NASA CONTRACTOR REPORT

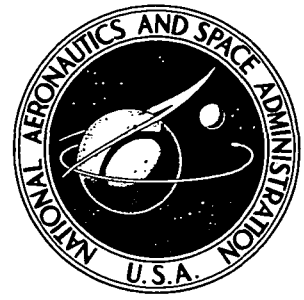

NASA CR-2434

NASA CR-2434

DEVELOPMENT OF AN APPARATUS TO MEASURE THERMOPHYSICAL PROPERTIES OF WIND TUNNEL HEAT TRANSFER MODELS

by Richard F. Romanowski and Ira H. Steinberg

Prepared by
GRUMMAN AEROSPACE CORPORATION
Bethpage, N.Y. 11714
for Langley Research Center

NATIONAL AERONAUTICS AND SPACE ADMINISTRATION • WASHINGTON, D. C. • SEPTEMBER 1974

1. Report No.	2. Government Accession No.	3. Recipient's Catalog No.
NASA CR-2434		

4. Title and Subtitle	5. Report Date
DEVELOPMENT OF AN APPARATUS TO MEASURE THERMOPHYSICAL PROPERTIES OF WIND TUNNEL HEAT TRANSFER MODELS	September 1974
	6. Performing Organization Code

7. Author(s)	8. Performing Organization Report No.
Richard F. Romanowski and Ira H. Steinberg	

9. Performing Organization Name and Address	10. Work Unit No.
Grumman Aerospace Corporation Bethpage, New York 11714	760-66-01-02
	11. Contract or Grant No.
	NAS1-11537
	13. Type of Report and Period Covered
12. Sponsoring Agency Name and Address	Contractor Report
National Aeronautics and Space Administration Washington, D. C. 20546	14. Sponsoring Agency Code

15. Supplementary Notes

Final report.

16. Abstract

A new apparatus and technique for measuring the thermophysical properties, $\sqrt{\rho ck}$, of models used with the phase-change paint technique for obtaining wind tunnel heat transfer data is described. This method allows rapid measurement of the combined properties in a transient manner similar to an actual wind tunnel test. Thus, an effective value of $\sqrt{\rho ck}$ can be determined which accounts for changes in thermal properties with temperature or with depth into the model surface. The apparatus was successfully tested at various heating rates between 1.9×10^4 and 12.4×10^4 W/m^2.

17. Key Words (Suggested by Author(s))	18. Distribution Statement
Thermophysical Properties Phase-Change Paint Technique Wind Tunnel Models	Unclassified - Unlimited STAR Category 33

19. Security Classif. (of this report)	20. Security Classif. (of this page)	21. No. of Pages	22. Price*
Unclassified	Unclassified	145	$4.75

*For sale by the National Technical Information Service, Springfield, Virginia 22151

TABLE OF CONTENTS

TABLE OF CONTENTS (Cont)

LIST OF TABLES

LIST OF ILLUSTRATIONS

SYMBOLS AND ABBREVIATIONS

SYMBOLS

A	Area, m^2
AC	Alternating current, A
c	Specific heat, J/(kg·K)
D	Diameter, cm or m
DC	Direct current, A
g	Gap width between specimen and concentric specimen mounting hole, m
J_λ	Spectral radiation of tungsten at wavelength λ, W/(cm^2·micron)
k	Thermal conductivity, W/(m·K)
L	Thickness, cm or m
M	Calorimeter mass, kg
Q	Rate of heat flow, W
$\dot{q}$	Heating rate, W/m^2
T	Temperature, K
T_i	Initial temperature, K
T_{pc}	Phase-change temperature, K
t	Time, s
X	Test plane coordinate normal to specimen rows, cm
x	Coordinate normal to calorimeter or sample face, m
Y	Test plane coordinate along specimen rows, cm
α	Thermal diffusivity, m^2/s
$\bar{\alpha}$	Average absorptance of phase-change coating

ε	Emissivity
λ	Wavelength, microns
ρ	Density, kg/m^3
ρ_λ	Spectral reflectance of phase-change coating at wavelength
$\bar{\rho}$	Average reflectance of phase-change coating
τ_λ	Spectral transmittance of phase-change coating at wavelength
$\bar{\tau}$	Average transmittance of phase-change coating

SUBSCRIPTS

abs	Absorbed
B	Denotes specimen mounting holes defined by test plane coordinate X = -2.857 cm (-1.125 in.)
C	Denotes specimen mounting holes defined by test plane coordinate X = 2.857 cm (1.125 in.)
cal	Calorimeter
cond	Conduction
cor	Corrected
e	Error
i	Incident
leak	Leakage
meas	Measured
nom	Nominal
rad	Radiation
refl	Reflected
sam	Sample
(0,0)	Center of test plane

UNITS

NOTE

All values are presented in the International System of Units (SI). In most cases, British System values are also presented, in parenthesis or brackets, following the SI values. Both sets of units are thus defined.

A	Amperes
Btu	British thermal unit
cm	Centimeter
F	Fahrenheit degrees
ft	Foot
gal	Gallon
Hz	Hertz
in.	Inch
kg	Kilogram
KW	Kilowatt
J	Joule
K	Kelvin degrees
lb	Pound mass
m	Meter
min	Minute
mm	Millimeter
N	Newton
s	Second
V	Volt
W	Watt

DEVELOPMENT OF AN APPARATUS TO MEASURE THERMOPHYSICAL PROPERTIES OF WIND TUNNEL HEAT TRANSFER MODELS

By R. Romanowski and I.H. Steinberg
Grumman Aerospace Corporation

Section 1

INTRODUCTION AND SUMMARY

1.1 INTRODUCTION

The phase-change coating technique, Reference 1, is a relatively simple and useful means of measuring aerodynamic heat transfer to small, complex wind tunnel models. It consists of using a model made from a low-conductivity material (usually plastic) covered with a phase-change coating which is an accurate indicator of surface temperature. One commercially available indicator, called "tempilaq," consists of wax crystals with a calibrated melting point; it is available in small temperature increments from 310.92 K(100 F) to 1644.26 K (2500 F). As a model is heated in a wind tunnel, the coating melts at various surface locations when the calibrated melting point is reached at the respective surface locations. With the melt temperature and the thermophysical properties of the model material known, the time required for each surface location to reach the melt temperature can be measured, and the heat transfer coefficient can be determined for all these body locations by using solutions to the transient one dimensional heat conduction equation.

Current methods of determining the thermophysical properties of the model material, specifically $\sqrt{\rho ck}$, where ρ is density, c is specific heat, and k is thermal conductivity, are costly, time consuming, and insufficiently accurate. Grumman thus initiated a study to determine whether the basic phase-change coating technique could be used with a specially constructed laboratory apparatus to determine these thermophysical properties more efficiently and accurately. That study led to the development of such an apparatus under a NASA-LRC funded program. This report describes the work

performed by Grumman in this program. The specific program objective was to develop an apparatus and technique for directly determining $\sqrt{\rho ck}$ as a function of both test time and surface temperature.

1.1.1 Apparatus and Test Technique

The apparatus used for the $\sqrt{\rho ck}$ determination must include a radiant heat source of variable intensity, a means for subjecting the model or test sample to a sudden step input in heating rate, control area of about one foot square which is subjected to a constant heating rate, several reference heat gages to measure imposed radiant heating rate, and a speciman holder. Thin-skin thermocouple calorimeters or other equally suitable devices can be used as the reference heat gages. The specimen and the reference heat gage should be coated with a layer of tempilaq with the melt temperature desired for a particular data point, so that the emissivity, and thus the heat rate, would be the same for both. The temperature of the radiant heat source should be high [about 3033.15 K (5000 F)] relative to the highest temperature for which $\sqrt{\rho ck}$ is to be determined [about 533.15 K (500 F)], so that the change in specimen wall temperature has a negligible effect on the imposed heat rate, and the heat rate can be considered constant during the test.

The test apparatus must include or provide for an external means of determining when the phase-change coating melts and the temperature-time response of the reference heat gage. The value of $\sqrt{\rho ck}$ can then be determined by solving the equation for one dimensional transient heating in a semi-infininte solid subjected to a step input of constant heating rate at the surface:

$$\sqrt{\rho ck} = \frac{\dot{q}}{T_{pc} - T_i} \frac{2}{\sqrt{\pi}} \sqrt{t}$$

where: $\dot{q}$ is the imposed heating rate

T_{pc} is the phase-change temperature

T_i is the initial temperature

t is the elapsed time at which the phase-change coating melts.

1.1.2 Tasks

The required tasks included development, construction, and test of apparatus as described in paragraph 1.1.1. Work was performed to demonstrate the following equipment characteristics:

- The one foot square control area is subjected to an essentially uniform heating rate (any variations must have a negligible effect on the $\sqrt{\rho ck}$ measurement).
- The apparatus can operate with a sufficient variety of heating rates to vary the time required to melt a 366.48 K (200 F) coating of tempilaq on a stycast plastic specimen from 0.1 second to 20 seconds; this variation corresponds to a heating rate range of 2.384×10^4 to 33.047×10^4 W/m^2 [2.1 to 29.1 $Btu/(ft^2 \cdot s)$].
- The specimen and reference heat gage have the same emissivity when coated with the same tempilaq.
- The apparatus can be used for accurately determining $\sqrt{\rho ck}$ of a representative plastic specimen at four surface temperatures, from 338.70 K (150 F) to 533.15 K (500 F), with three test times, from approximately 1 to 30 seconds, for each surface temperature.

1.2 SUMMARY

The apparatus that was designed and constructed, Figure 1-1, consists of a radiant heat source of variable intensity positioned above a 9.290×10^{-2} m^2 (1 ft^2) test plane containing tempilaq coated material samples and adjacent slug-calorimeter-type reference heat gages. The apparatus was successfully tested, yielding $\sqrt{\rho ck}$ values for a representative plastic at various heating rates between 1.930×10^4 and 12.492×10^4 W/m^2 [1.7 and 11.0 $Btu/(ft^2 \cdot s)$]; various test times between 0.3 and 20.6 seconds; and coating melt temperatures of 338.70 K [150 F], 366.48 K [200 F], 422.03 K [300 F], and 533.15 K [500 F]. The heating rate step inputs were effected by a spring-loaded shutter system. Motion picture and temperature recording equipment were used to respectively monitor sample coating melt time and reference gage heating rate, respectively, during these tests.

The apparatus that was developed has proven capable of producing nominal incident heating rates of 1.135×10^4 to 130.599×10^4 W/m^2 [1 to 115 Btu/(ft^2·s)]. Black body calibration data show that less than a 1.7 percent difference in incident heating rate exists between adjacent sample and reference gage ports. Calibration data also show that no more than half of the incident heat is absorbed by a given reference gage when coated with tempilaq. The difference in the amount of heat absorbed by the reference gage and the sample, for a given incident heating rate and coating thickness, is related to coating transmittance, $\bar{\tau}_1$, coating reflectance, $\bar{\rho}_1$, and sample reflectance $\bar{\rho}_3$, according to the following equation:

$$\left[\frac{\dot{q}_{cal} - \dot{q}_{sam}}{\dot{q}_i}\right]_{abs} = \frac{\bar{\rho}_3 \bar{\tau}_1^2}{1 - \bar{\rho}_1 \bar{\rho}_3} \quad . \tag{1-1}$$

Based on an experimentally determined maximum value of coating transmittance ($\bar{\tau}_1 = 0.20$) and its associated reflectance ($\bar{\rho}_1 = 0.57$), this difference is held to within 2.1 percent if sample reflectance ($\bar{\rho}_3$) is less than 0.40.

Reference gage heat losses are minimized by the application of aluminized h-film insulation. Copper slug type calorimeters, 3.810 cm (1.50 in.) in diameter, have been supplied in nominal thickness of 0.635 cm (0.25 in.) and 0.203 cm (0.08 in.). For their prescribed measurement ranges, the calorimeters experience less than a 2.1 percent loss when test times are limited to 35 seconds and 20 seconds for the larger and smaller thickness, respectively. The estimated heat loss for low conductivity plastic samples, based on a 35 second test time and a 56.782×10^4 W/m^2 [50 Btu/(ft^2·s)] absorbed heating rate is less than 1.75 percent.

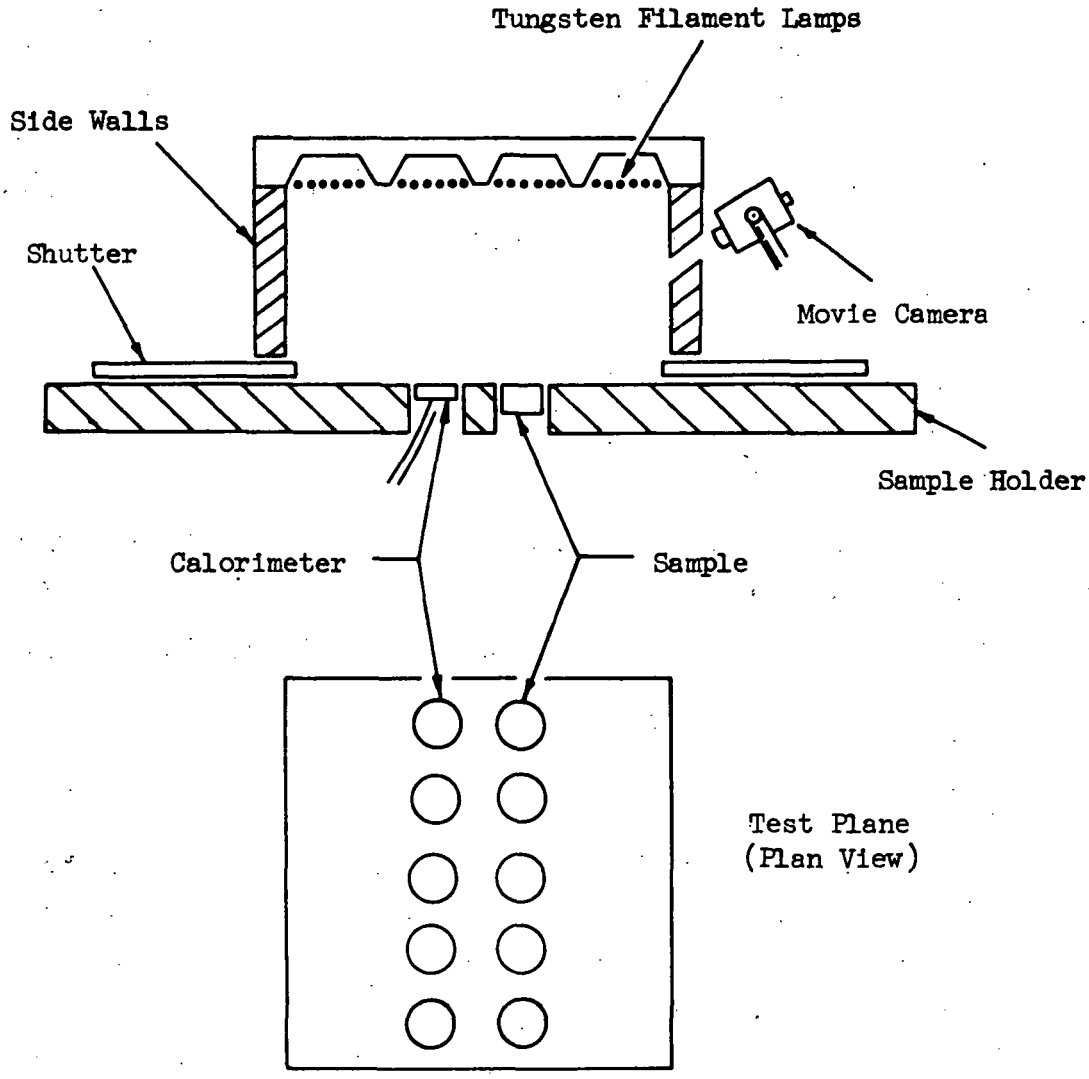

Figure 1-1 Thermophysical Properties Measurement Apparatus

Section 2

PROGRAM PLAN

The program plan for this study, Figure 2-1, consists of four basic tasks: the design, fabrication, and experimental verification of the prescribed thermophysical properties measurement apparatus, and evaluation of associated equipment and extended apparatus capability. Extensive analyses and supporting experimental investigations were performed in efforts to provide a "minimum-error" design.

The organization chart for this program is shown in Figure 2-2.

	Months From Go Ahead															Man Hours			
																Shop	Eng	Inst	Plang
	1	2	3	4	5	6	7	8	9	10	11	12	13	14	15	RC	RC	RC	RC
																20	10	11	52
DESIGN OF EQUIPMENT																			
Establish Design Requirements	80	75															155		
Design of Apparatus		40	40	35													115		
FABRICATION OF APPARATUS																			
Fabricate All Parts				80	80	75										230			5
Final Assembly						40	60									75		20	5
Operational Checkout								50	55							75		20	10
EXPERIMENTAL VERIFICATION																			
Optical Properties Tests			80	110												100	40	40	10
Develop Test Plan					20	20											40		
Define Heating Distribution								40	80							40	80		
Test Samples for $\sqrt{\rho ck}$									40	40	40	40				40	110		10
Modify Equipment and Checkout											40	40				40	40		
EQUIPMENT AND EXTENDED CAPABILITY EVALUATION																			
Evaluation of Cameras								40	40									80	
Cryogenic Cooling											40						40		
Extended Capability Evaluation												40					40		
REPORTS																			
Final Report and Users Manual													80	40			120		
Progress Report				▲			▲			▲			▲			600	780	160	40
PROGRAM MILESTONES																TOTAL			
NASA Review of Final Design				▲															
Operational Checkout Complete									▲										
Initial Sample Tested										▲									
Delivery														▲					
Issue Final Report															▲				

Figure 2-1 Program Plan

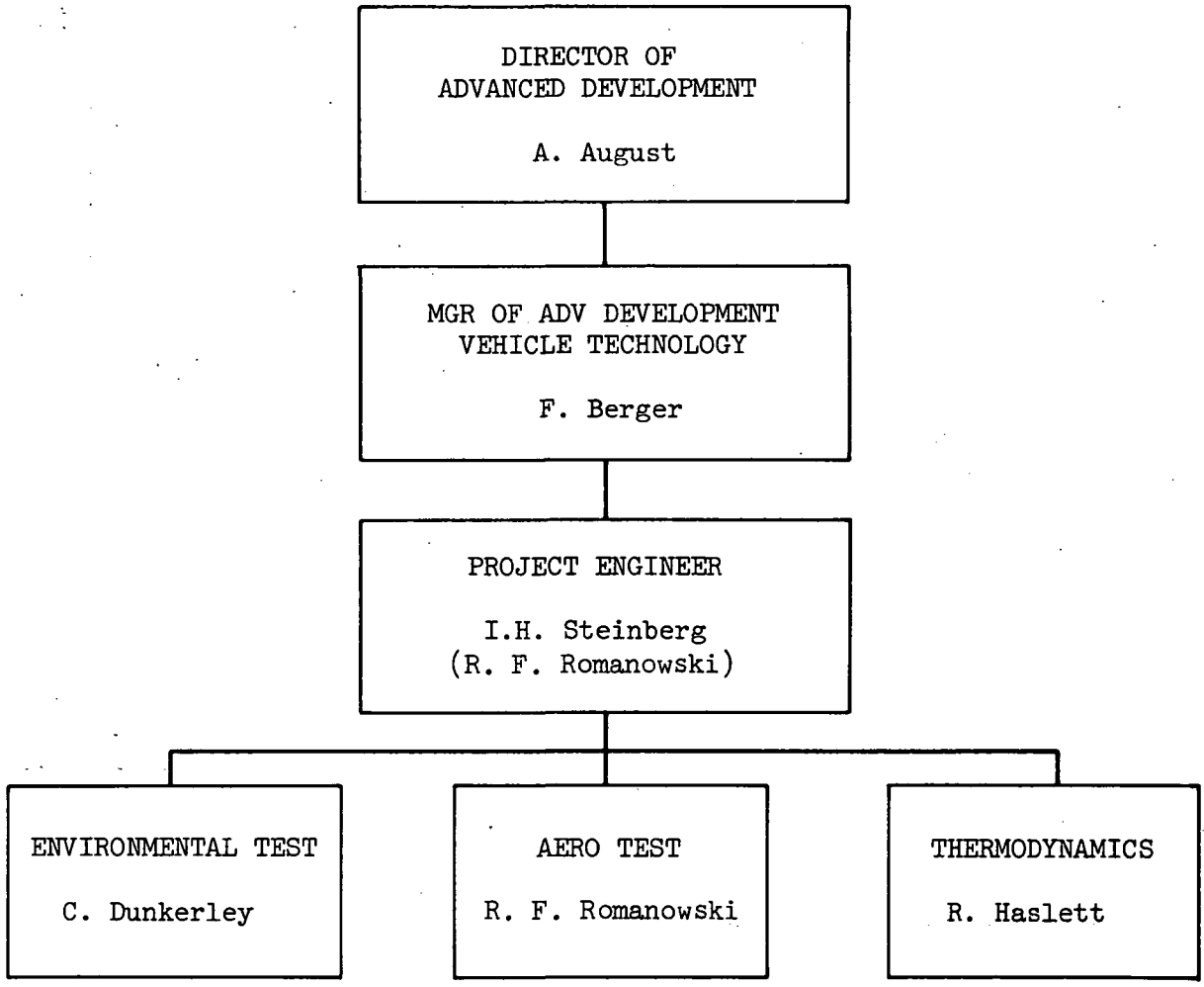

Figure 2-2 Program Organization

Section 3

BACKGROUND

The phase-change coating technique for measuring aerodynamic heat transfer to small complex wind tunnel models has proven to be an effective tool in experimental aerodynamics. The ever increasing use of this tool has led to a number of improvements over the last two years; New solutions which have been obtained allow for accurate data reduction on thin model sections heated at both surfaces; painting, lighting, and photographic techniques have been improved; methods for automating data reduction have been developed; and several promising new model materials have been studied. However, one factor currently exists which seriously limits the accuracy of the data, and thus the usefulness of the entire technique. This factor is the uncertainty in the thermophysical properties of the model material. The accuracy with which the heat transfer coefficient can be determined is directly dependent on the accuracy of thermophysical property $\sqrt{\rho ck}$. The uncertainty in $\sqrt{\rho ck}$ is large for a number of reasons. For example, one of the better model materials that has been used is a high temperature plastic which contains a filler. Experience with this material has shown a large variation to exist in $\sqrt{\rho ck}$ for a various models; $\sqrt{\rho ck}$ may also vary with depth near the surface, and with temperature. Thus, samples must be made for each model cast, and ρ, c, and k must be separately measured over a range of temperature in order to obtain acceptable accuracy. Unfortunately, the standard means of independently measuring these thermophysical properties have a number of disadvantages:

- Accuracy - The most serious disadvantage of the standard techniques, the inability to obtain accurate heat transfer data, is due to inaccuracies in determination of $\sqrt{\rho ck}$. Several factors are responsible for these inaccuracies. The standard techniques now used measure ρ, c, and k independently, under steady state conditions,

and these measurements are average values for the thickness or bulk of the sample. As a result, the total error in $\sqrt{\rho ck}$ is the square root of the product of the errors in each individual factor; but an even more important cause of inaccuracies is the fact that the thermophysical properties in a very thin layer near the surface may be different from the average value in the material. Since the transient tunnel testing technique allows heat to penetrate to only a small depth (dependent on time), an undetermined error is involved in the use of average values. Since different test times produce different depths of heat penetration in wind tunnel tests, a method of determining $\sqrt{\rho ck}$ in a transient environment similar to that experienced in a wind tunnel test should provide improved accuracy; this would be particularly true if $\sqrt{\rho ck}$ can be measured as one entity.

- Cost - The standard techniques for measuring heat transfer, Reference 2 for example, require elaborate equipment, specially trained technicians, and samples instrumented with thermocouples. The measurements cost for such a technique may exceed the fabrication cost for a complex wind tunnel model, depending upon the temperature range and the number of data points required.

- Time - Since instrumenting the thermal conductivity sample with thermocouples is very complex, and the actual measurements are best made in laboratories specializing in this type of work (which requires sending the samples elsewhere for analysis) the procedure is somewhat time consuming. Often, the models are received, the wind tunnel test program completed, and the data reduced several weeks before the thermophysical properties are determined.

- Samples - The thermophysical properties of the samples may be different from that of the model. Moreover, since some of the model materials contain fillers of variable concentration, especially near the surface, the thermophysical properties may vary with the size and shape of the casting, thickness of the section, or with the pouring technique and curing time. Thus, development of a nondestructive method for measuring $\sqrt{\rho ck}$ on small nearly flat surfaces of the model would be desirable.

Section 4

APPARATUS AND TEST TECHNIQUE

4.1 THERMOPHYSICAL PROPERTIES MEASUREMENT

The Thermophysical Properties Measurement (TPM) Apparatus, Figure 4-1, consists, essentially, of a bank of variable intensity, high density radiant heaters (1) which, when positioned above the base plate (5), is supported by two notched side tracks (7). The side tracks and end plates (8) completely enclose the heater bank around its perimeter and provide a nominal one foot square area of illumination to the base plate. This area, or test plane, can be shielded from illumination by split shutters (11), which slide along the channel formed by the base plate-side track junction. Rollers (18) guide the shutters in the channel. When retracted, the shutters provide a step input in heating to the test plane.

The heater, side track, and base plate assembly is supported by an inverted table frame (4) to which the shutter retraction system is mounted. This system consists of symmetrical shaft assemblies (15); associated linkage components (14), (16), (17), and (19); and a spring loading mechanism (22) and (23). The shutters are locked in place above the test plane by positioning a pivoted handle assembly (24), (25), and (26) so as to restrain the linkage when the springs are taut. This is accomplished by manually closing the shutters until the retainer (20) is located to the outside of the catch piece (25), pivoting the pull handle (26) until the retainer rests against the catch, and locking it in place with the safety latch (21). The pull handle is split to allow the left and right shutters to be set individually. The interlock (27) connects the two handle pieces so that both shutters release simultaneously.

The four units comprising the heater bank are both water and air cooled. Cooling manifolds are shown as components (2) and (3). Water is circulated

through the heater housings; air cools the lamp cavities and exhausts to the atmosphere. The shutters are also water cooled. Water source and exit lines for shutter cooling attach to fittings at the base of the apparatus. Metal tubing is routed from the entrance port along the frame, then jumped by means of flexible plastic tubing (13) to the shutters. Water leaves the shutters through similar jumpers (12) and is carried along metal return tubing to the exit port.

The base plate contains ten specimen mounting holes, Figure 4-2. Locations 1 through 5 accommodate material samples of nominal 3.810 cm (1.5 in.) diameter and 1.905 cm (0.75 in.) thickness. Corresponding reference heat gages of the same diameter are positioned symmetrically, adjacent to the samples, at location 6 through 10. Prior to installation, the samples and reference gages are sprayed with a uniform layer of tempilaq phase-change coating to equalize their emissivities. Testing begins by closing the shutters above the test plane and locking them in place, and then placing the radiant heater bank in position above the test area. The lamps are brought to a preselected intensity by application of a constant voltage. When conditions are stabilized the shutters are retracted, thereby subjecting the test plane to a constant heating rate step input. The resulting heating distribution provides the same average heating rate for each sample and its corresponding reference gage, even though the average heating rate from sample to sample (and thus from reference gage to reference gage) can differ in a uniform manner.

Data that must be acquired include the temperature-time responses of each reference heat gage, and the elapsed time between initial heating and melt (phase-change) of the tempilaq coating for each sample. The temperature-time data may be obtained from either a multi-arm pen recorder or digital computer. These data are used to determine the imposed sample heating rate. Time-to-melt is best determined from a motion picture film; a camera port is provided in the right end plate, component (10) of Figure 4-1. The value of $\sqrt{\rho ck}$ can then be determined from solution of the equation for one dimensional transient heating in a semi-infinite solid subjected to a step input of constant heating rate at the surface:

$$\sqrt{\rho ck} = \frac{\dot{q}}{T_{pc} - T_i} \frac{2}{\sqrt{\pi}} \sqrt{t} \qquad (4\text{-}1)$$

where $\dot{q}$ is the imposed heating rate

T_{pc} is the phase-change temperature

T_i is the initial temperature

t is the elapsed time at which the phase change coating melts.

4.2 TEMPERATURE CONTROL

A modular temperature control system was used in conjunction with the TPM apparatus to provide power regulation. The system basically consists of a temperature controller, proportional power controller, run control panel, circuit breaker, ammeter, and load voltage monitor.

The temperature controller is a solid state null balancing instrument designed for both high and low response closed loop control systems. It can be operated manually (by switch selection), from a set point dial, or by a remote programmer. Manual control allows for selection of 0 to 100 percent of full output for open-loop operation; the set point dial provides 1000 part logging for precise setting of the selected value. The remote control feature allows the instrument to accept commands from automatic programming devices.

A power controller regulates power to the radiant heaters in response to the temperature controller signals. The unit has a maximum input voltage of 480 VAC and maximum current rating of 450 amperes. Maximum power output at the maximum line voltage is 216.0 KW.

4.3 RECORDING EQUIPMENT

Any accurate means of recording the temperature-time response of the reference heat gages may be employed. Initial apparatus calibration and thermophysical properties measurements were performed using 4-pen millivoltmeter recorders with the following characteristics:

Accuracy: ±¼ percent of span, or 20 microvolts

Deadband: 0.1 percent of span maximum

Slidewire Resolution: Better than 0.1 percent of span

Minimum Span: 1 millivolt, DC

Source Impedance: 10,000 ohms maximum for 1 millivolt span

Pen Speeds: 2 or 4 seconds for full-scale travel

Standardization (Potentiometers): Zener diode reference voltage source

Primary Power: 120 volts, 50 or 60 Hz.

4.4 PHOTOGRAPHIC EQUIPMENT

The initial calibration tests performed at Grumman used a precision motion picture camera equipped with a 3.45 mm wide angle lens. This lens has a 2.879 radian (165 degree) field angle and maximum aperture of f 1.5. An N.D. filter was required when the apparatus was operated at high intensities. Camera speed was calibrated at 20 frames per second. Standard 16 mm positive color film with normal processing provided good results. The exposure settings used during the tests are given in Table 4-1.

Table 4-1. Camera Exposure Settings

Nominal Voltage, Volts	Nominal $\dot{q}$ (With Templaq Coating), 10^4 W/m^2 (Btu/(ft^2 · s)		Lens Opening, f	Filter
50	1.782	(1.57)	2.8	None
75	3.634	(3.20)	5.6	None
100	5.791	(5.10)	8.0	None
220	17.602	(15.50)	2.8	N.D. 4
460	58.485	(51.50)	5.6-8.0	N.D. 4

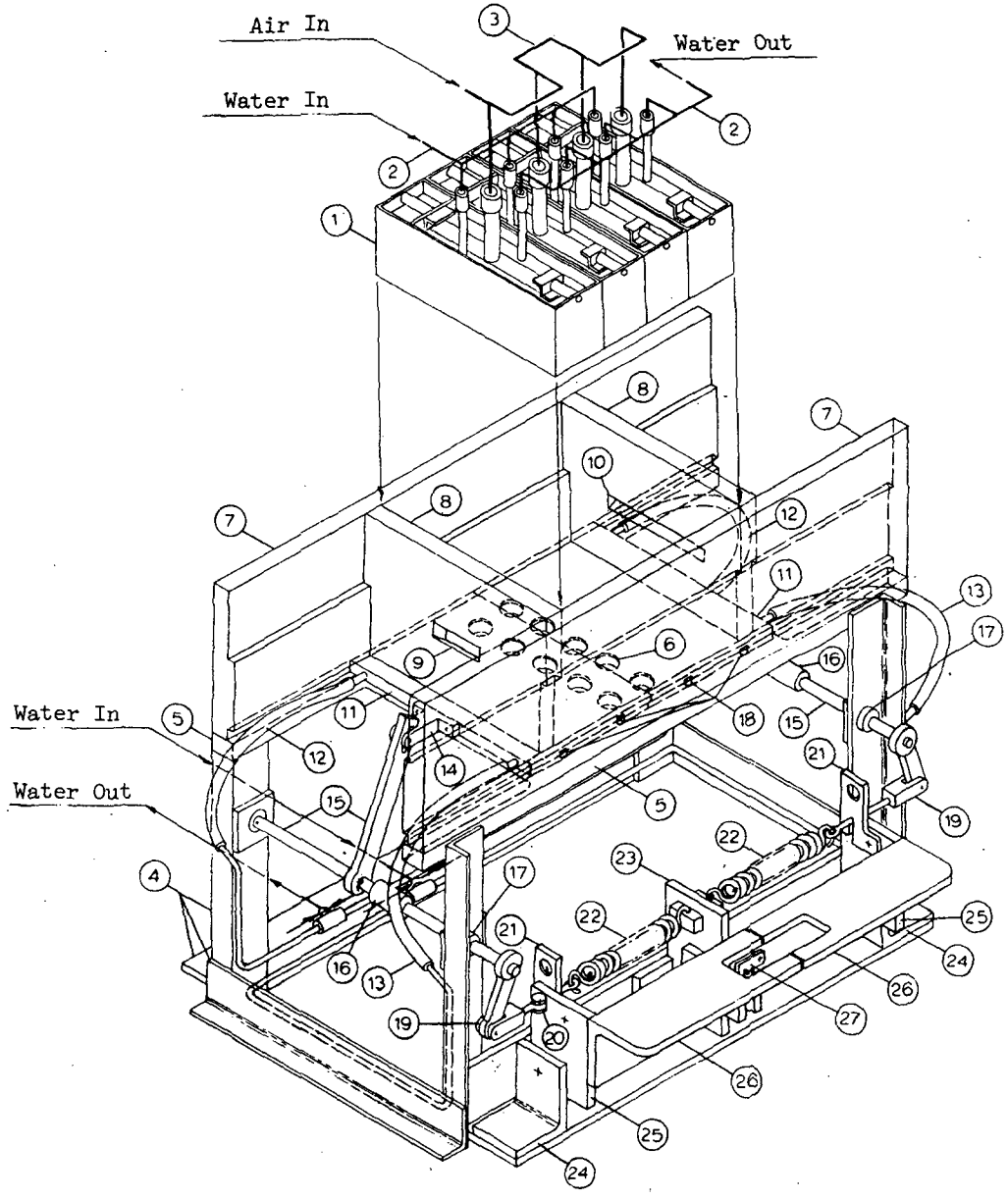

Legend

1. Quartz Lamp Array
2. Cooling Water Manifold
3. Cooling Air Manifold
4. Brace and Leg Assembly
5. Base Plant
6. Specimen Mounting Holes
7. Side Track
8. End Plate
9. Viewing Port
10. Camera Port
11. Water Cooled Shutters
12. Flexible Tubing (Water Supply)
13. Flexible Tubing (Water Exit)
14. Yoke
15. Shaft Assembly
16. Union
17. Collar
18. Shutter Rollers
19. Clevis
20. Retainer
21. Safety
22. Spring
23. Spring Mount
24. Catch Mount
25. Catch
26. Pull Handle
27. Interlock

Figure 4-1 Thermophysical Properties Measurement Apparatus

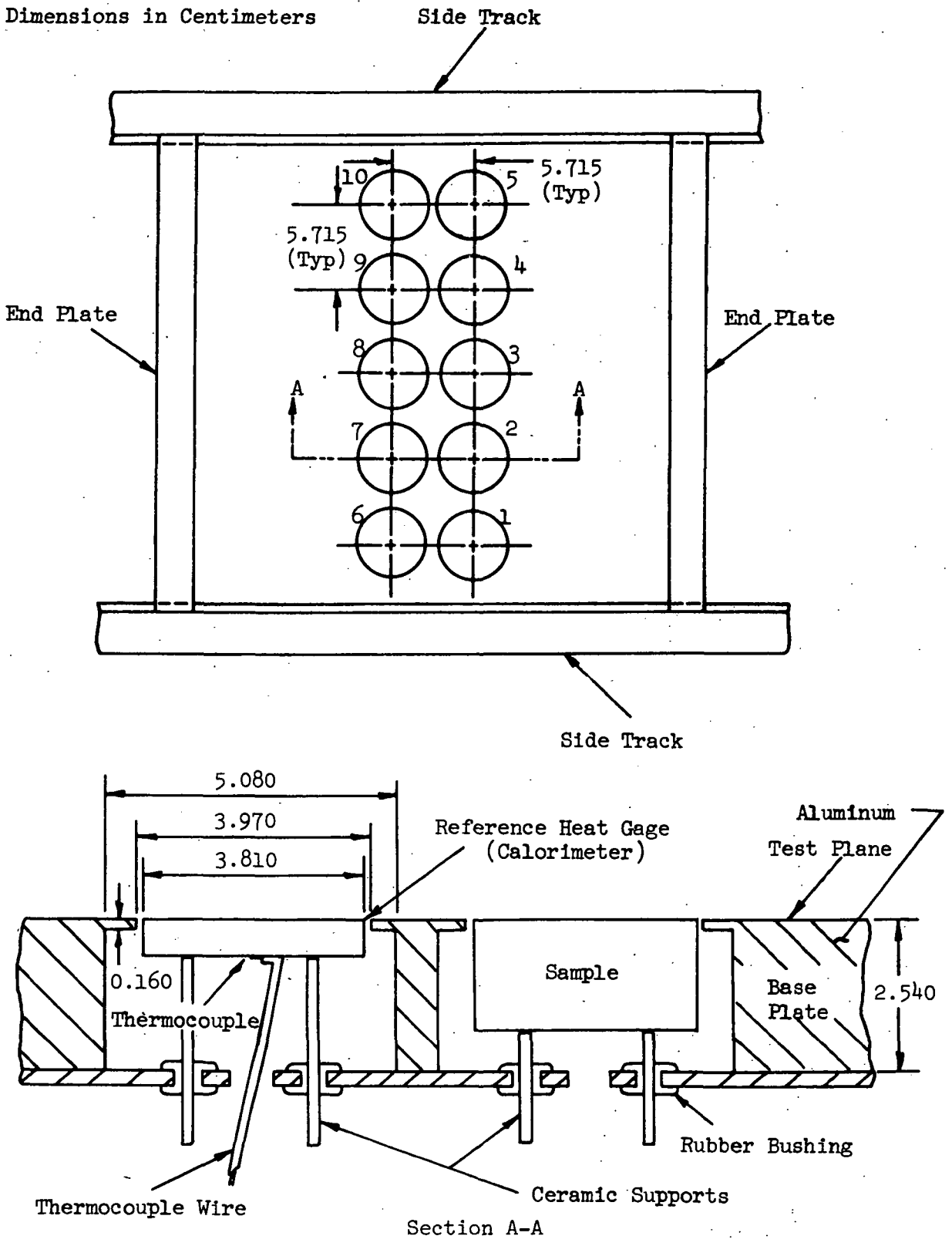

Figure 4-2 Reference Heat Gage and Material Sample Installation

Section 5

COMPONENT DESIGN

5.1 RADIANT HEATER BANK

The heater bank is comprised of four high density modular radiant heater units, assembled as shown in Figure 5-1. Each unit has six tungsten filament lamps installed in a water cooled reflector housing. Clear quartz windows seal the lamp cavity at the housing base and thus provide a cooling air passage. (Figure 4-1 shows the cooling air and water manifold.) An argon atmosphere surrounds the tungsten filaments which are enclosed in clear quartz tubes of 0.952 cm (0.375 in.) outer diameter. The filaments of each unit operate between 2477.59 K (4000 F) and 3255.37 K (5400 F) over their half to full rated voltage range as follows:

Rated Voltage: 480 VAC

Total Power Dissipated at Rated Voltage: 36.0 KW

Net Heat Flux at Window Surface at Rated Voltage: 1.209×10^{6} W/m^{2} (780 W/in.^{2})

Current at Rated Voltage: 75 amperes

Cooling Water Flow Recommended: 4.163×10^{-3} m^{3}/min (1.1 gal/min)

Cooling Air Recommended: Plenum Gage Pressure at Port P = 158.579×10^{3} N/m^{2} (23 psig); Flow = 0.877 m^{3}/min (31 ft^{3}/min)

5.2 TEST SAMPLES

The TPM apparatus is designed to accept samples of 3.810 cm (1.5 in.) diameter and 1.905 cm (0.75 in.) thickness. This thickness permits the testing of a wide range of materials, from low conductivity plastics to stainless steel, covering the range of thermophysical properties $0.408 \times 10^{3} \leqq \sqrt{\rho ck} \leqq 8.176 \times 10^{3}$ J/(m$^{2}\cdot$s$^{\frac{1}{2}}\cdot$K) [$0.02 \leqq \sqrt{\rho ck} \leqq 0.40$ Btu/(ft$^{2}\cdot$s$^{\frac{1}{2}}\cdot$F)]. Maximum test time before the

semi-infinite slab assumption is violated is approximately 300 seconds for low conductivity plastic and 30 seconds for stainless steel; these times are more than adequate for TPM apparatus operation. An analysis of conduction and radiation heat leakage experienced by samples of these two materials under test conditions resulted in the selection of the 3.810 cm (1.5 in.) sample diameter. The detailed analysis is presented as Appendix A. Figure 5-2 summarizes the results: The stainless steel sample experiences a net heat gain whereas the low conductivity plastic sample experiences a net heat loss. However, in both cases, the magnitude of heat leakage increases with time, and is relatively insensitive to absorbed heating rate.

The percentage of heat gained by the stainless steel sample is less than 1.2 percent for a 30 second test time with a 56.782×10^4 W/m^2 [50 Btu/(ft^2·s)] absorbed heating rate. This value represents the heat gained by the entire sample; the error at the center of the sample face should be significantly less. The heat loss from the low conductivity plastic sample is, coincidently, of the same order of magnitude as the heat gained by the stainless steel sample. Thus, the plastic sample heat leakage for a 35 second test time and 56.782×10^4 W/m^2 [50 Btu/(ft^2·s)] absorbed heating rate is less than 1.75 percent, as determined from the applicable curve for stainless steel.

5.3 REFERENCE HEAT GAGES

The details of an analysis performed to determine the proper design of reference heat gages for use in the measurement of sample heating rate are presented in Appendix B. A 3.810 cm (1.5 in.) diameter, pure-copper-slug-type calorimeter, instrumented with a backface thermocouple and insulated with aluminized h-film, was selected as the optimum design, Figure 5-3. Thermocouple wires were 0.127 mm (0.005 in.) diameter chromel and alumel, with refrasil insulation. Calorimeter and sample diameter were kept the same so that when each is located in zones of similar heating, the calorimeter measures the same average heating rate as the sample absorbs. Calorimeters with thicknesses of 0.203 cm (0.08 in.), 0.635 cm (0.25 in.), and 1.270 cm (0.50 in.) thus are needed to measure material thermophysical properties across the $0.408 \times 10^3 \leqq \sqrt{\rho ck} \leqq 8.176 \times 10^3$ J/(m^2·s$^{1/2}$·K) range [$0.02 \leqq \sqrt{\rho ck} \leqq 0.40$ Btu/(ft^2·s$^{1/2}$·F) range]

for selected nominal incident heating rates from 1.135×10^4 W/m^2 [1 Btu/ft^2·s)] to 113.565×10^4 W/m^2 [100 Btu/(ft^2·s)]. For a given material and incident heating rate, calorimeter thickness must be selected to insure a temperature rise sufficiently large and rapid to provide an accurate heating rate reading; in addition, this temperature rise must lag behind that of the sample surface so that the phase-change coating on the sample melts before the coating on the calorimeter.

Design considerations dictate that a thin coating [approximately 0.025 mm (0.001 in.)] of high temperature/high emissivity black paint be applied to the calorimeter face prior to application of the phase-change coating. Many commercial precoats are available for this purpose; almost all may be cured following application for high temperature operation. Since the curing renders them solvent resistant, tempilaq coatings may be repeatedly applied and removed without affecting the black base coat.

One commercially available precoat, "sperex," is supplied in spray cans for ease of application. A thinly applied coating air dries in 15 to 30 minutes. Baking for 30 to 60 minutes at 588.70 K (600 F) to 616.48 K (650 F) improves the finish and provides a more durable surface. Drying and curing sperex coatings as described enables them to survive temperatures of 922.03 K (1200 F).

The calorimeter heat leakage for the prescribed heating rate measurement ranges is shown in Figure 5-4. Heat leakage may be minimized by limiting test time. For example, a tempilaq coated calorimeter subjected to an incident heating rate of 45.426×10^4 W/m^2 [40 Btu/(ft^2·s)] absorbs about half of the incident flux; and, Figure 5-4(a) shows that a 0.203 cm (0.08 in.) thick calorimeter loses no more than 2.1 percent of the heat it absorbs if test time is limited to 20 seconds. If a 0.635 cm (0.25 in.) thick calorimeter is used, test time may be increased to as much as 39 seconds before a 2.1 percent heat loss is incurred, as shown in Figure 5-4(b).

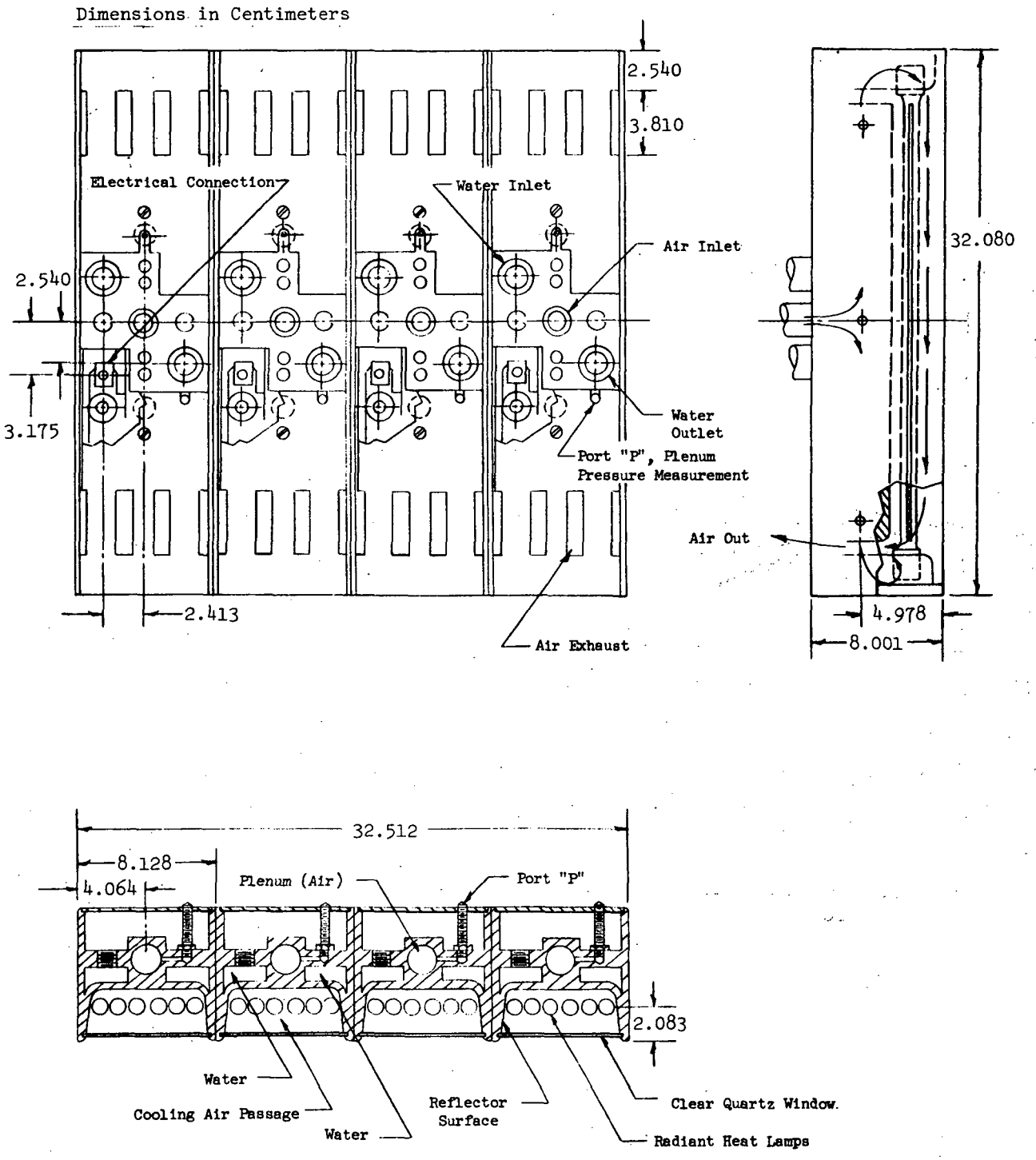

Figure 5-1 Radiant Heater Bank

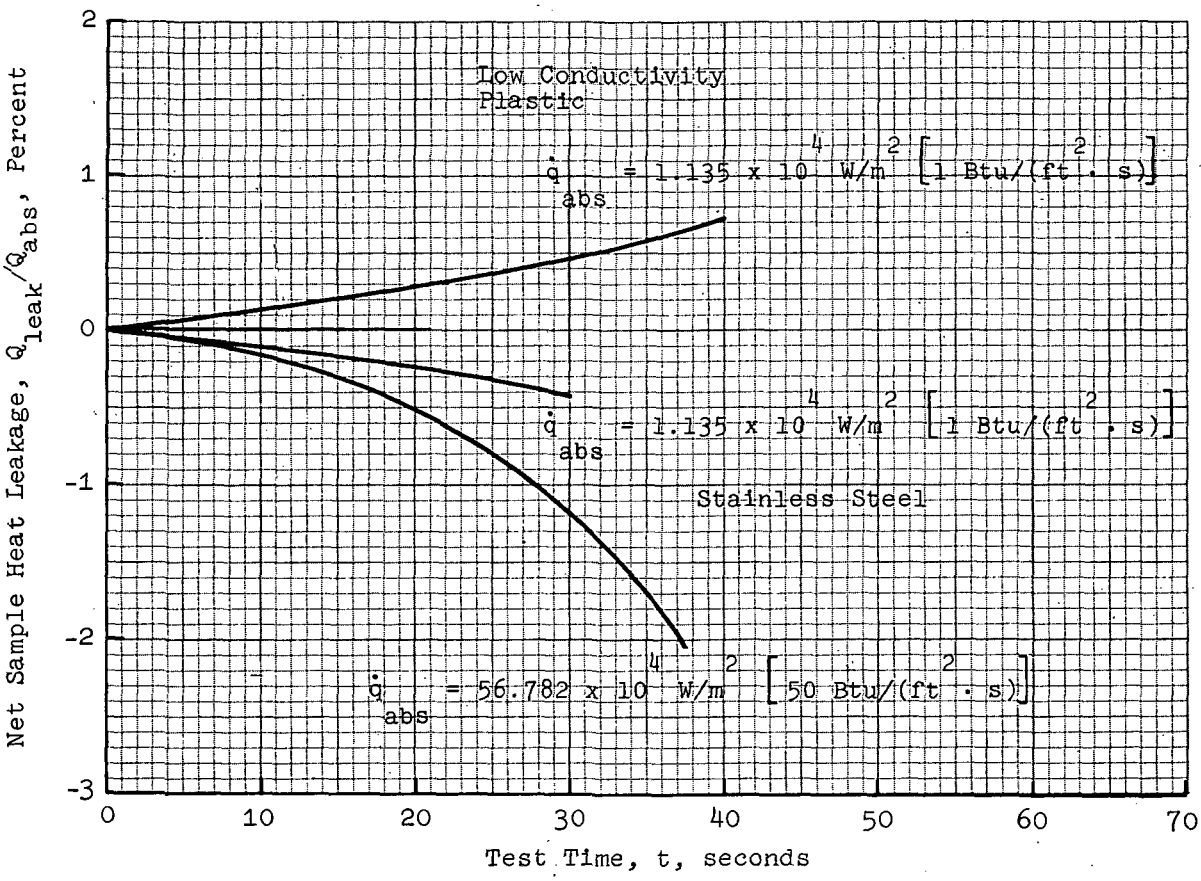

Figure 5-2 Sample Heat Leakage

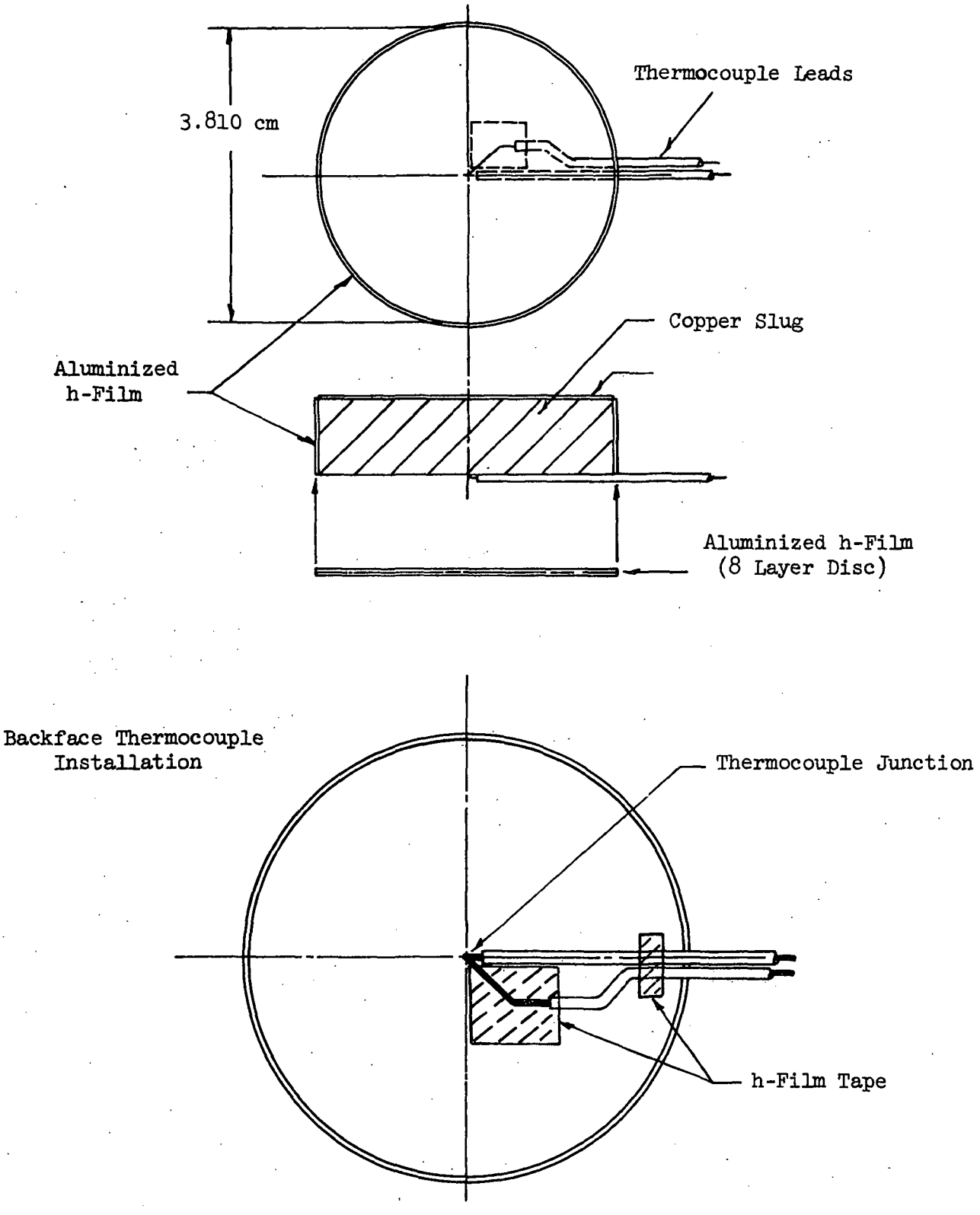

Figure 5-3 Instrumented Copper Slug Calorimeter

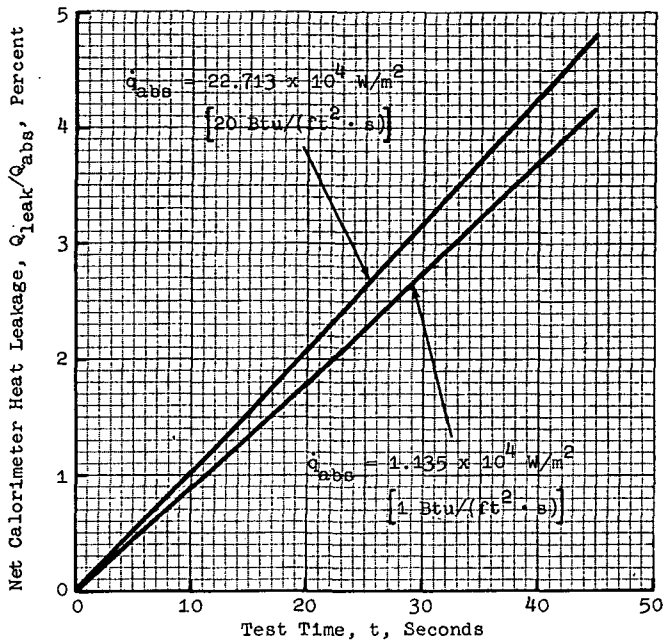

a. Thickness = 0.203 cm (0.08 in.)

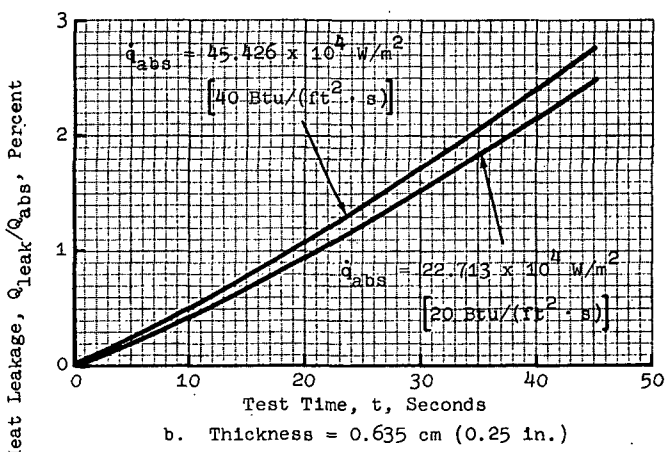

b. Thickness = 0.635 cm (0.25 in.)

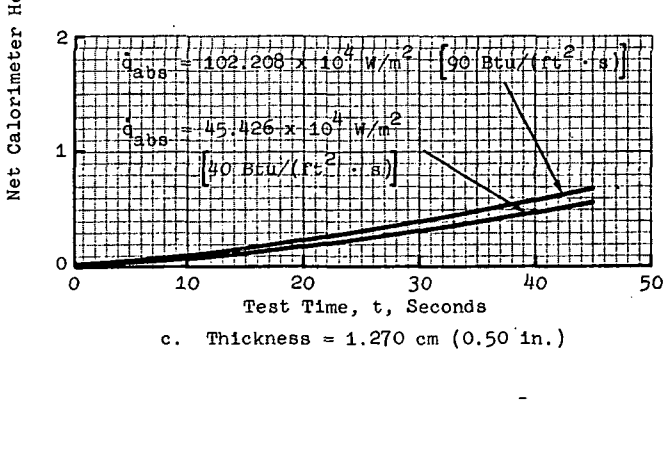

c. Thickness = 1.270 cm (0.50 in.)

Figure 5-4 Calorimeter Heat Leakage

Section 6

TEST RESULTS

6.1 HEATING DISTRIBUTION

Heating across the test plane was measured to demonstrate uniformity of distribution and to verify that adjacent reference gage and sample ports had essentially the same heating rates. Preliminary distribution measurements were made, for optimization purposes, prior to assembly of the TPM apparatus. Calibration heating distribution measurements were made after assembly of the apparatus.

6.1.1 Preliminary Measurements

Preliminary measurements of the test plane heating distribution were made by mounting the radiant heater bank to a four-legged frame and track assembly, and positioning the lamps above the base plate as shown in Figure 6-1. Calorimeters coated with a 0.025 mm (0.001 in.) layer of sperex flat black paint were installed in all ten base plate ports, Figure 6-2. Four nominal lamp voltages were selected: 50, 100, 220, and 460 volts; and three sets of heating rate data were taken at each voltage. The first set of data was obtained with the lamps on center, Figure 6-2(a), the second with the lamps positioned 5.715 cm (2.25 in.) to the left of center, Figure 6-2(b), and the third with the lamps positioned 5.715 cm (2.25 in.) to the right of center, Figure 6-2(c).

The heating rate data are presented in Tables 6-1 through 6-4. Data in each of the three sets, presented in columns (1) and (2), (3) and (4), and (5) and (6), respectively, were taken simultaneously, at the nominal voltage. Asterisks denote interpolated data which were substituted for faulty calorimeter measurements. Note that columns (2) and (3), and likewise columns (4) and (5), represent duplicate measurements taken on separate runs. Correction factors K_1 and K_2 were applied to the data in columns (1) and (2) and columns (5) and (6), respectively, to compensate for slight nominal voltage differences between runs. The average heating rate across both stations B and C (Figure 6-2) thus is conserved, and a fourth order curve fit to the corrected data at

these stations [columns (2) through (5)] can be used to obtain the heating rate at the center of the test plane (X = 0, Y = 0). Corrected heating rate data are normalized with respect to this value, and plotted in Figures 6-3 through 6-6. Solid symbols in these figures represent interpolated data substituted for faulty calorimeter measurements.

In general, the heating distributions varied uniformly along calorimeter rows (Y direction), reaching a maximum at the center of the test plane, and the tapering off to between 85 and 89 percent of maximum at the outer ports. Heating rate levels remained relatively constant across calorimeter rows (X direction); the maximum incident heating rate varied from 2.908×10^4 W/m^2 (2.562 Btu/[ft^2·s]) at 50 volts to 118.684×10^4 W/m^2 (104.507 Btu/[ft^2·s]) at 460 volts.

6.1.2 Final Measurements

Calibration heating distributions obtained for the assembled apparatus are presented in Tables 6-5 through 6-8 and plotted in Figure 6-7. These data show the distributions to be more uniform than in the preliminary measurements, and the edge effects to be slightly less severe (due to the side track and endplate enclosure of the heater bank). Maximum incident heating rates at the various voltage settings were increased by an average of 6 percent over preliminary values.

Percentage differences in heating rate between corresponding pairs of calorimeters are presented in Table 6-9. Since the greatest difference is no more than 1.7 percent over the apparatus operating range, the fact that corresponding sample and reference gage ports are located in zones of similar heating is verified.

6.2 OPTICAL PROPERTIES OF PHASE-CHANGE COATINGS

Results of transmittance and reflectance tests on phase-change coatings verified the absorption of equivalent amounts of heat by identically coated calorimeters and samples located in zones of similar heating. This equivalent absorption is a necessary requirement for the calorimeter measurement to represent the sample heating rate accurately. Other requirements include

establishing that the phase-change coating, and not the substrate, is the prime variable that determines the amount of heat entering the sample or calorimeter, determining the transmittance and reflectance characteristics of various temperature phase-change coatings, and applying these data to estimate the differences, if any, in the amount of heat absorbed by the sample and calorimeter under test conditions.

6.2.1 Effect of Substrate

Spectral reflectance measurements of a 422.03 K (300 F) phase-change coating applied to both high and low emissivity substrates were obtained by means of a heated cavity reflectometer. Reflectance versus wavelength data for both cases, Figures 6-8 and 6-9, bear marked similarities and result in identical values of near normal emittance: 0.895. The substrate can thus be considered to have no appreciable effect on the reflectance characteristics of tempilaq phase-change coatings.

6.2.2 Transmittance and Reflectance Tests

Results of transmittance and reflectance tests of 318.15 K (113 F) and 533.15 K (500 F) phase-change coatings are presented in Figures 6-10 through 6-17. Data were obtained for each coating at two nominal thicknesses: 0.177 mm (0.007 in.) and 0.406 mm (0.016 in.). The average values of transmittance, reflectance, and hence absorptance, are determined by integrating the curves of Figures 6-10 through 6-17 over the quartz lamp spectrum as follows:

$$\bar{\tau} = \frac{\int_0^\infty \tau_\lambda J_\lambda \, d\lambda}{\int_0^\infty J_\lambda \, d\lambda} \qquad (6\text{-}1)$$

$$\bar{\rho} = \frac{\int_0^\infty \rho_\lambda J_\lambda \, d\lambda}{\int_0^\infty J_\lambda \, d\lambda} \qquad (6\text{-}2)$$

$$\bar{\alpha} = 1 - (\bar{\tau} + \bar{\rho}) \qquad (6\text{-}3)$$

where $\bar{\tau}$ = average transmittance

$\bar{\rho}$ = average reflectance

$\bar{\alpha}$ = average absorptance

λ = wavelength, microns

τ_λ = transmittance at wavelength λ

ρ_λ = reflectance at wavelength λ

J_λ = watts radiated per square centimeter of surface, per micron wavelength band at wavelength λ, for tungsten at a selected filament temperature.

Results of these integrations are shown in Table 6-10 for filament temperatures of 810.92 K (1000 F) and 3255.37 K (5400 F). These temperatures cover the entire voltage range of quartz lamp operation. In general, values of average transmittance and reflectance increase as filament temperature increases; as expected, increasing coating thickness reduces transmittance and increases reflectance.

6.2.3 Coated Calorimeter and Sample Heat Absorption

Differences in heat absorption between tempilaq coated calorimeters and samples must be minimized to insure that calorimeter measurements accurately represent sample heating rates. Fortunately, an analytical method for estimating the differences that do exist is available. The analytical heating models used in the analysis are shown in Figure 6-18. The calorimeter is assumed to have a base coating of black paint with an emissivity of 1.0; any incident heat passing through the phase-change coating thus should be absorbed by the black paint, and transmitted via conduction to the copper slug, Figure 6-18(a). The amount of heat reflected thus is given by

$$(\dot{q}_{cal})_{refl} = \bar{\rho}_1 \, \dot{q}_i \qquad (6\text{-}4)$$

where $\bar{\rho}_1$ is the average reflectance of the phase-change coating and $\dot{q}_i$ is the incident heating rate. The amount of heat absorbed, therefore, is

$$(\dot{q}_{cal})_{abs} = (1 - \bar{\rho}_1)\ \dot{q}_i \tag{6-5}$$

Figure 6-18(b) shows the mechanism by which heat is transmitted to the sample. The incident heat first strikes the phase-change coating, where some is reflected, some absorbed, and the remainder transmitted to the sample. A portion of the transmitted heat is absorbed by the sample; the remainder is reflected back to the paint where, again, some is transmitted away, and some reflected back to the sample. The total reflected heat may be expressed as an infinite series:

$$(\dot{q}_{sam})_{refl} = \bar{\rho}_1\ \dot{q}_i + \bar{\rho}_3(\bar{\tau}_1)^2\dot{q}_i + \bar{\rho}_1(\bar{\rho}_3)^2(\bar{\tau}_1)^2\dot{q}_i + (\bar{\rho}_1)^2(\bar{\rho}_3)^3(\bar{\tau}_1)^2\dot{q}_i + \cdots \tag{6-6}$$

where subscripts 1 and 3 denote phase-change coating and sample, respectively. Dividing through by $\dot{q}_i$, Equation 6-6 becomes

$$\frac{(\dot{q}_{sam})_{refl}}{\dot{q}_i} = \bar{\rho}_1 + \bar{\rho}_3\ (\bar{\tau}_1)^2\ [1 + \bar{\rho}_1\ \bar{\rho}_3 + (\bar{\rho}_1\ \bar{\rho}_3)^2 + \cdots] \tag{6-7}$$

Equation 6-7 may be reduced as follows:

$$\frac{(\dot{q}_{sam})_{refl}}{\dot{q}_i} = \bar{\rho}_1 + \bar{\rho}_3(\bar{\tau}_1)^2\ \frac{(1 - \bar{\rho}_1\bar{\rho}_3)}{(1 - \bar{\rho}_1\bar{\rho}_3)}\ [1 + \bar{\rho}_1\bar{\rho}_3 + (\bar{\rho}_1\bar{\rho}_3)^2 + \cdots] \tag{6-8}$$

$$\frac{(\dot{q}_{sam})_{refl}}{\dot{q}_i} = \bar{\rho}_1 + \frac{\bar{\rho}_3(\bar{\tau}_1)^2}{1 - \bar{\rho}_1\bar{\rho}_3}\ [1 - (\bar{\rho}_1\bar{\rho}_3)^2 + \cdots] \tag{6-9}$$

Neglecting higher order terms, Equation 6-9 becomes

$$\frac{(\dot{q}_{sam})_{refl}}{\dot{q}_i} = \bar{\rho}_1 + \frac{\bar{\rho}_3(\bar{\tau}_1)^2}{1 - \bar{\rho}_1\bar{\rho}_3} \tag{6-10}$$

The amount of heat absorbed by the sample is

$$\frac{(\dot{q}_{sam})_{abs}}{\dot{q}_i} = 1 - \left[\bar{\rho}_1 + \frac{\bar{\rho}_3(\bar{\tau}_1)^2}{1 - \bar{\rho}_1\bar{\rho}_3}\right] \tag{6-11}$$

Using Equations 6-5 and 6-11, the difference in the amount of heat absorbed by the calorimeter and sample may be written as

$$\left[\frac{\dot{q}_{cal} - \dot{q}_{sam}}{\dot{q}_i}\right]_{abs} = \frac{\bar{\rho}_3(\bar{\tau}_1)^2}{1 - \bar{\rho}_1\bar{\rho}_3} \tag{6-12}$$

The data in Table 6-10 show that the maximum average transmittance of a 0.203 mm (0.008 in.) thick 318.15 K (114 F) tempilaq coating is about 0.200. Substituting this value along with its associated reflectance of 0.566 into Equation 6-12 yields an expression dependent solely on sample reflectance:

$$\left[\frac{\dot{q}_{cal} - \dot{q}_{sam}}{\dot{q}_i}\right]_{abs} = \frac{0.04\bar{\rho}_3}{1 - 0.566\,\bar{\rho}_3} \tag{6-13}$$

As long as sample reflectance is less than 0.40, the error in heat absorption between sample and calorimeter is less than 2.1 percent; if a material with a reflectance greater than 0.40 is tested, a high emissivity coating must be applied to the sample face before application of the phase-change coating.

6.3 APPARATUS CALIBRATION

Results of tests conducted to determine the variation of maximum absorbed heating rate as a function of voltage for tempilaq coated calorimeters are shown in Table 6-11 and Figure 6-19(a). Phase-change coatings in a variety of

temperatures and colors were used. Figure 6-19(a) shows that the absorbed heating rate is approximately half the incident value when phase-change coatings are applied. This permits material samples to be tested in the 1.703×10^4 W/m^2 [1.5 Btu (ft^2·s)] to 56.782×10^4 W/m^2 [50 Btu/(ft^2·s)] heating rate range. Figure 6-19(b) presents approximate filament temperature and current as a function of voltage.

Heating rate measurements obtained with tempilaq coated specimens in all ten base plate ports show that the non-dimensional heating distributions of paragraph 6.1.2 still apply, Table 6-12 and Figures 6-20 and 6-21.

6.4 THERMOPHYSICAL PROPERTIES MEASUREMENTS

A final series of TPM apparatus tests were performed to obtain thermophysical properties measurements on samples of a low conductivity plastic suitable for fabrication into tunnel models. Four phase-change coatings, 338.70 K (150 F), 366.48 K (200 F), 422.03 K (300 F), and 533.15 K (500 F), were tested at three different heating rates; the results are presented in Table 6-13.

The accuracy of the Table 6-13 measurements can be determined, and subsequently corrected, by estimating the errors incurred due to absorbed and incident heating rate differences between sample and calorimeter, their respective heat leakages, and by measurement of temperature at the calorimeter backface. These errors are defined by Equation 6-13; Table 6-9; Figures 5-2, 5-4, and 5-5; and Appendix B (Figure B-2). Table 6-14 lists the errors for the complete set of thermophysical properties measurements. Data corrections are derived as follows:

- Error in Absorbed Heating Rate - From Equation 6-13

$$\frac{(\dot{q}_{cal})_{abs} - (\dot{q}_{sam})_{abs}}{\dot{q}_i} = \frac{0.04\ \bar{\rho}_3}{1 - 0.566\ \bar{\rho}_3}$$

Assuming sample reflectance, $\bar{\rho}_3$, = 0.30, and $(\dot{q}_{cal})_{abs} = \dot{q}_i$, then,

$$(\dot{q}_{sam})_{abs} = \dot{q}_i\ (1 - 0.014) = 0.986\ \dot{q}_i \qquad (6\text{-}14)$$

- Percent Error in Incident Heating Rate - From Table 6-9

$$(\dot{q}_i)_e = \left[\frac{(\dot{q}_i)_{cal} - (\dot{q}_i)_{sam}}{(\dot{q}_i)_{lamps}} \right] 100 \qquad (6\text{-}15)$$

Assuming $(\dot{q}_i)_{cal} = (\dot{q}_i)_{lamps}$, then,

$$(\dot{q}_i)_{sam} = (\dot{q}_i)_{lamps} \left[1 - \frac{(\dot{q}_i)_e}{100} \right] \qquad (6\text{-}16)$$

- Accumulated Error in Absorbed Sample Heating Rate - Substituting Equation 6-16 into Equation 6-14 yields

$$(\dot{q}_{sam})_{abs} = (\dot{q}_i)_{lamps} \left[1 - \frac{(\dot{q}_i)_e}{100} \right] (0.986) \qquad (6\text{-}17)$$

- Sample Heat Leakage - From Figure 5-2 and Appendix A (Table A-2), and as defined by Equation A-6,

$$\left[\frac{Q_{leak}}{Q_{abs}} \right]_{sam} = \frac{L_{sam}}{0.25\ D_{sam}} \left[\frac{\dot{q}_{leak}}{(\dot{q}_{sam})_{abs}} \right] 100 \qquad (6\text{-}18)$$

where

L_{sam} is sample thickness (1.905 cm)
D_{sam} is sample diameter (3.810 cm)

Sample heat leakage as a percent of total absorbed heating rate is defined as

$$(\dot{q}_{sam})_{leak} = \frac{\dot{q}_{leak}}{(\dot{q}_{sam})_{abs}} \quad (100) \qquad (6\text{-}19)$$

Substituting Equation 6-18 into Equation 6-19 yields

$$(\dot{q}_{sam})_{leak} = \frac{0.25\ D_{sam}}{L_{sam}} \left[\frac{Q_{leak}}{Q_{abs}}\right]_{sam} = 0.5 \left[\frac{Q_{leak}}{Q_{abs}}\right]_{sam} \quad (6\text{-}20)$$

- Net Sample Absorbed Heating Rate

$$(\dot{q}_{sam})_{net} = (\dot{q}_{sam})_{abs} \left[1 - \frac{\dot{q}_{leak}}{(\dot{q}_{sam})_{abs}}\right] \quad (6\text{-}21)$$

Substituting Equations 6-17 and 6-19 into Equation 6-21 yields

$$(\dot{q}_{sam})_{net} = (\dot{q}_{i})_{lamps} \left[1 - \frac{(\dot{q}_{i})_{e}}{100}\right] (0.986) \left[1 - \frac{(\dot{q}_{sam})_{leak}}{100}\right] \quad (6\text{-}22)$$

where $(\dot{q}_{sam})_{leak}$ is defined by Equation 6-20.

- Calorimeter Heat Leakage - From Figures 5-4 and 5-5 and Appendix B (Table B-1),

$$\left[\frac{Q_{leak}}{Q_{abs}}\right]_{cal} = \frac{L_{cal}}{0.25\ D_{cal}} \left[\frac{\dot{q}_{leak}}{(\dot{q}_{cal})_{abs}}\right] 100 \quad (6\text{-}23)$$

where

L_{cal} is calorimeter thickness
D_{cal} is calorimeter diameter (3.810 cm)

Calorimeter heat leakage as a percent of total absorbed heating rate is defined as

$$(\dot{q}_{cal})_{leak} = \frac{\dot{q}_{leak}}{(\dot{q}_{cal})_{abs}} (100) \quad (6\text{-}24)$$

Substituting Equation 6-23 into Equation 6-24 yields

$$(\dot{q}_{cal})_{leak} = \frac{0.25\ D_{cal}}{L_{cal}} \left[\frac{Q_{leak}}{Q_{abs}}\right]_{cal} \tag{6-25}$$

For a calorimeter thickness of 0.203 cm (0.08 in.),

$$(\dot{q}_{cal})_{leak} = 4.6875 \left[\frac{Q_{leak}}{Q_{abs}}\right]_{cal} \tag{6-26}$$

For a calorimeter thickness of 0.635 cm (0.25 in.)

$$(\dot{q}_{cal})_{leak} = 1.5 \left[\frac{Q_{leak}}{Q_{abs}}\right]_{cal} \tag{6-27}$$

- Net Calorimeter Absorbed Heating Rate

$$(\dot{q}_{cal})_{net} = (\dot{q}_{cal})_{abs} \left[1 - \frac{\dot{q}_{leak}}{(\dot{q}_{cal})_{abs}}\right] \tag{6-28}$$

Assuming $(\dot{q}_{cal})_{abs} = (\dot{q}_i)_{lamps}$ and substituting Equation 6-24 into Equation 6-28 yields

$$(\dot{q}_{cal})_{net} = (\dot{q}_i)_{lamps} \left[1 - \frac{(\dot{q}_{cal})_{leak}}{100}\right] \tag{6-29}$$

where $(\dot{q}_{cal})_{leak}$ is defined by Equations 6-26 and 6-27.

- Calorimeter Measurement Error - From Appendix B (Figure B-2), calorimeter measurement error is expressed as a percent of net absorbed heating rate as follows:

$$(\dot{q}_{meas})_e = \left[1 - \frac{(\dot{q}_{cal})_{meas}}{(\dot{q}_{cal})_{net}}\right] (100) \tag{6-30}$$

Solving for $(\dot{q}_{cal})_{meas}$ yields

$$(\dot{q}_{cal})_{meas} = (\dot{q}_{cal})_{net} \left[1 - \frac{(\dot{q}_{meas})_e}{100}\right] \qquad (6\text{-}31)$$

Substituting Equation 6-29 into Equation 6-31 yields

$$(\dot{q}_{cal})_{meas} = (\dot{q}_i)_{lamps} \left[1 - \frac{(\dot{q}_{cal})_{leak}}{100}\right]\left[1 - \frac{(\dot{q}_{meas})_e}{100}\right] \qquad (6\text{-}32)$$

Equation 6-32 may be used to calculate the imposed heating rate, $(\dot{q}_l)_{lamps}$, with values of $(\dot{q}_{cal})_{meas}$, $(\dot{q}_{cal})_{leak}$, and $(\dot{q}_{meas})_e$, as defined in Table 6-14. Corrected values for calorimeter heating rate, $(\dot{q}_{cal})_{net}$, can subsequently be determined from Equation 6-29. Similarly, corrected values for sample heating rate $(\dot{q}_{sam})_{net}$, can be determined from Equation 6-22, with values of $(\dot{q}_i)_e$ and $(\dot{q}_{sam})_{leak}$ defined in Table 6-14. Corrected $\sqrt{\rho ck}$ values are obtained by re-reducing the thermophysical properties data using $(\dot{q}_{sam})_{net}$ in place of $(\dot{q}_{cal})_{meas}$.

The total percent error in $\sqrt{\rho ck}$ measurements may be expressed as

$$(\sqrt{\rho ck})_e = \left[\frac{\sqrt{\rho ck} - (\sqrt{\rho ck})_{cor}}{\sqrt{\rho ck}}\right] 100 \qquad (6\text{-}33)$$

Corrected sample and calorimeter heating rates, together with corrected $\sqrt{\rho ck}$ values and their respective measurement errors, are given in Table 6-14.

Figure 6-21(a) is a comparison of laboratory and corrected TPM apparatus measurements, as a function of temperature on samples of a low conductivity plastic suitable for wind tunnel model fabrication. Different sample sets cast from the same batch of material were used for each method of measurement. The variation of corrected TPM apparatus thermophysical properties measurements with the square root of time-to-phase-change and with corrected sample heating rate are presented in Figure 6-22(b) and (c), respectively.

Table 6-1. Preliminary Heating Distribution, Nominal Voltage = 50 V

Calorimeter Measurements with 0.025 mm (0.001 in.) Sperex Coating, $\dot{q}_{cal}$, 10^4 W/m^2 (Btu/[ft^2·s])

Y, cm (in.)	Sta A	Sta B		Sta C		Sta D
	(1)	(2)	(3)	(4)	(5)	(6)
-11.430 (-4.50)	2.591 (2.282)	2.562 (2.256)	2.568 (2.262)	2.584 (2.276)	2.405 (2.118)	2.421 (2.132)
-5.715 (-2.25)	2.861 (2.520)	2.794 (2.461)	2.791 (2.458)	2.794 (2.461)	2.577* (2.270)*	2.654 (2.337)
0.0 (0.0)	2.987 (2.631)	2.950 (2.598)	2.917 (2.569)	2.903 (2.557)	2.682 (2.362)	2.786 (2.454)
5.715 (2.25)	2.873* (2.530)*	2.849 (2.509)	2.793* (2.460)*	2.801 (2.467)	2.589* (2.280)*	2.778 (2.447)
11.430 (4.50)	2.641 (2.326)	2.660 (2.343)	2.594 (2.285)	2.614 (2.302)	2.431 (2.141)	2.542 (2.239)
Average $\dot{q}_{cal}$		2.7630 (2.4334)	2.7326 (2.4068)	2.7392 (2.4126)	2.5368 (2.2342)	
		$K_1 = \frac{2.7326 \times 10^4}{2.7630 \times 10^4} = 0.9890$		$K_2 = \frac{2.7392 \times 10^4}{2.5368 \times 10^4} = 1.0798$		

Corrected Heating Distribution, $\dot{q}_{cor}$, 10^4 W/m^2 (Btu/[ft^2·s])

Y, cm (in.)	Sta A	Sta B		Sta C		Sta D
	(1)	(2)	(3)	(4)	(5)	(6)
-11.430 (-4.50)	2.562 (2.257)	2.534 (2.231)	2.568 (2.262)	2.584 (2.276)	2.597 (2.287)	2.614 (2.302)
-5.715 (-2.25)	2.830 (2.492)	2.763 (2.434)	2.791 (2.458)	2.794 (2.461)	2.783* (2.451)*	2.866 (2.524)
0.0 (0.0)	2.954 (2.602)	2.918 (2.570)	2.917 (2.569)	2.903 (2.557)	2.896 (2.551)	3.008 (2.650)
5.715 (2.25)	2.841* (2.502)*	2.818 (2.482)	2.793* (2.460)*	2.801 (2.467)	2.796* (2.462)*	3.000 (2.642)
11.430 (4.50)	2.612 (2.301)	2.631 (2.317)	2.594 (2.285)	2.614 (2.302)	2.625 (2.312)	2.745 (2.418)

Fourth order curve fit to corrected data at stations B and C except for interpolated data (with asterisks):

$$\dot{q}_{cor} = (A0) + (A1)Y + (A2)Y^2 + (A3)Y^3 + (A4)Y^4$$

(A0) = 2.90848810 x 10^4 (2.56168175)
(A1) = 24.7042619 (0.00548470)
(A2) = 37.8449600 (-0.02148666)
(A3) = -0.03757720 (-0.00005139)
(A4) = 0.10505580 (0.00038385)
Standard Deviation = 0.016 (0.014)

Heating Rate at Center of Plate: $\dot{q}_{(0,0)}$ = 2.908 x 10^4 W/m^2 (2.562 Btu/[ft^2·s])

Normalized Heating Distribution, $\dot{q}_{cor}/\dot{q}_{(0,0)}$

Y, cm (in.)	Sta A	Sta B		Sta C		Sta D
	(1)	(2)	(3)	(4)	(5)	(6)
-11.430 (-4.50)	0.881	0.871	0.883	0.888	0.893	0.899
-5.715 (-2.25)	0.973	0.950	0.959	0.961	0.957*	0.985
0.0 (0.0)	1.015	1.003	1.003	0.998	0.996	1.034
5.715 (2.25)	0.977*	0.969	0.960*	0.963	0.961*	1.031
11.430 (4.50)	0.898	0.904	0.892	0.899	0.902	0.944

*Since valid readings could not be obtained these data were interpolated.

Table 6-2. Preliminary Heating Distribution, Nominal Voltage = 100 V

Calorimeter Measurements with 0.025 mm (0.001 in.) Sperex Coating, $\dot{q}_{cal}$, 10^4 W/m^2 (Btu/[ft^2·s])

Y, cm (in.)	Sta A (1)	Sta B (2)	Sta B (3)	Sta C (4)	Sta C (5)	Sta D (6)
-11.430 (-4.50)	8.266 (7.279)	7.990 (7.036)	8.102 (7.135)	8.225 (7.243)	8.407 (7.403)	8.460 (7.450)
-5.715 (-2.25)	9.077 (7.993)	8.877 (7.817)	8.866 (7.807)	8.901 (7.838)	9.147 (8.055)	9.347 (8.231)
0.0 (0.0)	9.505 (8.370)	9.202 (8.103)	9.246 (8.142)	9.342 (8.227)	9.505 (8.370)	9.600 (8.454)
5.715 (2.25)	9.153* (8.060)*	8.971 (7.900)*	8.892* (7.830)*	8.923 (7.858)	9.153 (8.060)*	9.417 (8.293)
11.430 (4.50)	8.369 (7.370)	8.429 (7.423)	8.158 (7.184)	8.265 (7.278)	8.369 (7.370)	8.574 (7.550)*
Average q_{cal}		8.6938 (7.6558)	8.6528 (7.6196)	8.7312 (7.6888)	8.9162 (7.8516)	
		$K_1 = \frac{8.6528 \times 10^4}{8.6938 \times 10^4} = 0.9953$		$K_2 = \frac{8.7312 \times 10^4}{8.9162 \times 10^4} = 0.9793$		

Corrected Heating Distribution, $\dot{q}_{cor}$, 10^4 W/m^2 (Btu/[ft^2·s])

Y, cm (in.)	Sta A (1)	Sta B (2)	Sta B (3)	Sta C (4)	Sta C (5)	Sta D (6)
-11.430 (-4.50)	8.227 (7.245)	7.952 (7.003)	8.102 (7.135)	8.225 (7.243)	8.233 (7.250)	8.285 (7.296)
-5.715 (-2.25)	9.034 (7.955)	8.835 (7.780)	8.866 (7.807)	8.901 (7.838)	8.958 (7.888)	9.154 (8.060)
0.0 (0.0)	9.460 (8.330)	9.159 (8.065)	9.246 (8.142)	9.342 (8.227)	9.308 (8.196)	9.401 (8.279)
5.715 (2.25)	9.110* (8.022)*	8.929* (7.863)*	8.892* (7.830)*	8.923 (7.858)	8.964* (7.893)*	9.222 (8.121)
11.430 (4.50)	8.330 (7.335)	8.389 (7.388)	8.158 (7.184)	8.265 (7.278)	8.196 (7.217)	8.397* (7.393)*

Fourth order curve fit to corrected data at stations B and C except for interpolated data (with asterisks):

$$\dot{q}_{cor} = (A0) + (A1)Y + (A2)Y^2 + (A3)Y^3 + (A4)Y^4$$

(A0) = 9.26370838×10^4 (8.15731812)
(A1) = 20.4420934 (0.00480609)
(A2) = -118.417439 (-0.06718361)
(A3) = 0.25873787 (0.00036067)
(A4) = 0.27733081 (0.00101289)
Standard Deviation = 0.083 (0.733)

Heating Rate at Center of Plate: $\dot{q}_{(0,0)} = 9.264 \times 10^4$ W/m^2 (8.157 Btu/[ft^2·s])

Normalized Heating Distribution, $\dot{q}_{cor}/\dot{q}_{(0,0)}$

Y, cm (in.)	Sta A (1)	Sta B (2)	Sta B (3)	Sta C (4)	Sta C (5)	Sta D (6)
-11.430 (-4.50)	0.888	0.859	0.875	0.888	0.889	0.894
-5.715 (-2.25)	0.975	0.954	0.957	0.961	0.967	0.988
0.0 (0.0)	1.021	0.989	0.998	1.009	1.005	1.015
5.715 (2.25)	0.983*	0.964*	0.960*	0.963	0.968*	0.996
11.430 (4.50)	0.899	0.906	0.881	0.892	0.885	0.906*

*Since valid readings could not be obtained these data were interpolated.

Table 6-3. Preliminary Heating Distribution, Nominal Voltage = 220 V

Calorimeter Measurements with 0.025 mm (0.001) Sperex Coating, $\dot{q}_{cal}$, 10^4 W /m^2 (Btu/[ft^2·s])

Y, cm (in.)	Sta A	Sta B		Sta C		Sta D
	(1)	(2)	(3)	(4)	(5)	(6)
-11.430 (-4.50)			31.525 (27.760)	32.433 (28.559)	32.109 (28.274)	32.550 (28.662)
-5.715 (-2.25)			35.300 (31.084)	35.345 (31.124)	35.300 (31.084)	35.816 (31.538)
0.0 (0.0)			36.821 (32.423)	37.114 (32.681)	36.939 (32.527)	37.135* (32.700)*
5.715 (2.25)			35.205 (31.000)*	35.553 (31.307)	35.318* (31.100)*	36.496 (32.137)
11.430 (4.50)			31.442 (27.687)	32.377 (28.510)	32.138* (28.300)*	32.730 (28.821)
Average $\dot{q}_{cal}$			34.0586 (29.9908)	34.5644 (30.4362)	34.3608 (30.2570)	
		K_1 =		$K_2 = \frac{34.5644 \times 10^4}{34.3608 \times 10^4} = 1.00592$		

Corrected Heating Distribution, $\dot{q}_{cor}$, 10^4 W /m^2 (Btu/[ft^2·s])

Y, cm (in.)	Sta A	Sta B		Sta C		Sta D
	(1)	(2)	(3)	(4)	(5)	(6)
-11.430 (-4.50)			31.525 (27.760)	32.433 (28.559)	32.299 (28.441)	32.743 (28.832)
-5.715 (-2.25)			35.300 (31.084)	35.345 (31.124)	35.509 (31.268)	36.028 (31.725)
0.0 (0.0)			36.821 (32.423)	37.114 (32.681)	37.158 (32.720)	37.355* (32.894)*
5.715 (2.25)			35.205 (31.000)*	35.553 (31.307)	35.527* (31.284)*	36.712 (32.327)
11.430 (4.50)			31.442 (27.687)	32.377 (28.510)	32.328* (28.468)*	32.924 (28.992)

Fourth order curve fit to corrected data at stations B and C except for interpolated data (with asterisks):

$$\dot{q}_{cor} = (A0) + (A1)Y + (A2)Y^2 + (A3)Y^3 + (A4)Y^4$$

(A0) = 37.0308654 x 10^4 (32.6073914)
(A1) = 222.124226 (0.04982978)
(A2) = -509.220557 (-0.28898382)
(A3) = -2.29005914 (-0.00331086)
(A4) = 0.94879315 (0.00346363)
Standard Deviation = 0.303 (0.267)

Heating Rate at Center of Plate: $\dot{q}_{(0,0)}$ = 37.031 x 10^4 W/m^2 (32.607 Btu/[ft^2·s])

Normalized Heating Distribution, $\dot{q}_{cor}/\dot{q}_{(0,0)}$

Y, cm (in.)	Sta A	Sta B		Sta C		Sta D
	(1)	(2)	(3)	(4)	(5)	(6)
-11.430 (-4.50)			0.851	0.876	0.872	0.884
-5.715 (-2.25)			0.953	0.955	0.959	0.973
0.0 (0.0)			0.994	1.002	1.003	1.009*
5.715 (2.25)			0.951*	0.960	0.959*	0.991
11.430 (4.50)			0.849	0.874	0.873*	0.889

*Since valid readings could not be obtained these data were interpolated.

Table 6-4. Preliminary Heating Distribution, Nominal Voltage = 460 V

Calorimeter Measurements With 0.025 mm (0.001 in.) Sperex Coating, $\dot{q}_{cal}$, 10^4 W/m^2 (Btu/[ft^2·s])

Y, cm (in.)	Sta A	Sta B		Sta C		Sta D
	(1)	(2)	(3)	(4)	(5)	(6)
-11.430 (-4.50)	96.530* (85.000)*	96.828 (85.263)	101.697 (89.550)	101.294 (89.195)	99.946 (88.008)	100.589 (88.574)
-5.715 (-2.25)	109.773 (96.661)	109.443 (96.371)	112.236 (98.830)	113.201 (99.680)	111.180 (97.900)	111.861*(98.500)*
0.0 (0.0)	118.109 (104.002)	114.736 (101.032)	118.698 (104.520)	118.249 (104.125)	118.581 (104.417)	118.951 (104.743)
5.715 (2.25)	111.747* (98.400)*	111.136 (97.862)	113.565*(100.000)*	113.962 (100.350)	113.565* (100.000)*	115.375 (101.594)
11.430 (4.50)	100.524 (88.517)	100.309 (88.328)	102.511 (90.267)	103.017 (90.712)	101.926 (89.752)	103.606 (91.231)
	Average $\dot{q}_{cal}$	106.4904 (93.7712)	109.7414 (96.6334)	109.9446 (96.8124)	109.03961 (96.0154)	
		$K_1 = \frac{109.7414 \times 10^4}{106.4904 \times 10^4} = 1.03052$		$K_2 = \frac{109.9446 \times 10^4}{109.0396 \times 10^4} = 1.0083$		

Corrected Heating Distribution, $\dot{q}_{cor}$, 10^4 W/m^2 (Btu/[ft^2·s])

Y, cm (in.)	Sta A	Sta B		Sta C		Sta D
	(1)	(2)	(3)	(4)	(5)	(6)
-11.430 (-4.50)	99.476* (87.594)*	99.783 (87.866)	101.697 (89.550)	101.294 (89.195)	100.776 (88.739)	101.424 (89.309)
-5.715 (-2.25)	113.123 (99.611)	112.783 (99.313)	112.236 (98.830)	113.201 (99.680)	112.103 (98.713)	112.789* (99.318)*
0.0 (0.0)	121.714 (107.176)	118.238 (104.116)	118.698 (104.520)	118.249 (104.125)	119.565 (105.284)	119.938 (105.612)
5.715 (2.25)	115.158* (101.403)*	114.528 (100.849)	113.565*(100.000)*	113.962 (100.350)	114.508*(100.830)*	116.333 (102.437)
11.430 (4.50)	103.592 (91.219)	103.370 (91.024)	102.511 (90.267)	103.017 (90.712)	102.772 (90.497)	104.466 (91.988)

Fourth order curve fit to corrected data at stations B and C except for interpolated data (with asterisks):

$$\dot{q}_{cor} = (A0) + (A1)Y + (A2)Y^2 + (A3)Y^3 + (A4)Y^4$$

(A0) = 118.684082 x 10^4 (104.507324)
(A1) = 1646.22068 (0.36812830)
(A2) = -1723.54817 (-0.97873401)
(A3) = -5.8034854 (-0.00837127)
(A4) = 3.36016761 (0.01229667)
Standard Deviation = 0.517 (0.456)

Heating Rate at Center of Plate: $\dot{q}_{(0,0)}$ = 118.684 x 10^4 W/m^2 (104.507 Btu/[ft^2·s])

Normalized Heating Distribution, $\dot{q}_{cor}/\dot{q}_{(0,0)}$

Y, cm (in.)	Sta A	Sta B		Sta C		Sta D
	(1)	(2)	(3)	(4)	(5)	(6)
-11.430 (-4.50)	0.838*	0.841	0.857	0.853	0.849	0.854
-5.715 (-2.25)	0.953	0.950	0.946	0.954	0.945	0.950*
0.0 (0.0)	1.026	0.996	1.000	0.996	1.007	1.011
5.715 (2.25)	0.971*	0.965	0.957*	0.960	0.965*	0.980
11.430 (4.50)	0.873	0.871	0.864	0.868	0.866	0.880

*Since valid readings could not be obtained these data were interpolated

Table 6-5. Final Central Heating Distribution, Nominal Voltage = 50 V

Calorimeter Measurements with 0.025 mm (0.001 in.) Sperex Coating, $\dot{q}_{cal}$, 10^4 W/m^2 (Btu/[ft^2·s])					
Y, cm (in.)		Sta B		Sta C	
		(1)		(2)	
-11.430	(-4.50)	2.896	(2.550)	2.868	(2.525)
-5.715	(-2.25)	3.166	(2.788)	3.124	(2.751)
0.0	(0.0)	3.176	(2.797)	3.208	(2.825)
5.715	(2.25)	3.150	(2.774)	3.132	(2.758)
11.430	(4.50)	2.899	(2.553)	2.896	(2.550)

Fourth order curve fit to data at stations B and C:

$$\dot{q}_{cal} = (A0) + (A1)Y + (A2)Y^2 + (A3)Y^3 + (A4)Y^4$$

(A0) =	3.19195366 x 10^4	(2.81097794)
(A1) =	-6.93924259	(-0.00155720)
(A2) =	-12.27768140	(-0.00700062)
(A3) =	0.10503383	(0.00015372)
(A4) =	-0.08309158	(-0.00030417)
Standard Deviation =	0.015	(0.013)

Heating Rate at Center of Plate: $\dot{q}_{(0,0)}$ = 3.192 x 10^4 W/m^2 (2.811 Btu/[ft^2·s])

Normalized Central Heating Distribution, $\dot{q}_{cal}/\dot{q}_{(0,0)}$			
Y, cm (in.)		Sta B	Sta C
		(1)	(2)
-11.430	(-4.50,	0.907	0.898
-5.715	(-2.25)	0.992	0.979
0.0	(0.0)	0.995	1.005
5.715	(2.25)	0.987	0.981
11.430	(4.50)	0.908	0.907

Table 6-6. Final Central Heating Distribution, Nominal Voltage = 100 V

Calorimeter Measurements with 0.025 mm (0.001 in.) Sperex Coating, $\dot{q}_{cal}$, 10^4 W/m^2 (Btu/[ft^2·s])

Y, cm (in.)		Sta B (1)		Sta C (2)	
-11.430	(-4.50)	8.442	(7.434)	8.461	(7.450)
-5.715	(-2.25)	9.239	(8.135)	9.177	(8.081)
0.0	(0.0)	9.628	(8.478)	9.475	(8.343)
5.715	(2.25)	9.261	(8.155)	9.273	(8.166)
11.430	(4.50)	8.416	(7.411)	8.369	(7.369)

Fourth order curve fit to data at stations B and C:

$$\dot{q}_{cal} = (A0) + (A1)Y + (A2)Y^2 + (A3)Y^3 + (A4)Y^4$$

(A0) = 9.55122375 x 10^4 (8.41030121)
(A1) = 112.411380 (0.01748697)
(A2) = -105.377436 (-0.05632966)
(A3) = -1.05800689 (-0.00114891)
(A4) = 0.14493838 (0.00035680)
Standard Deviation = 0.048 (0.036)

Heating Rate at Center of Plate: $\dot{q}_{(0,0)}$ = 9.551 x 10^4 W/m^2 (8.410 Btu/[ft^2·s])

Normalized Central Heating Distribution, $\dot{q}_{cal}/\dot{q}_{(0,0)}$

Y, cm (in.)		Sta B (1)	Sta C (2)
-11.430	(-4.50)	0.884	0.886
-5.715	(-2.25)	0.967	0.961
0.0	(0.0)	1.008	0.992
5.715	(2.25)	0.970	0.971
11.430	(4.50)	0.881	0.876

Table 6-7. Final Central Heating Distribution, Nominal Voltage = 220 V

Calorimeter Measurements with 0.025 mm (0.001 in.) Sperex Coating, $\dot{q}_{cal}$, 10^4 W/m^2 (Btu/[ft^2·s])

Y, cm (in.)		Sta B (1)		Sta C (2)	
-11.430	(-4.50)	33.842	(29.800)	34.060	(29.992)
-5.715	(-2.25)	36.808	(32.411)	37.288	(32.834)
0.0	(0.0)	38.767	(34.136)	38.474	(33.878)
5.715	(2.25)	36.829	(32.430)	37.455	(32.981)
11.430	(4.50)	33.017	(29.073)	33.364	(29.379)

Fourth order curve fit to data at stations B and C:

$$\dot{q}_{cal} = (A0) + (A1)Y + (A2)Y^2 + (A3)Y^3 + (A4)Y^4$$

(A0)	= 38.6200867 x 10^4	(34.0068970)
(A1)	= 220.623612	(0.04943123)
(A2)	= -493.824184	(-0.28049922)
(A3)	= -4.23524063	(-0.00611742)
(A4)	= 0.82138052	(0.00300955)
Standard Deviation	= 0.221	(0.194)

Heating Rate at Center of Plate: $\dot{q}_{(0,0)}$ = 38.620 x 10^4 W/m^2 (34.007 Btu/[ft^2·S])

Normalized Central Heating Distribution, $\dot{q}_{cal}/\dot{q}_{(0,0)}$

Y, cm (in.)		Sta B (1)	Sta C (2)
-11.430	(-4.50)	0.876	0.882
-5.715	(-2.25)	0.953	0.966
0.0	(0.0)	1.004	0.996
5.715	(2.25)	0.954	0.970
11.430	(4.50)	0.855	0.864

Table 6-8. Final Central Heating Distribution, Nominal Voltage = 460 V

Calorimeter Measurements with 0.025 mm (0.001 in.) Sperex Coating, $\dot{q}_{cal}$, 10^4 W/m^2 (Btu/[ft^2·s])

Y, cm (in.)	Sta B (1)	Sta C (2)
-11.430 (-4.50)	109.287 (96.233)	108.933 (95.921)
-5.715 (-2.25)	119.977 (105.646)	121.187 (106.712)
0.0 (0.0)	127.051 (111.875)	126.444 (111.341)
5.715 (2.25)	120.396 (106.015)	120.438 (106.052)
11.430 (4.50)	106.953 (94.178)	108.786 (95.792)

Fourth order curve fit to data at stations B and C:

$$\dot{q}_{cal} = (A0) + (A1)Y + (A2)Y^2 + (A3)Y^3 + (A4)Y^4$$

(A0) = 126.744995 x 10^4	(111.604675)
(A1) = -11.8901767	(-0.00272573)
(A2) = -2083.67229	(-1.18319035)
(A3) = -4.06254781	(-0.00585640)
(A4) = 5.25328796	(0.01922951)
Standard Deviation = 0.544	(0.479)

Heating Rate at Center of Plate: $\dot{q}_{(0,0)}$ = 126.744 x 10^4 W/m^2 (111.605 Btu/[ft^2·s])

Normalized Central Heating Distribution, $\dot{q}_{cal}/\dot{q}_{(0,0)}$

Y, cm (in.)	Sta B (1)	Sta C (2)
-11.430 (-4.50)	0.862	0.859
-5.715 (-2.25)	0.947	0.956
0.0 (0.0)	1.002	0.998
5.715 (2.25)	0.950	0.950
11.430 (4.50)	0.844	0.858

Table 6-9. Percent Difference in Adjacent Colorimeter Measurements*

V_{nom}, Volts	Y, cm (in.)	$100\frac{(\dot{q}_B - \dot{q}_C)}{\dot{q}_B}$, Percent
50	-11.430 (-4.50)	0.12
	-5.715 (-2.25)	0.98
	0.0 (0.0)	1.33
	5.715 (2.25)	-1.00
	11.430 (4.50)	-0.51
100	-11.430 (-4.50)	-0.22
	-5.715 (-2.25)	0.66
	0.0 (0.0)	1.59
	5.715 (2.25)	-0.13
	11.430 (4.50)	0.57
220	-11.430 (-4.50)	-0.64
	-5.715 (-2.25)	-1.31
	0.0 (0.0)	0.76
	5.715 (2.25)	-1.70
	11.430 (4.50)	-1.05
460	-11.430 (-4.50)	0.32
	-5.715 (-2.25)	-1.01
	0.0 (0.0)	0.48
	5.715 (2.25)	-0.03
	11.430 (4.50)	-1.71

*From Tables 6-5 through 6-8.

Table 6-10. Average Transmittance, Reflectance, and Absorptance of Phase-Change Coatings

T_{pc}, K (F)	Paint Color	Coating Thickness, mm (in.)	Transmittance, $\bar{\tau}$		Reflectance, $\bar{\rho}$		Absorptance, $\bar{\alpha}$	
			$T_{filament}$ = 810.92 K (1000 F)	$T_{filament}$ = 3255.37 K (5400 K)	$T_{filament}$ = 810.92 K (1000 F)	$T_{filament}$ = 3255.37 K (5200 K)	$T_{filament}$ = 810.92 K (1000 K)	$T_{filament}$ = 3255.37 K (5400 K)
318.15 (113)	Lt Orange	0.203 (0.008)	0.031	0.200	0.137	0.566	0.832	0.234
		0.381 (0.015)	0.002	0.131	0.144	0.635	0.854	0.234
533.15 (500)	Dk Blue	0.152 (0.006)	0.039	0.163	0.151	0.531	0.810	0.306
		0.431 (0.017)	0.008	0.043	0.137	0.540	0.855	0.417

Table 6-11. Calorimeter Measurements with Phase Change Coatings*

T_{pc} K (F)	Color	Run Number	V_{nom}, volts	$\dot{q}_{cal}$, 10^4 W/m^2 (Btu/[ft^2·s])
338.70 (150)	Lt Green	28	50	1.884 (1.659)
		29	75	3.100 (2.730)
		7	80	3.929 (3.460)
		30	100	6.946 (6.117)
366.48 (200)	Dk Violet	16	100	6.528 (5.749)
		17	115	7.834 (6.899)
366.48 (200)	Lt Violet	26	50	2.237 (1.970)
		25	75	3.296 (2.903)
		24	100	5.220 (4.597)
366.48 (200)	Off White	1	50	1.764 (1.554)
422.03 (300)	Pink	2	50	1.694 (1.492)
		22	75	4.074 (3.588)
		11	80	3.713 (3.270)
		9	100	4.876 (4.294)
		21	100	6.322 (5.567)
		10	115	6.301 (5.549)
		12	145	9.628 (8.478)
		23	160	10.793 (9.504)
		13	170	12.003 (10.570)
533.15 (500)	White	31	50	1.976 (1.740)
		32	50	1.779 (1.567)
		3	100	5.082 (4.475)
		4	100	5.294 (4.662)
		20	100	5.619 (4.948)
		19	130	8.851 (7.794)
		18	160	12.503 (11.010)
		34	220	16.858 (14.845)
		5	220	17.561 (15.464)
		6	460	57.602 (50.722)
		33	460	61.115 (53.815)
		35	460	59.007 (51.959)

*Calorimeter located at Sta B: X = 2.857 cm (-1.125 in.), Y = 0.0.

Table 6-12. Central Heating Distribution Measurements With Phase-Change Coated Calorimeters

Run Number	V_{nom}, Volts	Calorimeter Number	Location, Sta B, Y, cm (in.)	T_{pc}, K (F)	Paint Color	$\dot{q}_{cal}$, 10^4 W/m^2 (Btu/[ft^2·S])	$\frac{\dot{q}_{cal}}{\dot{q}_{cal}\ (Y=0)}$
1	50	6	-11.430 (-4.50)	366.48 (200)	Off White	1.541 (1.357)	0.873
		7	-5.715 (-2.25)			1.688 (1.487)	0.957
		8	0.0 (0.0)			1.764 (1.554)	1.000
		9	5.715 (2.25)			1.750 (1.541)	0.992
		10	11.430 (4.50)			1.543 (1.359)	0.875
2	50	6	-11.430 (-4.50)	422.03 (300)	Pink	- -	-
		7	-5.715 (-2.25)			1.618 (1.425)	0.955
		8	0.0 (0.0)			1.694 (1.492)	1.000
		9	5.715 (2.25)			1.679 (1.479)	0.991
		10	11.430 (4.50)			- -	-
3	100	6	-11.430 (-4.50)	533.15 (500)	White	4.413 (3.886)	0.869
		7	-5.715 (-2.25)			4.854 (4.275)	0.955
		8	0.0 (0.0)			5.082 (4.475)	1.000
		9	5.715 (2.25)			4.899 (4.314)	0.964
		10	11.430 (4.50)			4.348 (3.829)	0.856
4	100	6	-11.430 (-4.50)	533.15 (500)	White	- -	-
		7	-5.715 (-2.25)			5.136 (4.523)	0.970
		8	0.0 (0.0)			5.294 (4.662)	1.000
		9	5.715 (2.25)			- -	-
		10	11.430 (4.50)			4.558 (4.014)	0.861
5	220	1	-11.430 (-4.50)	533.15 (500)	White	15.500 (13.649)	0.883
		2	-5.715 (-2.25)			- -	-
		3	0.0 (0.0)			17.561 (15.464)	1.000
		4	5.715 (2.25)			- -	-
		5	11.430 (4.50)			14.834 (13.063)	0.845
6	460	1	-11.450 (-4.50)	533.15 (500)	White	49.354 (43.459)	0.857
		2	-5.715 (-2.25)			- -	-
		3	0.0 (0.0)			57.602 (50.722)	1.000
		4	5.715 (2.25)			- -	-
		5	11.430 (4.50)			48.035 (42.298)	0.834

Table 6-13. Material Thermophysical Properties Measurements (TPM Apparatus Tests on Material G Sample)

T_{pc}, K (F)	T_i K (F)	Run Number	$(\dot{q}_{cal})_{meas}$, 10^4 W/m^2 (Btu/[ft^2.s])		t, Seconds	$\sqrt{\rho ck}$, 10^3 J/[m^2.s$^{\frac{1}{2}}$.K] (Btu/[ft^2. s$^{\frac{1}{2}}$.F])	
338.70 (150)	294.26 (70)	28	1.884	(1.659)	4.75	1.042	(0.05099)
		29	3.100	(2.730)	1.40	0.931	(0.04556)
		30	6.946	(6.117)	0.30	0.965	(0.04725)
366.48 (200)	294.26 (70)	26	2.237	(1.970)	9.15	1.057	(0.05172)
		25	3.296	(2.903)	3.60	0.977	(0.04780)
		24	5.220	(4.597)	1.50	0.999	(0.04886)
422.03 (300)	294.26 (70)	22	4.074	(3.588)	8.80	1.067	(0.05221)
		21	6.322	(5.567)	4.10	1.130	(0.05530)
		23	10.793	(9.504)	0.95	0.928	(0.04544)
533.15 (500)	294.26 (70)	20	5.619	(4.948)	20.55	1.203	(0.05886)
		19	8.851	(7.794)	7.30	1.129	(0.05525)
		18	12.503	(11.010)	4.10	1.196	(0.05850)

NOTE: $\sqrt{\rho ck} = \dfrac{(q_{cal})_{meas}}{T_{pc} - T_i} \dfrac{2}{\sqrt{\pi}} \sqrt{t}$

Table 6-14. Corrected Thermophysical Properties Data

Run No.	$(\dot{q}_{cal})_{meas}$, 10^4 W/m^2 (Btu/[ft^2·s])	Error In Absorbed Heating Rate, percent	$(\dot{q}_i)_e$, percent	$(\dot{q}_{sam})_{leak}$, percent	$(\dot{q}_{cal})_{leak}$, percent	$(\dot{q}_{meas})_e$, percent
28	1.884 (1.659)	1.4	1.33	0.025	2.11	0.75
29	3.100 (2.730)		1.46	0.010	0.70	2.50
30	6.946 (6.117)		1.59	0.005	0.23	6.00
26	2.237 (1.970)	1.4	1.33	0.060	3.98	0.50
25	3.296 (2.903)		1.46	0.050	1.64	1.00
24	5.220 (4.597)		1.59	0.015	0.70	2.50
22	4.074 (3.588)	1.4	1.46	0.065	1.35	0.50
21	6.322 (5.567)		1.59	0.050	0.60	2.00
23	10.793 (9.504)		1.18	0.010	0.47	7.00
20	5.619 (4.948)	1.4	1.59	0.150	3.00	0.10
19	8.851 (7.794)		1.39	0.050	0.90	1.00
18	12.503 (11.010)		1.18	0.050	0.45	2.00

	$(\dot{q}_{cal})_{net}$, 10^4 W/m^2 (Btu/[ft^2·s])	$(\dot{q}_{sam})_{net}$, 10^4 W/m^2 (Btu/[ft^2·s])	$(\sqrt{\rho ck})_{cor}$, 10^3 J/[m^2·s$^{1/2}$·K] (Btu/[ft^2·s$^{1/2}$·F])	Total Error In $\sqrt{\rho ck}$, percent
28	1.898 (1.671)	1.886 (1.661)	1.043 (0.05106)	-0.1
29	3.179 (2.800)	3.110 (2.739)	0.934 (0.04571)	-1.3
30	7.390 (6.507)	7.187 (6.328)	0.999 (0.04888)	-3.5
26	2.248 (1.979)	2.276 (2.004)	1.075 (0.05261)	-1.7
25	3.330 (2.932)	3.287 (2.895)	0.974 (0.04767)	0.3
24	5.354 (4.714)	5.231 (4.606)	1.001 (0.04896)	-0.2
22	4.095 (3.606)	4.030 (3.549)	1.055 (0.05165)	1.1
21	6.451 (5.680)	6.294 (5.542)	1.125 (0.05505)	0.4
23	11.605 (10.219)	11.360 (10.003)	0.977 (0.04783)	-5.2
20	5.624 (4.952)	5.618 (4.947)	1.202 (0.05884)	-0.1
19	8.940 (7.872)	8.767 (7.720)	1.119 (0.05473)	0.9
18	12.758 (11.234)	12.481 (10.990)	1.193 (0.05839)	0.2

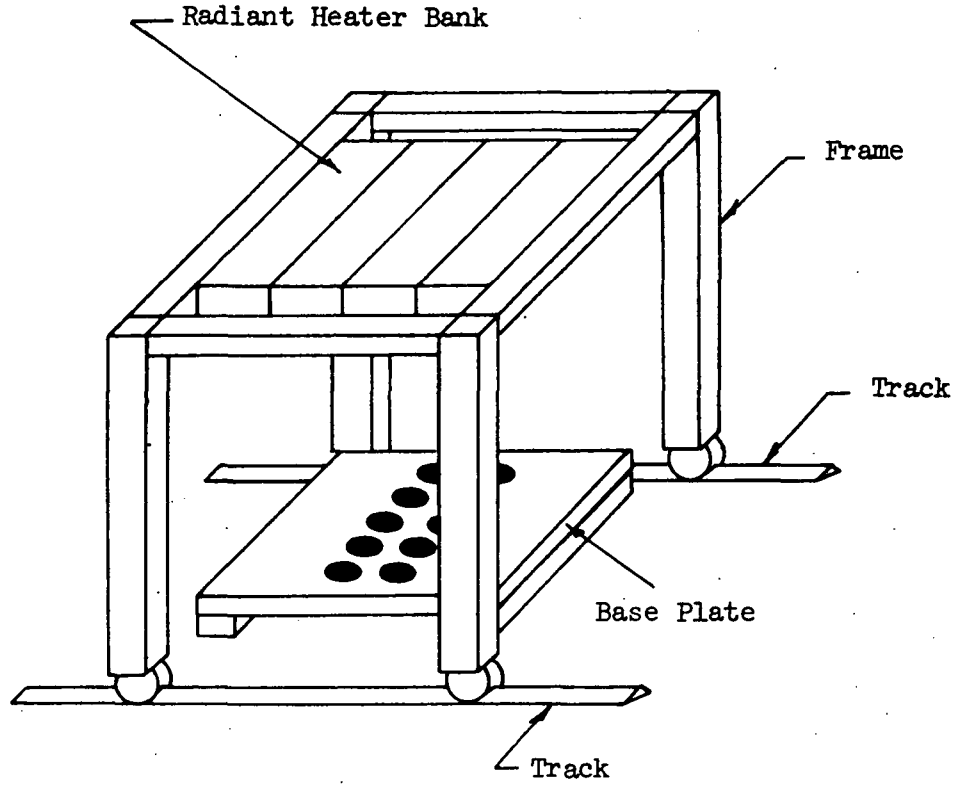

Figure 6-1 Test Setup - Preliminary Heating Distribution

Dimensions in Centimeters

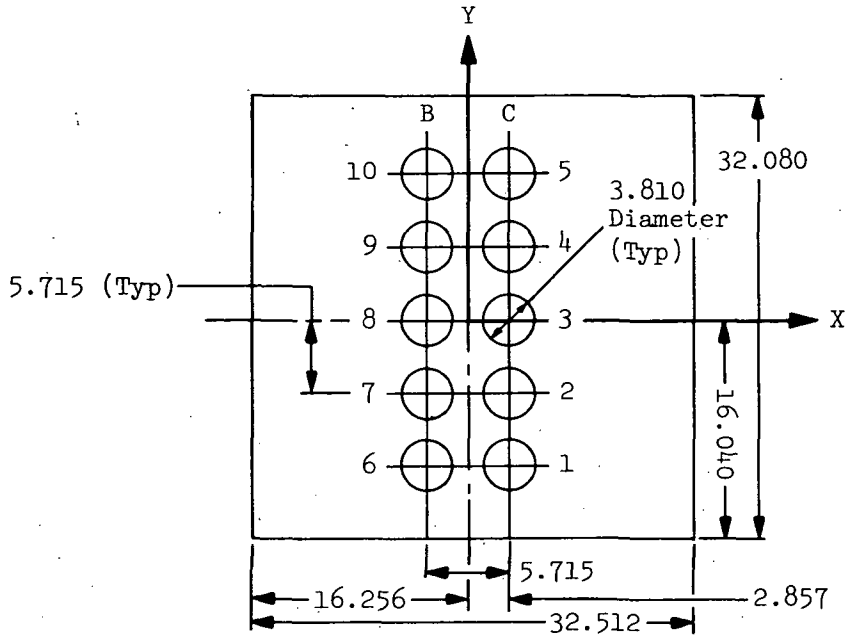

a. Lamps on Center

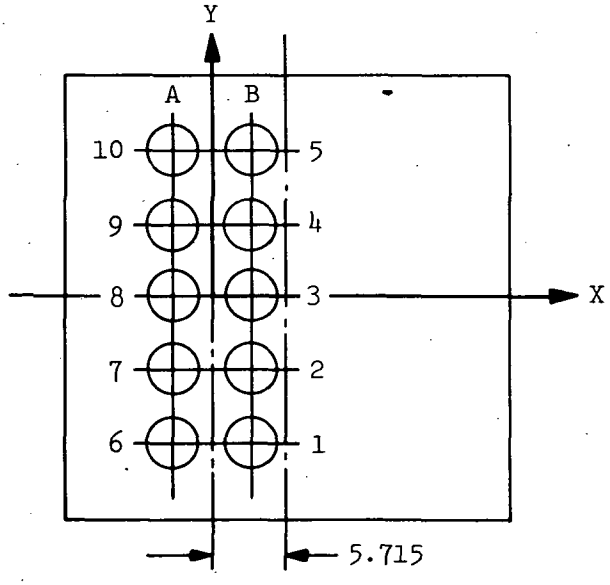

b. Lamps Left of Center

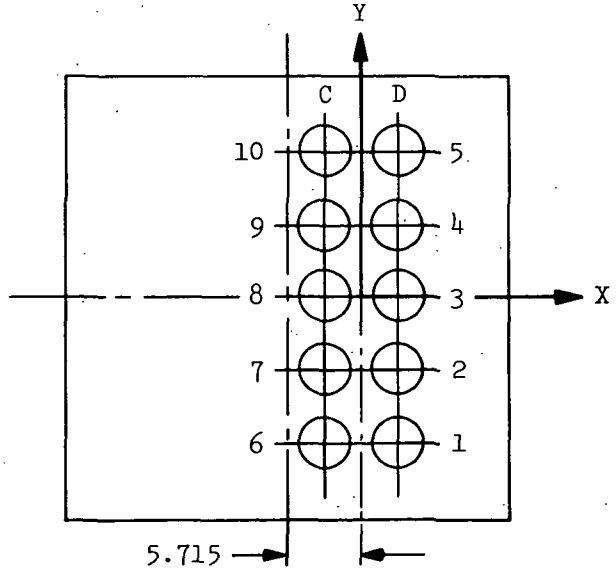

c. Lamps Right of Center

Figure 6-2 Radiant Heater Bank Position With Respect to Test Specimens - Preliminary Heating Distribution

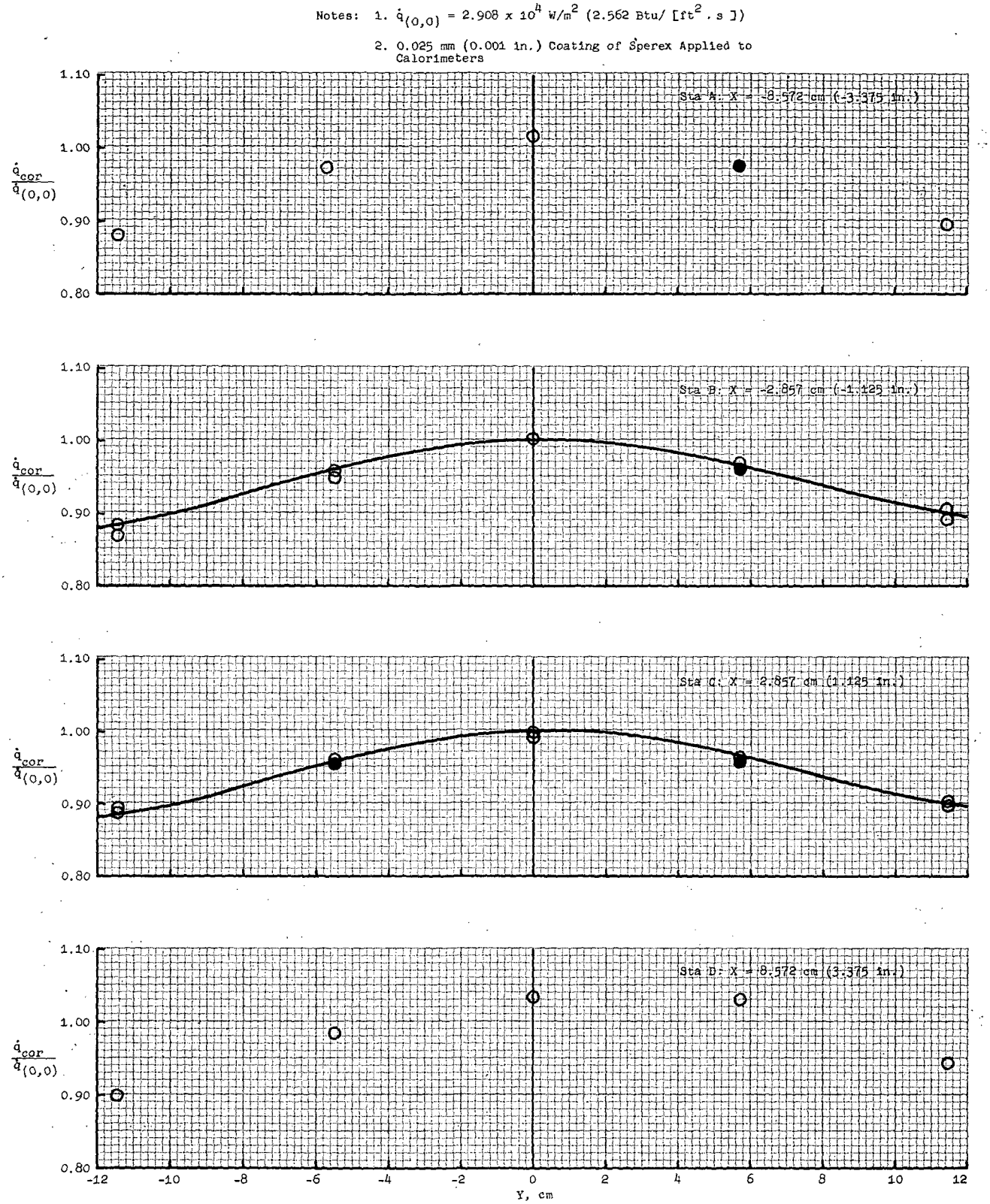

Figure 6-3 Preliminary Heating Distribution, Nominal Voltage = 50V

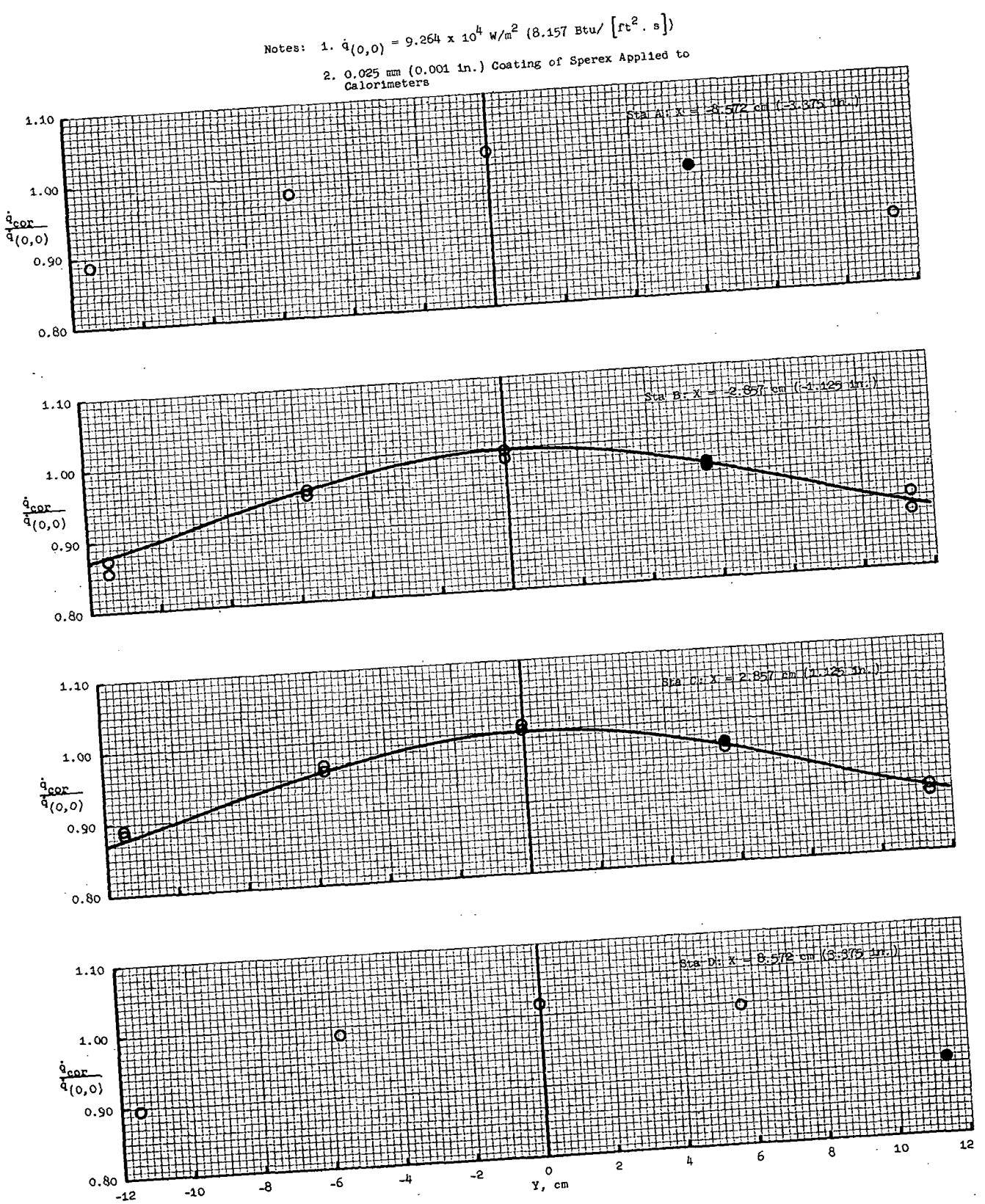

Figure 6-4 Preliminary Heating Distribution, Nominal Voltage = 100V

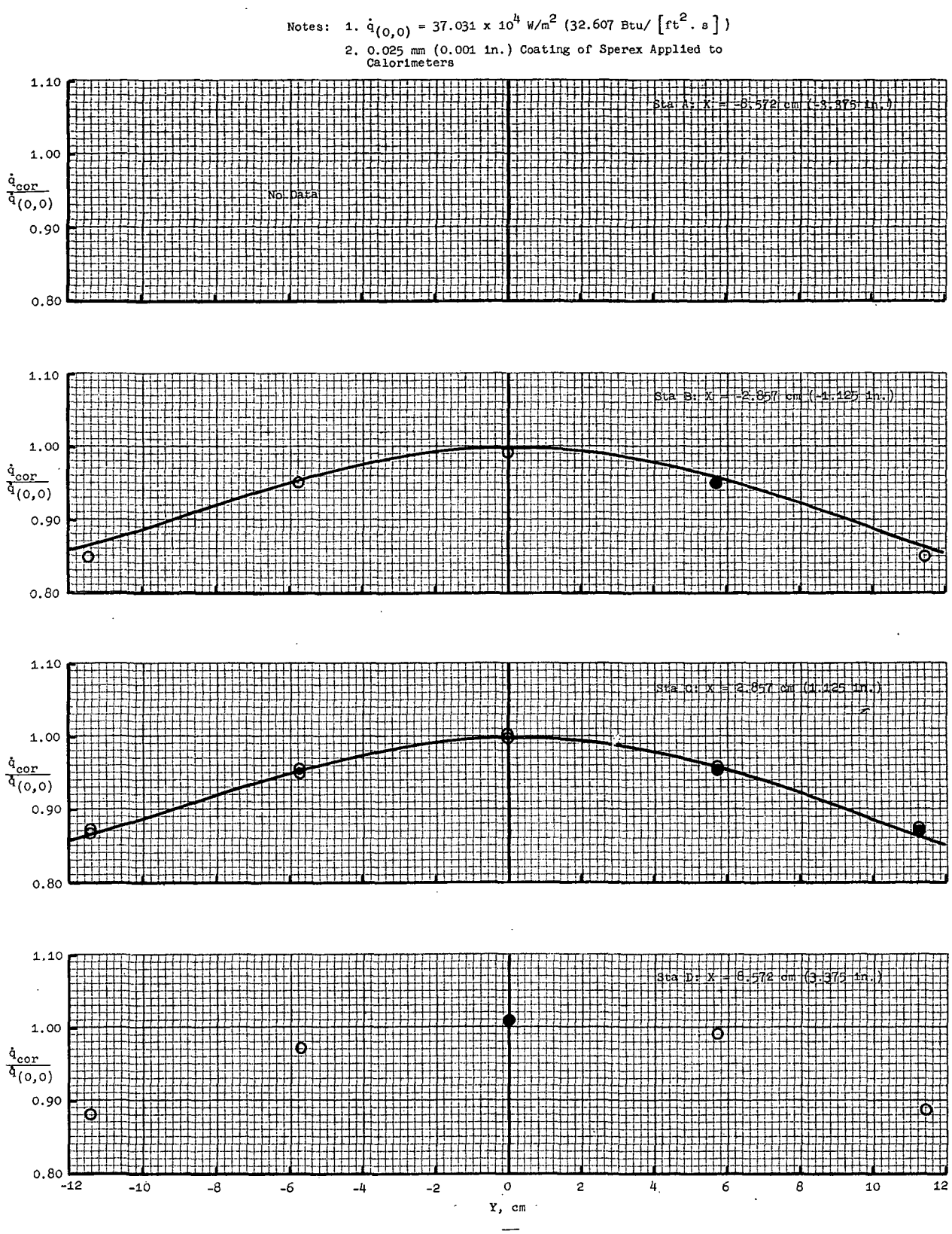

Figure 6-5 Preliminary Heating Distribution, Nominal Voltage = 220V

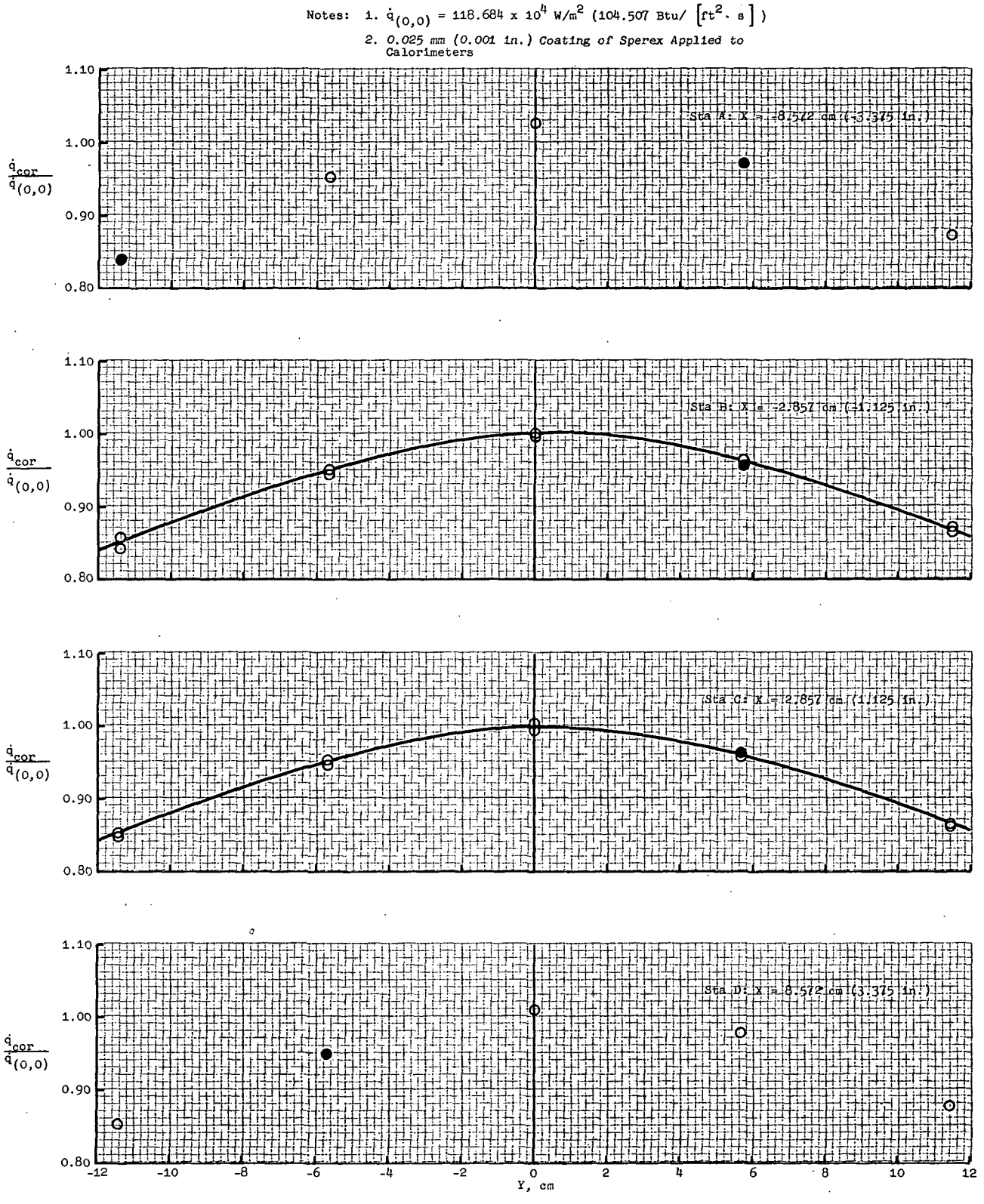

Figure 6-6 Preliminary Heating Distribution, Nominal Voltage = 460V

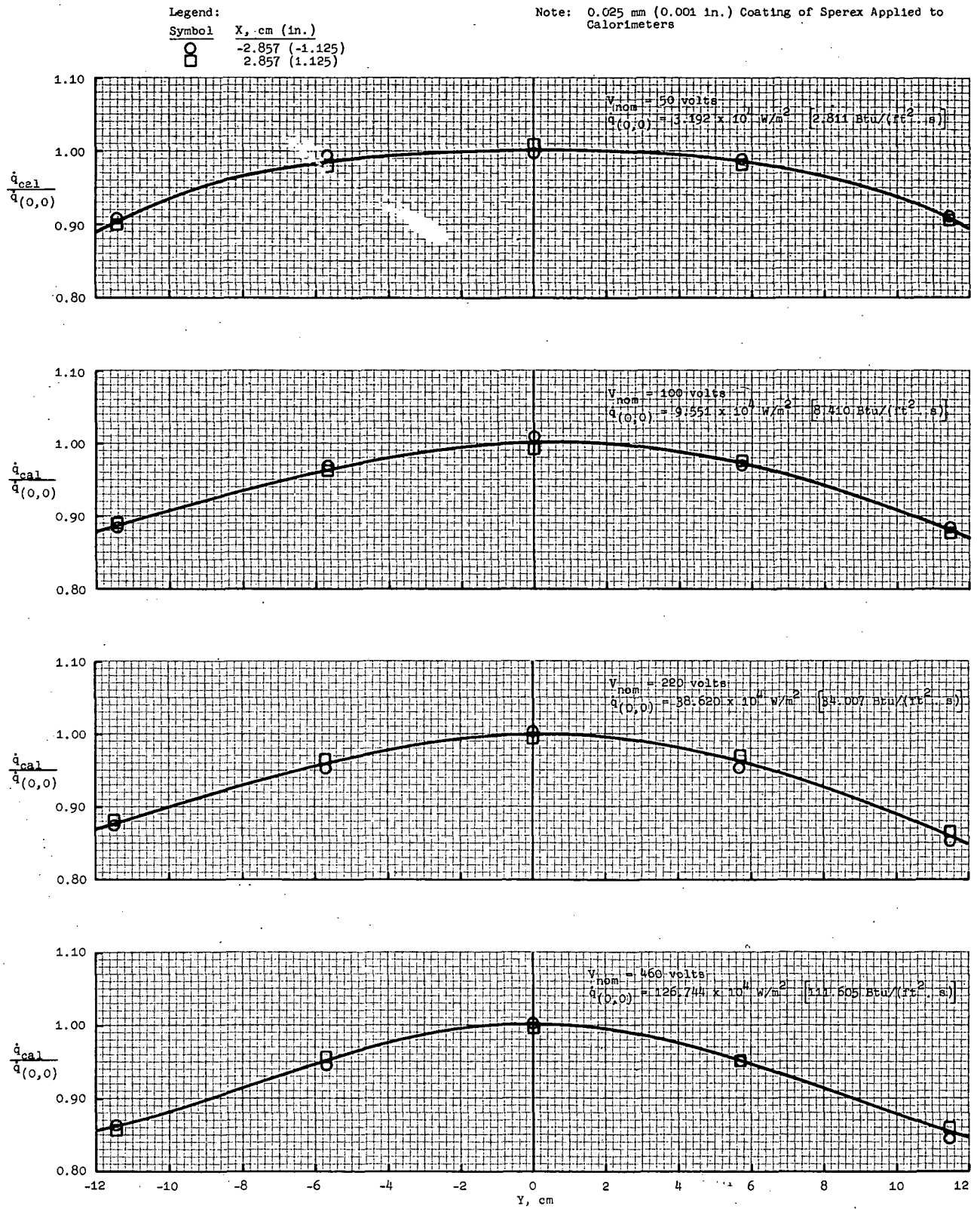

Figure 6-7 Final Central Heating Distribution

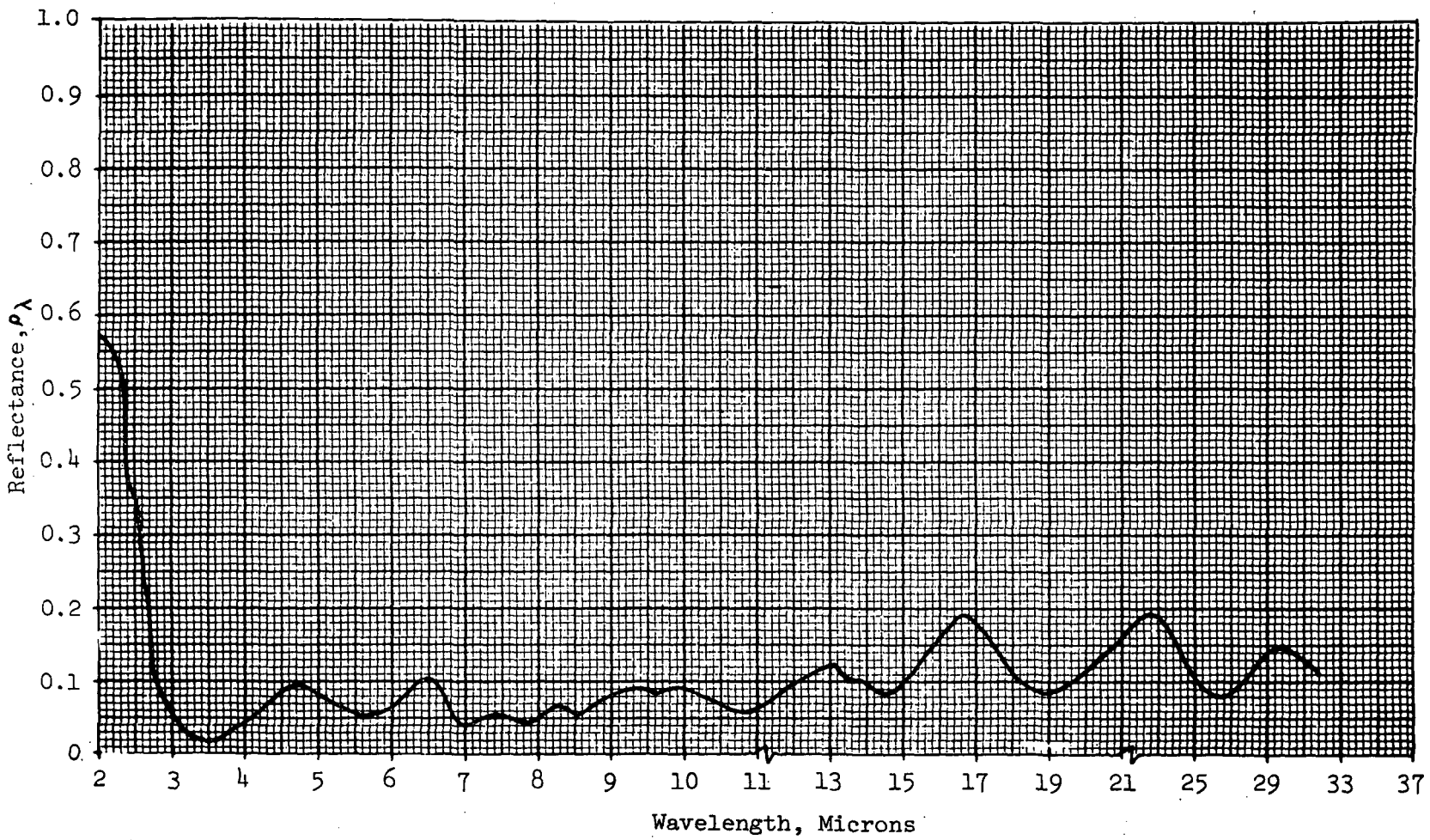

Figure 6-8 Spectral Reflectance of 422.03 K (300 F) Phase-Change Coating on Aluminum Substrate

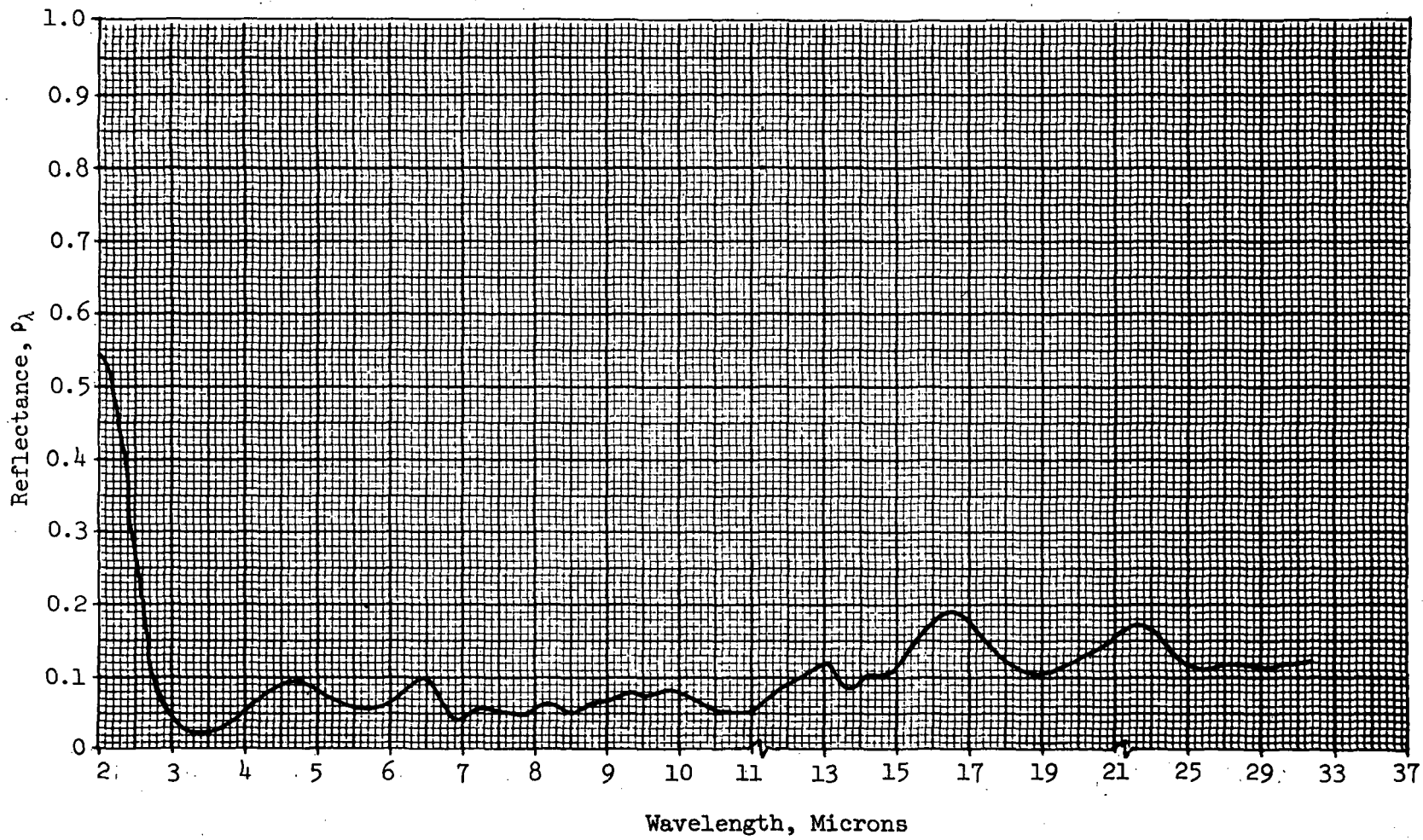

Figure 6-9 Spectral Reflectance of 422.03 K (300 F) Phase-Change Coating on Black Paint Substrate

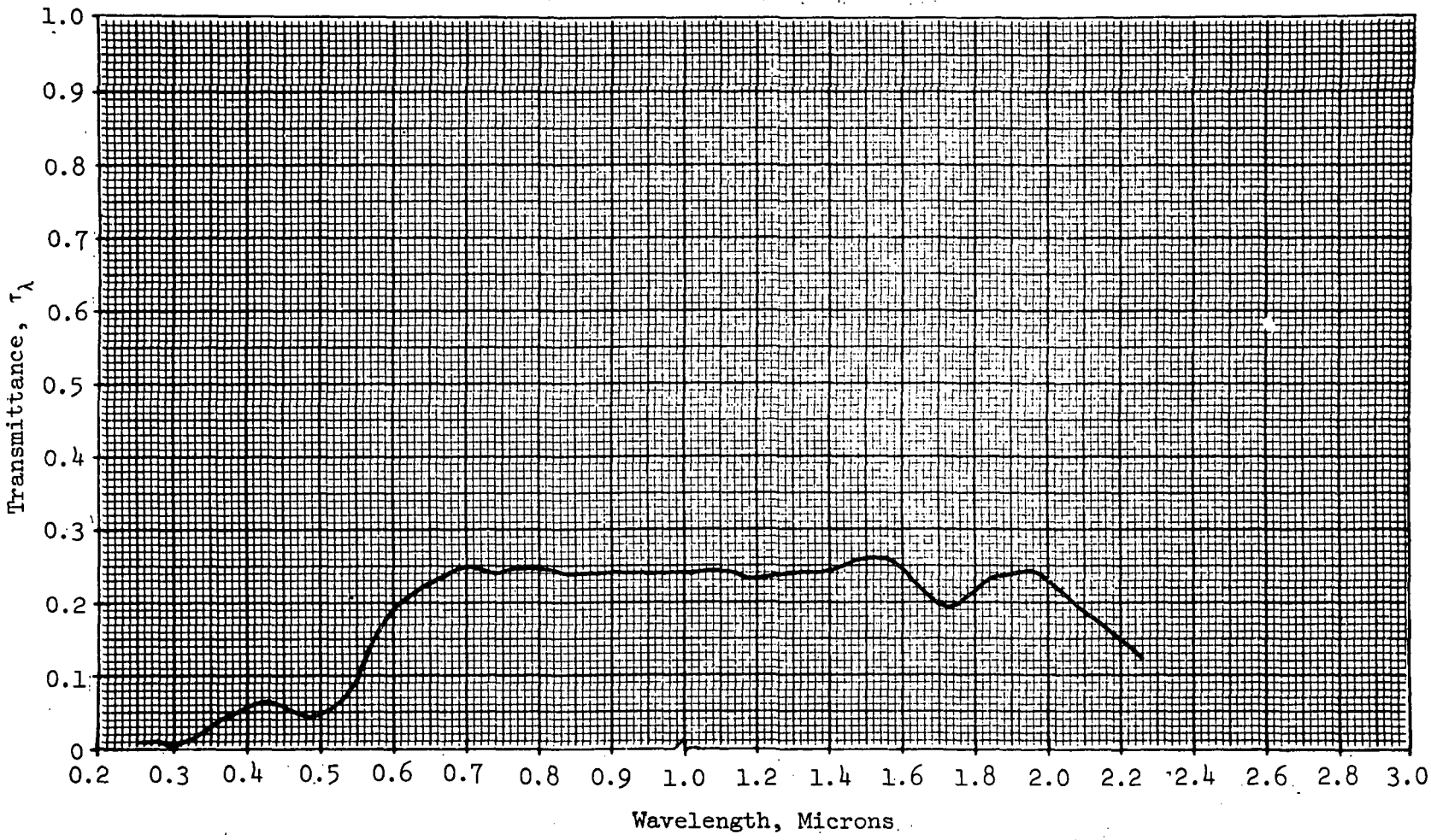

Figure 6-10 Spectral Transmittance of 318.15 K (113 F) Phase-Change Coating, 0.203 mm (0.008 in.) Thick

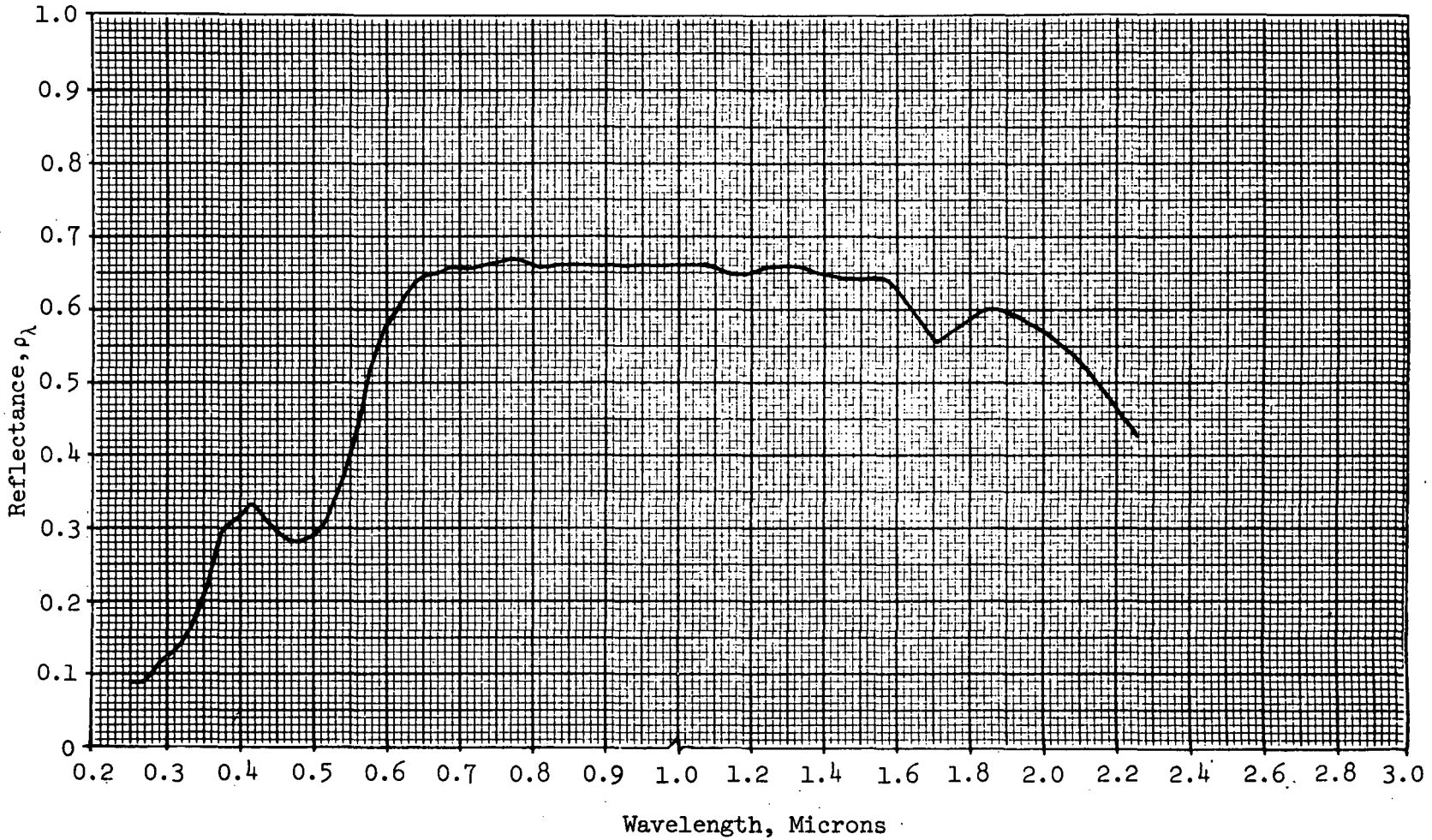

Figure 6-11 Spectral Reflectance of 318.15 K (113 F) Phase-Change Coating, 0.203 mm (0.008 in.) Thick

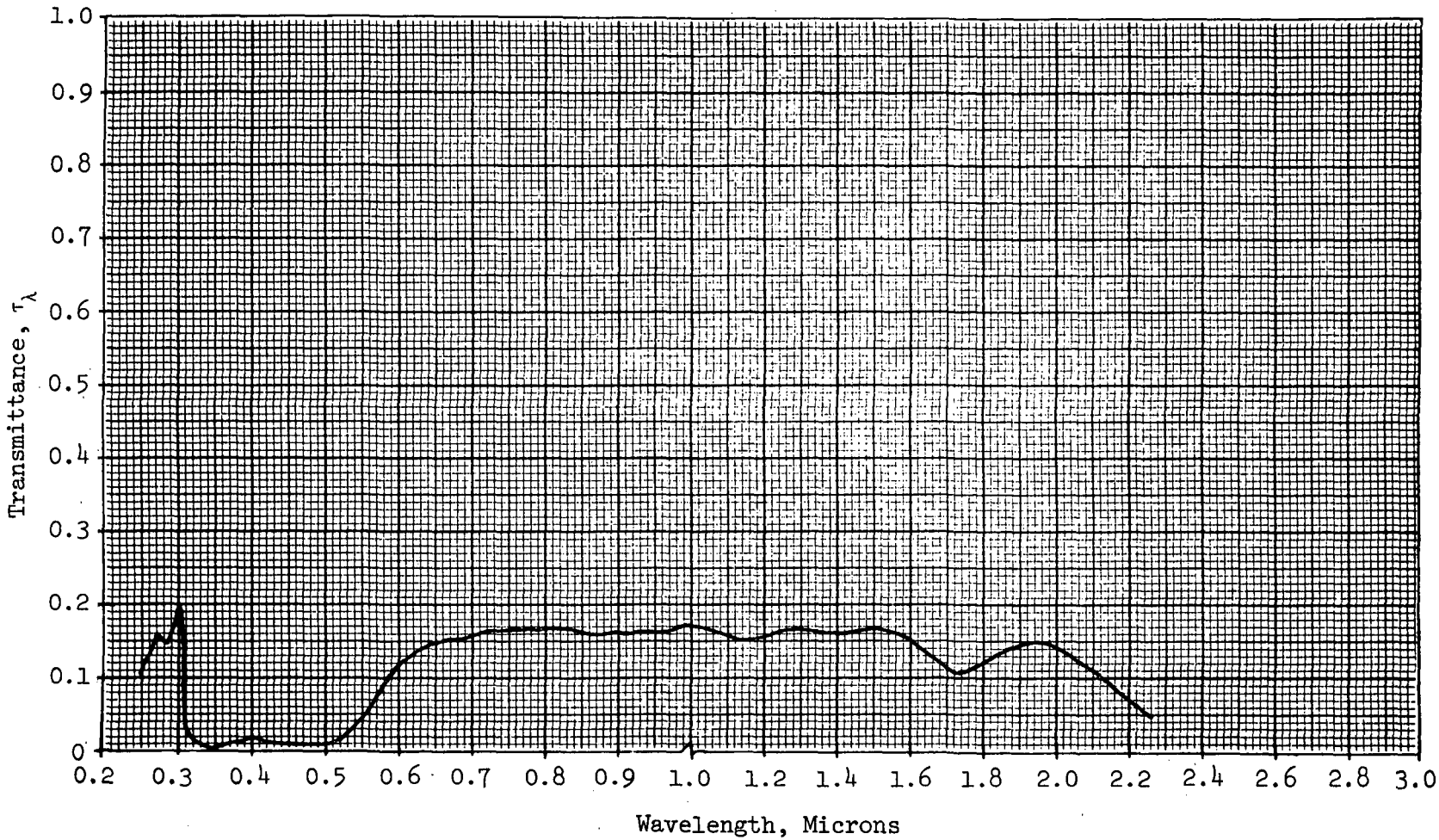

Figure 6-12 Spectral Transmittance of 318.15 K (113 F) Phase-Change Coating, 0.381 mm (0.015 in.) Thick

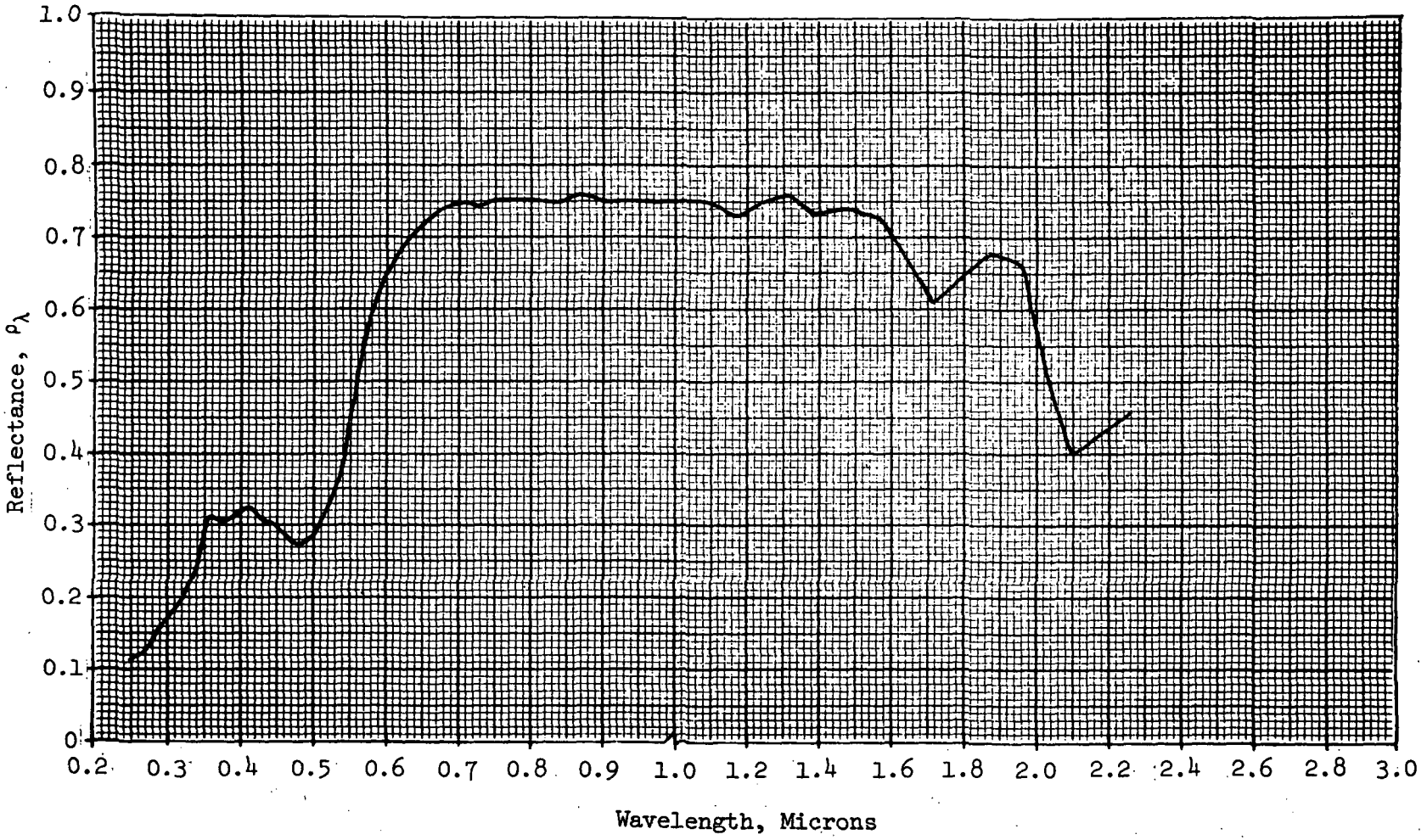

Figure 6-13 Spectral Reflectance of 318.15 K (113 F) Phase-Change Coating, 0.381mm (0.015 in.) Thick

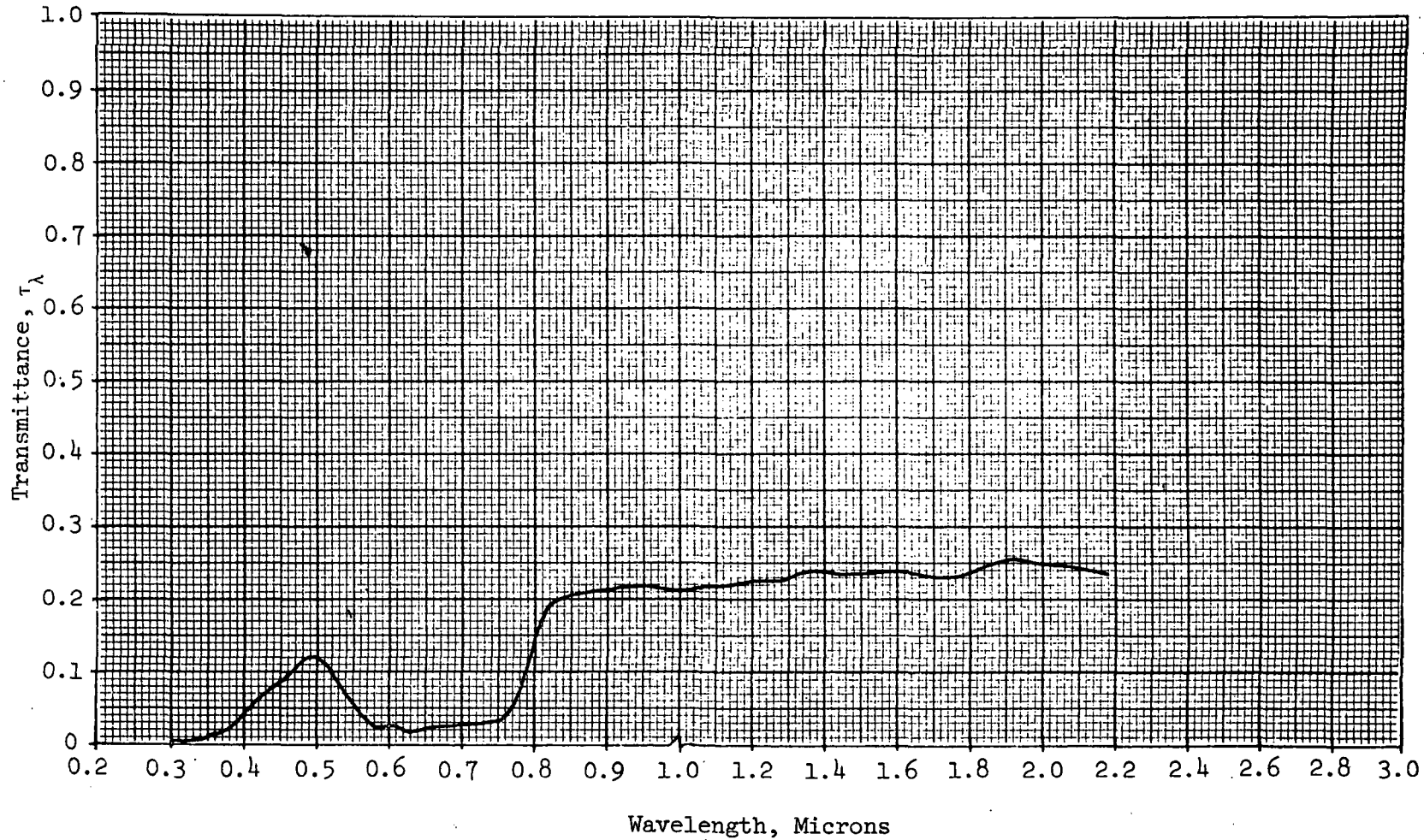

Figure 6-14 Spectral Transmittance of 533.15 K (500 F) Phase-Change Coating, 0.152mm (0.006 in.) Thick

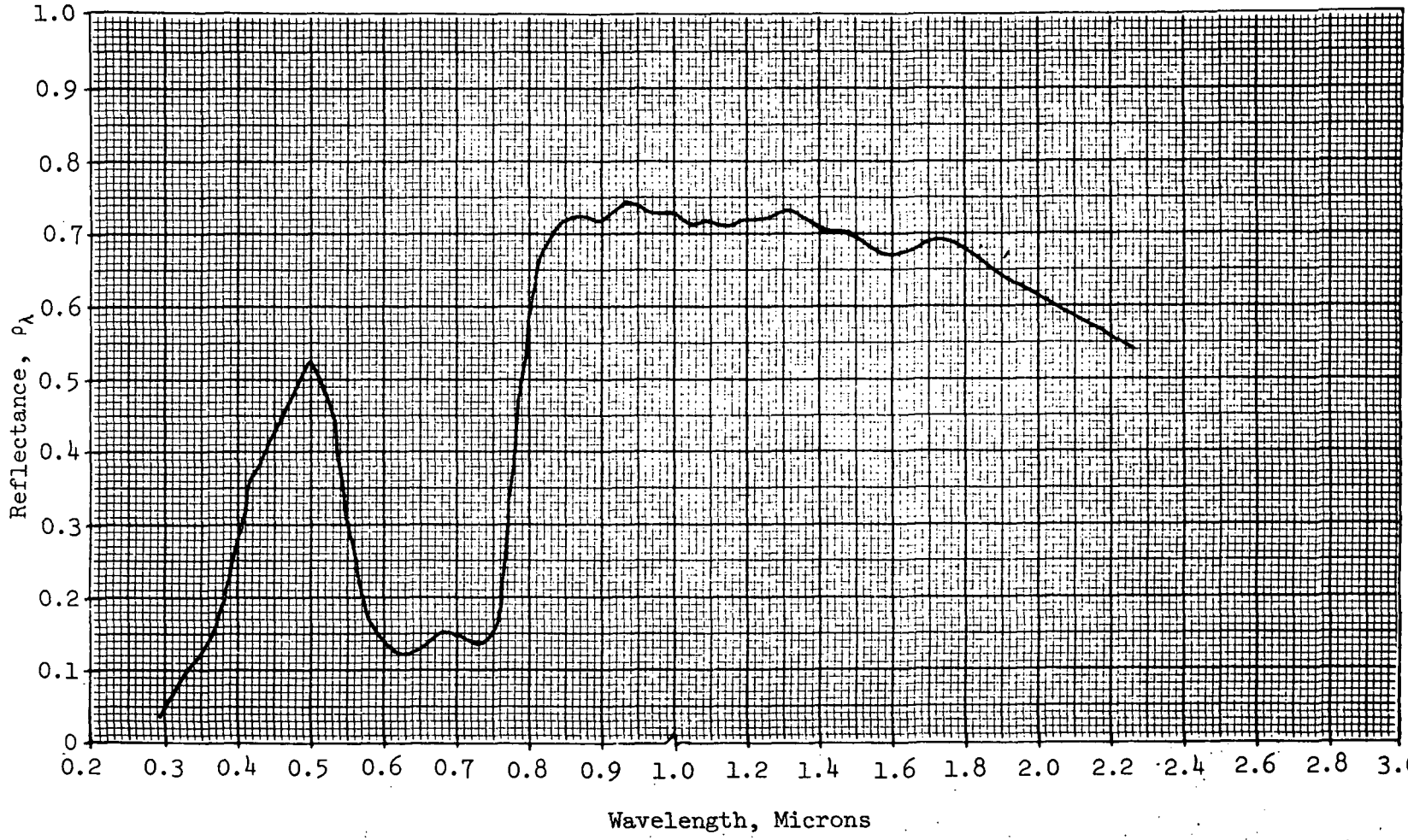

Figure 6-15 Spectral Reflectance of 533.15 K (500 F) Phase-Change Coating, 0.152 mm (0.006 in.) Thick

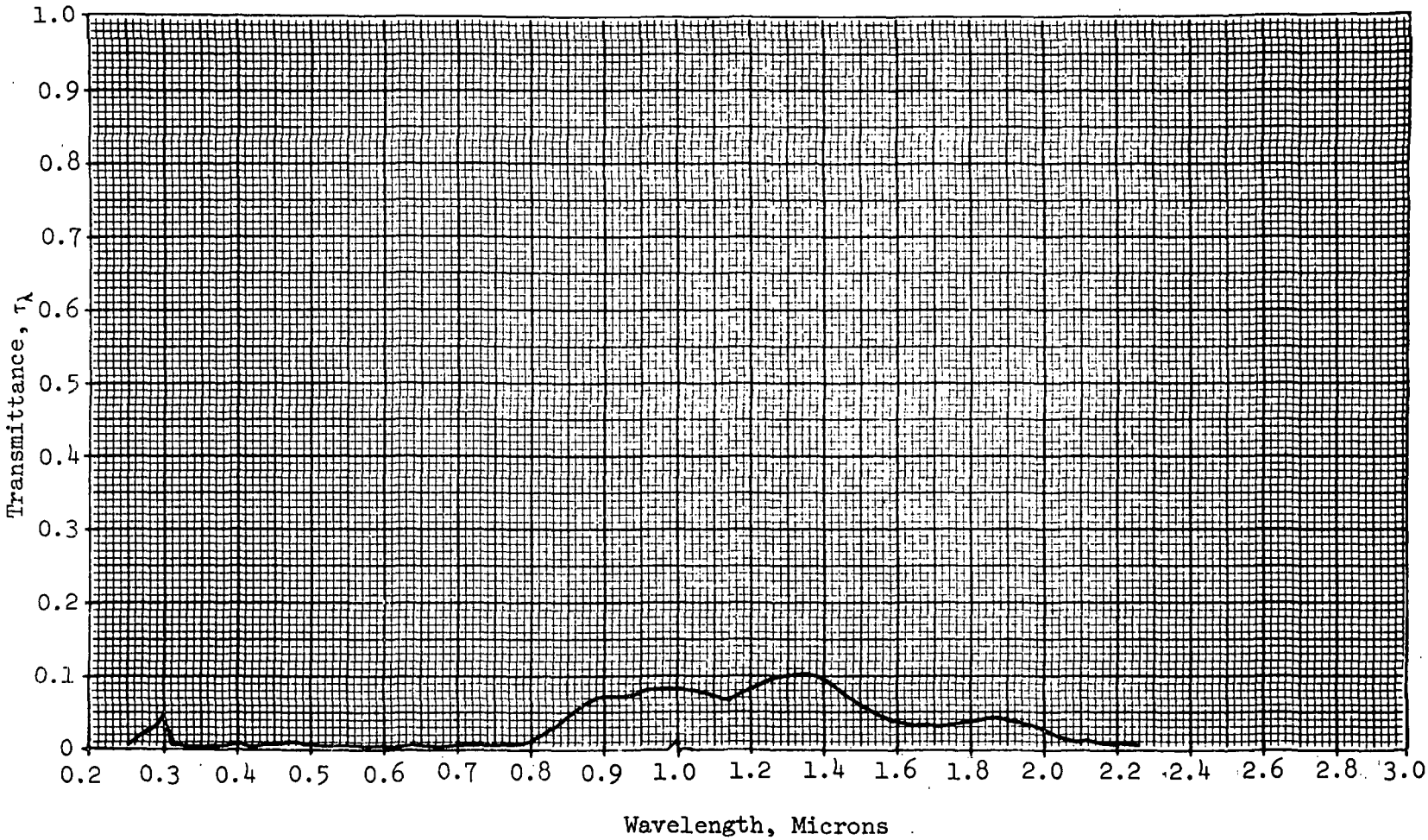

Figure 6-16 Spectral Transmittance of 533.15 K (500 F) Phase-Change Coating, 0.431 mm (0.017 in.) Thick

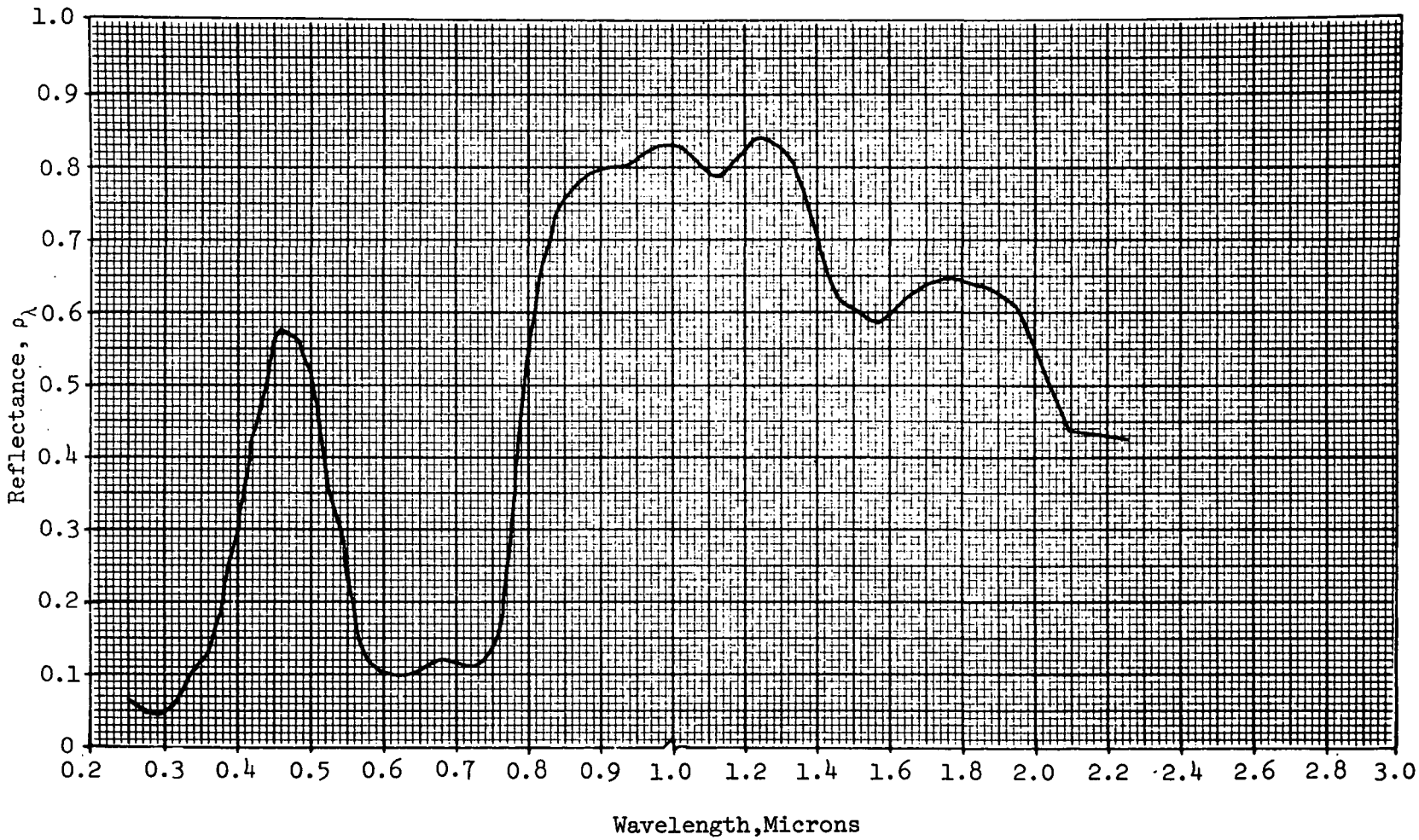

Figure 6-17 Spectral Reflectance of 533.15 K (500 F) Phase-Change Coating, 0.431 mm (0.017 in.) Thick

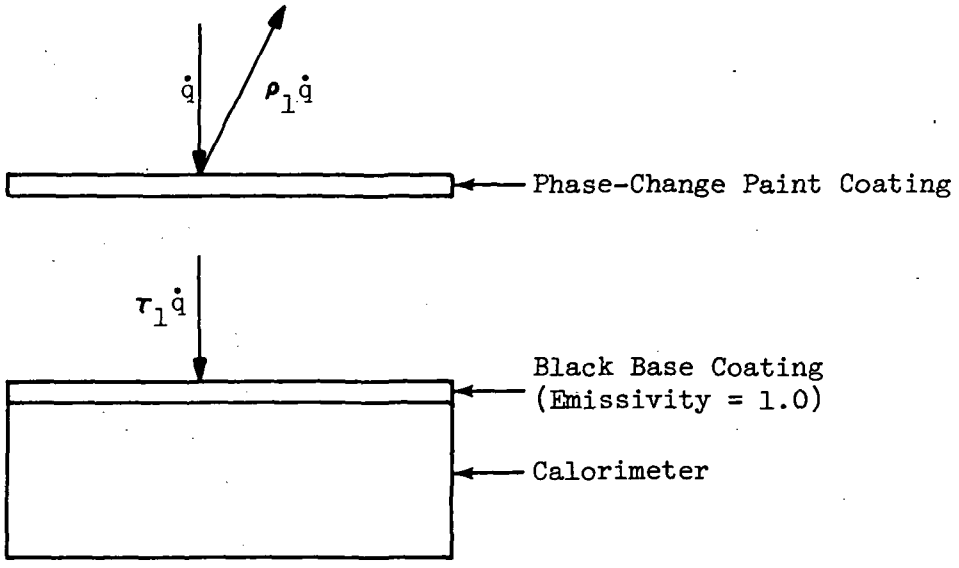

a. Incident Heat Absorbed by Black Paint

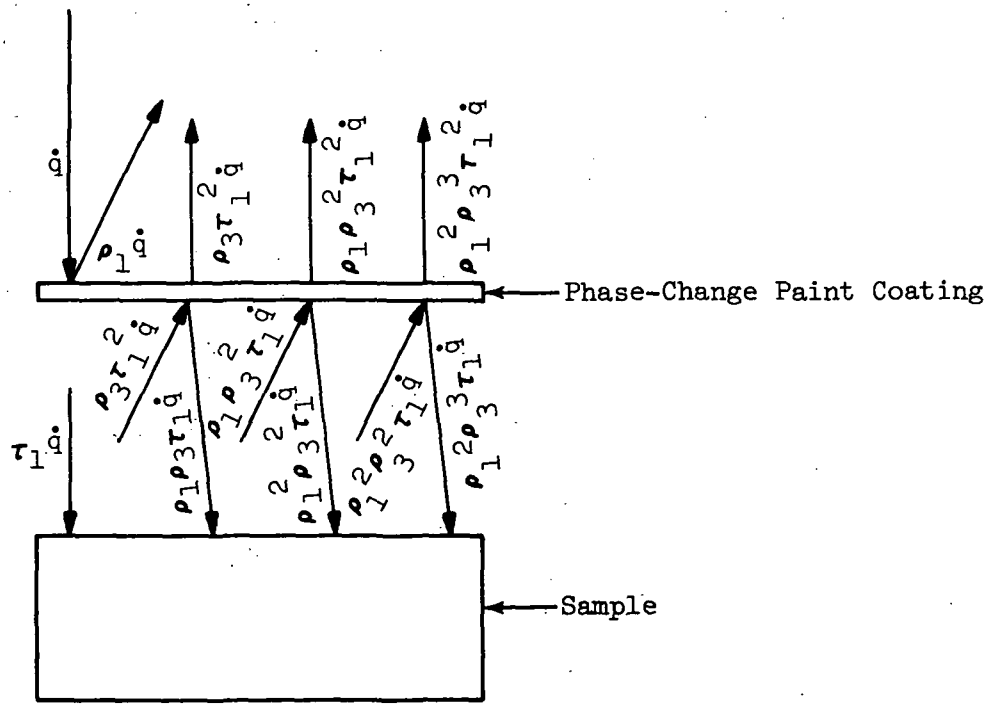

b. Heat Transmission to Sample

Figure 6-18 Analytical Heating Models

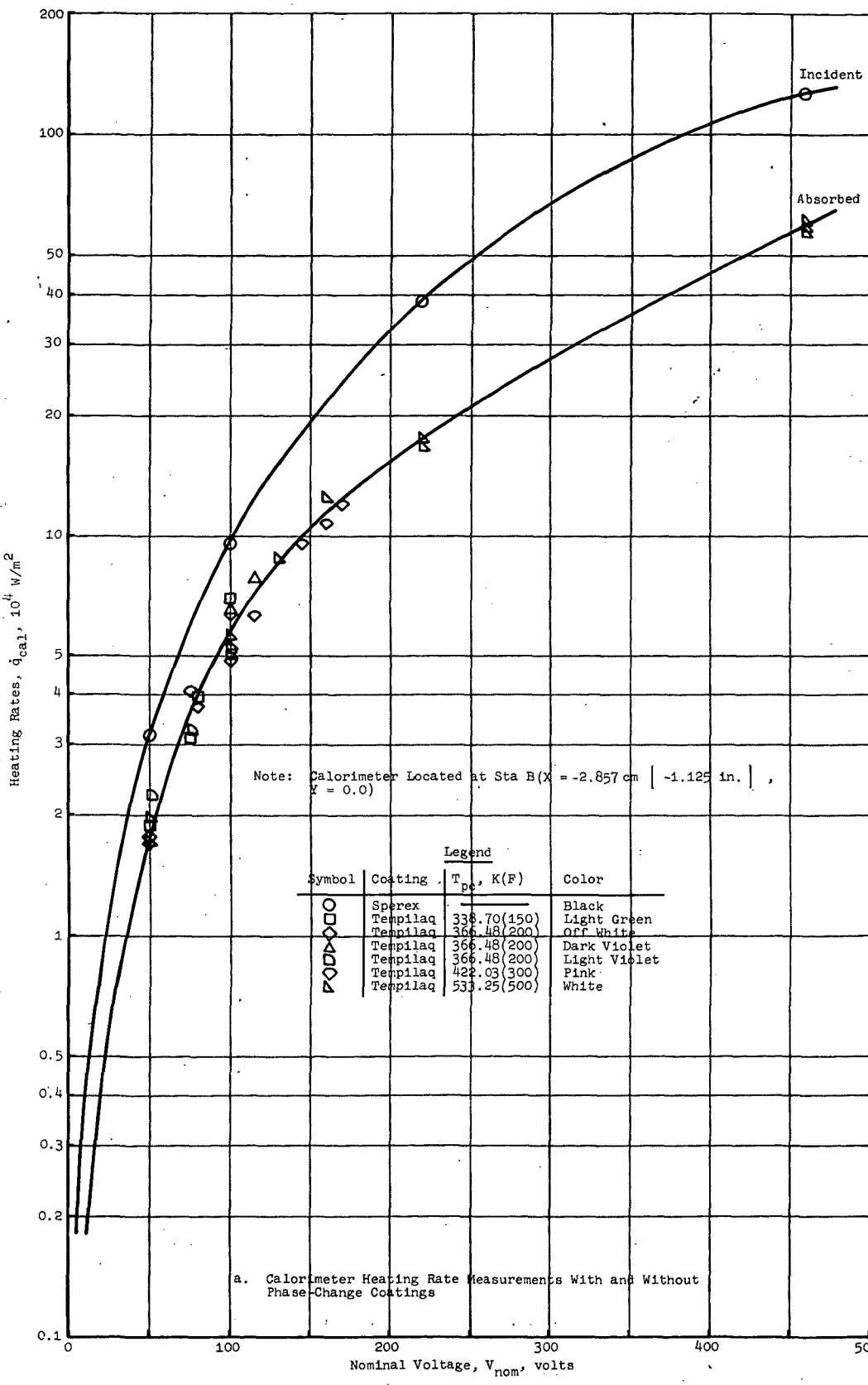

a. Calorimeter Heating Rate Measurements With and Without Phase-Change Coatings

Figure 6-19 Maximum Heating Rate Calibration Curves, Sheet 1 of 4

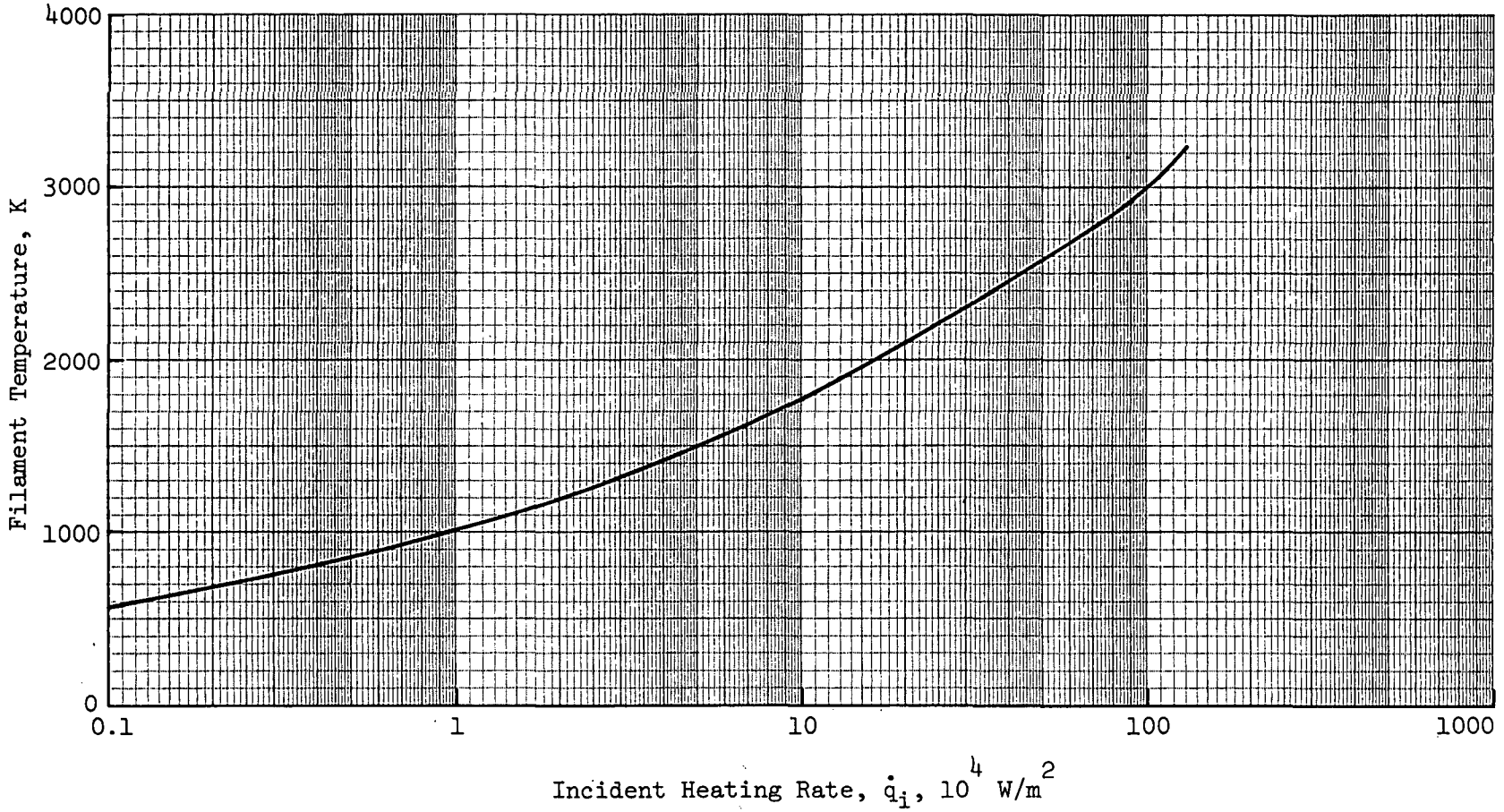

b. Typical Filament Temperature Variation with Incident Heating Rate

Figure 6-19 Maximum Heating Rate Calibration Curves, Sheet 2 of 4

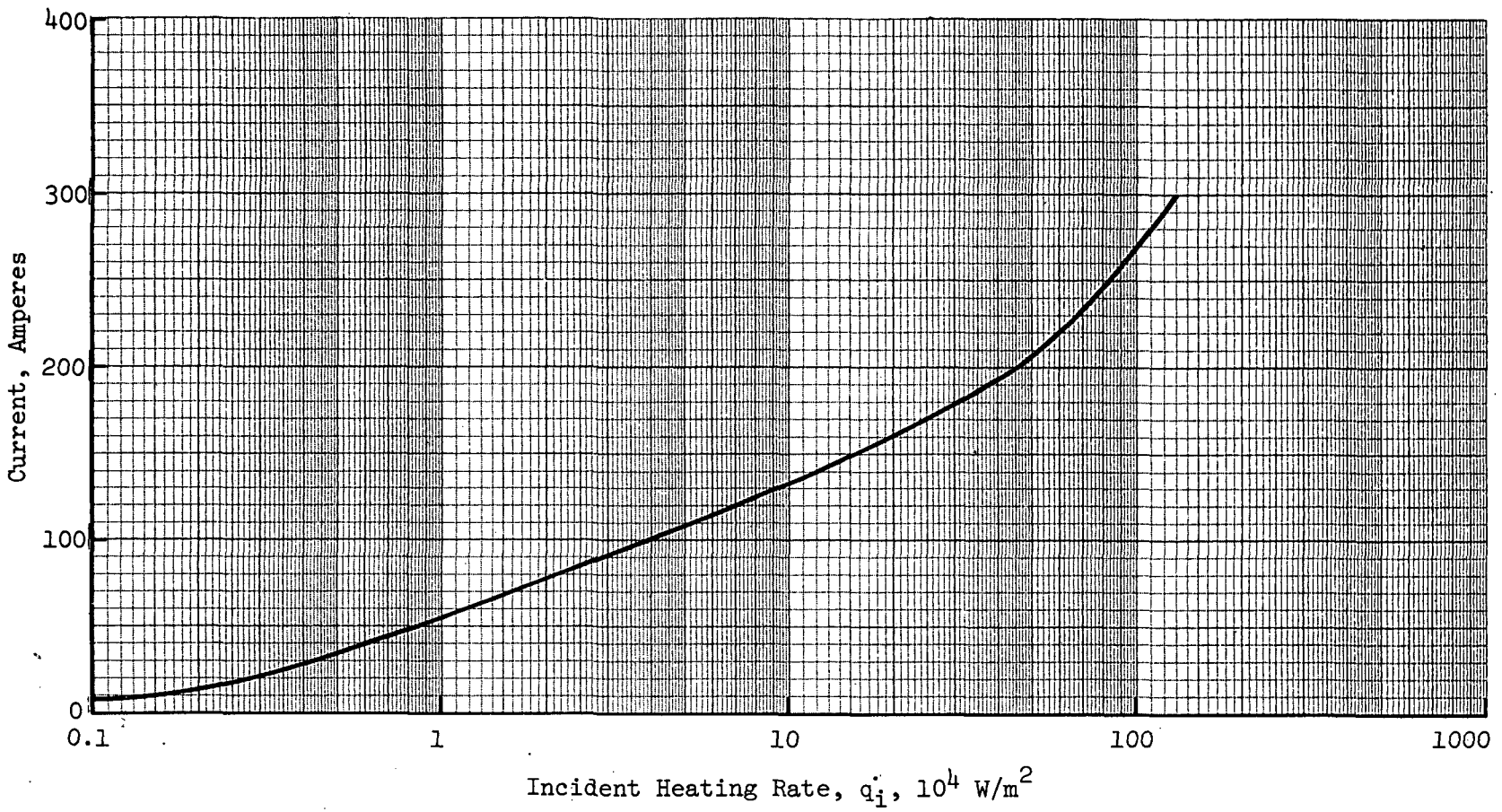

c. Typical Current Variation with Incident Heating Rate

Figure 6-19 Maximum Heating Rate Calibration Curves, Sheet 3 of 4

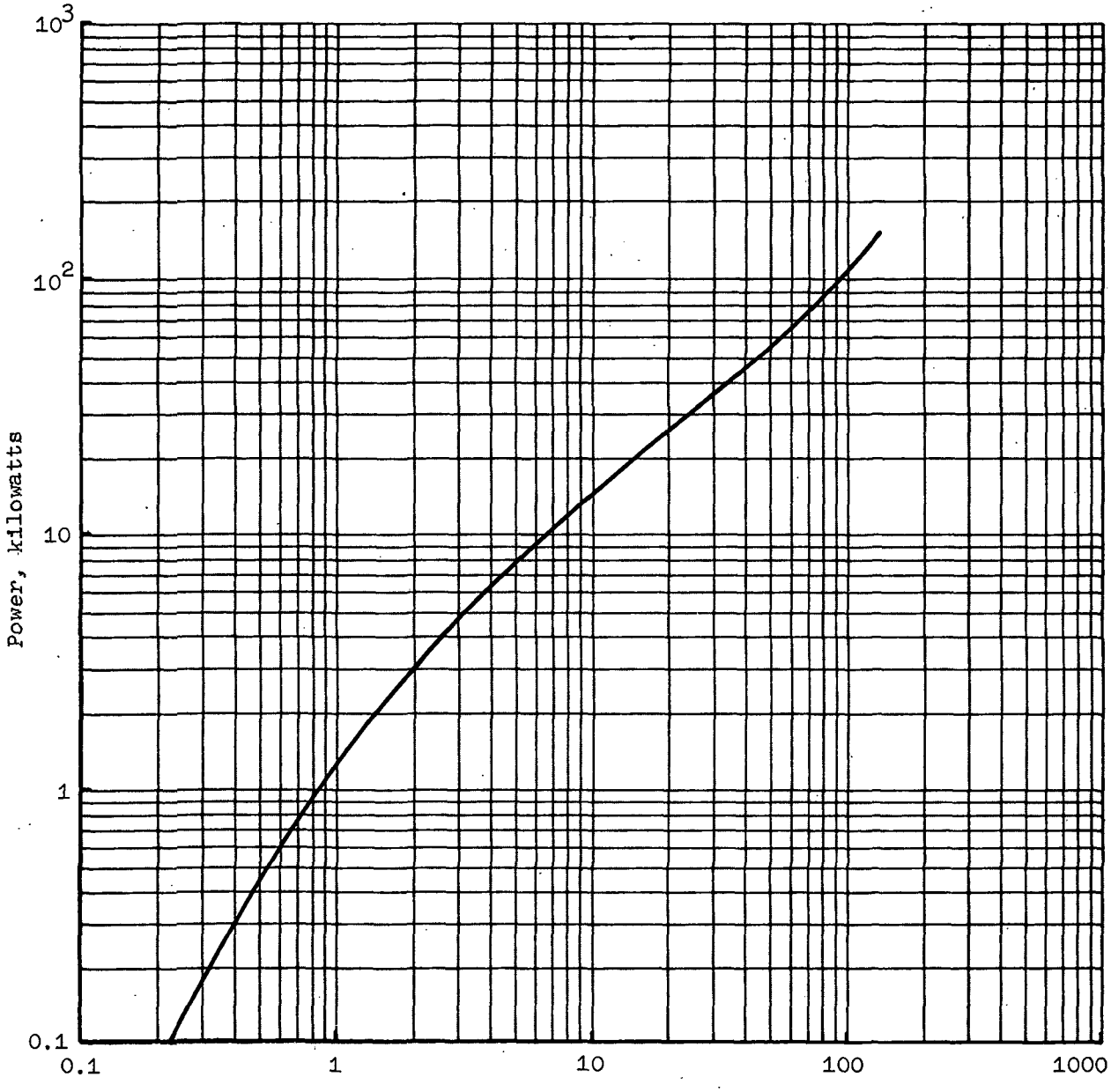

d. Typical Power Variation with Incident Heating Rate

Figure 6-19 Maximum Heating Rate Calibration Curves, Sheet 4 of 4

Symbol	Sta	X, cm(in.)	Coating	Color	$\dot{q}_{(0,0)}$, 10^4 W/m^2 [Btu/(ft^2 · s)]
○	B	-2.857(-1.125)	Sperex	Black	3.192 (2.811)
	C	2.857(1.125)			
△	B	-2.857(-1.125)	T_{pc} = 366.48K(200F)	Off White	1.764 (1.554) = $\dot{q}_{cal}$ (Y=0)
□	B	-2.857(-1.125)	T_{pc} = 422.03K(300F)	Pink	1.694 (1.492) = $\dot{q}_{cal}$ (Y=0)

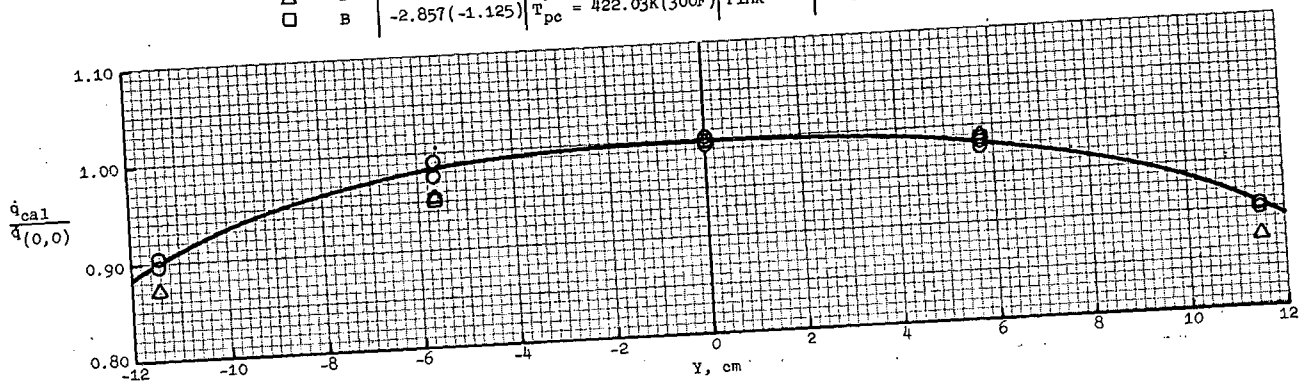

a. Nominal Voltage = 50 V

Symbol	Sta	X, cm(in.)	Coating	Color	$\dot{q}_{(0,0)}$, 10^4 W/m^2 [Btu/(ft^2 · s)]
○	B	-2.857(-1.125)	Sperex	Black	9.550 (8.420)
	C	2.857(1.125)			
△	B	-2.857(-1.125)	T_{pc} = 533.25K(500F)	White	5.082 (4.475) = $\dot{q}_{cal}$ (Y=0)
□	B	-2.857(-1.125)	T_{pc} = 533.15K(500F)	White	5.294 (4.662) = $\dot{q}_{cal}$ (Y=0)

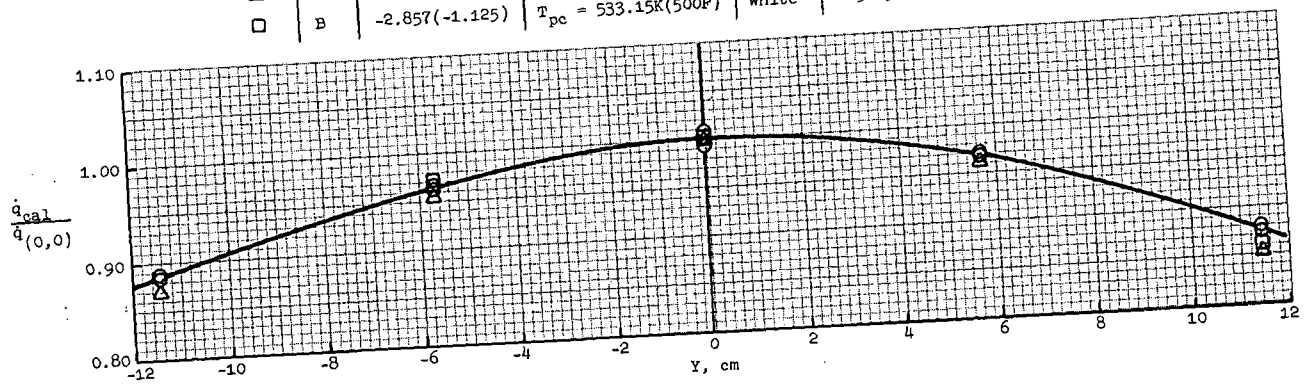

b. Nominal Voltage = 100 V

Figure 6-20 Comparison of Central Heating Distributions With and Without Phase-Change Coatings, Sheet 1 of 2

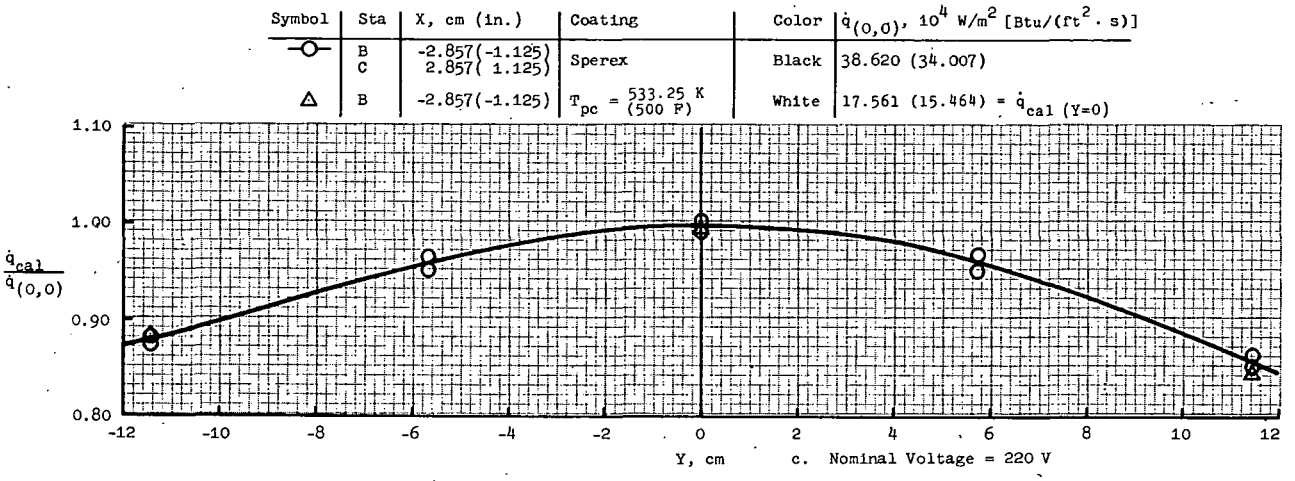

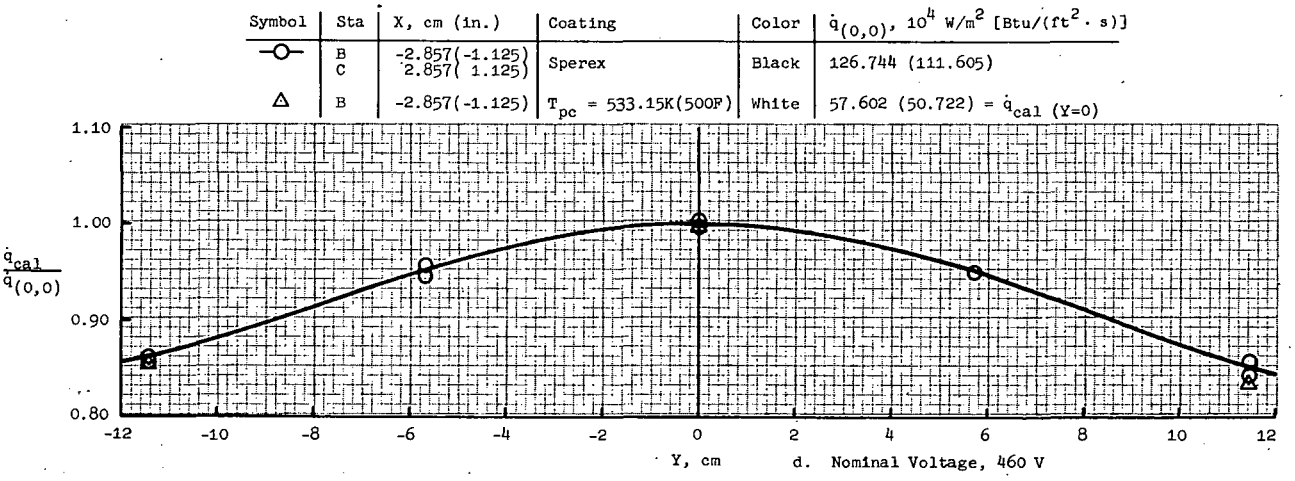

Figure 6-20 Comparison of Central Heating Distributions With and Without Phase-Change Coatings, Sheet 2 of 2

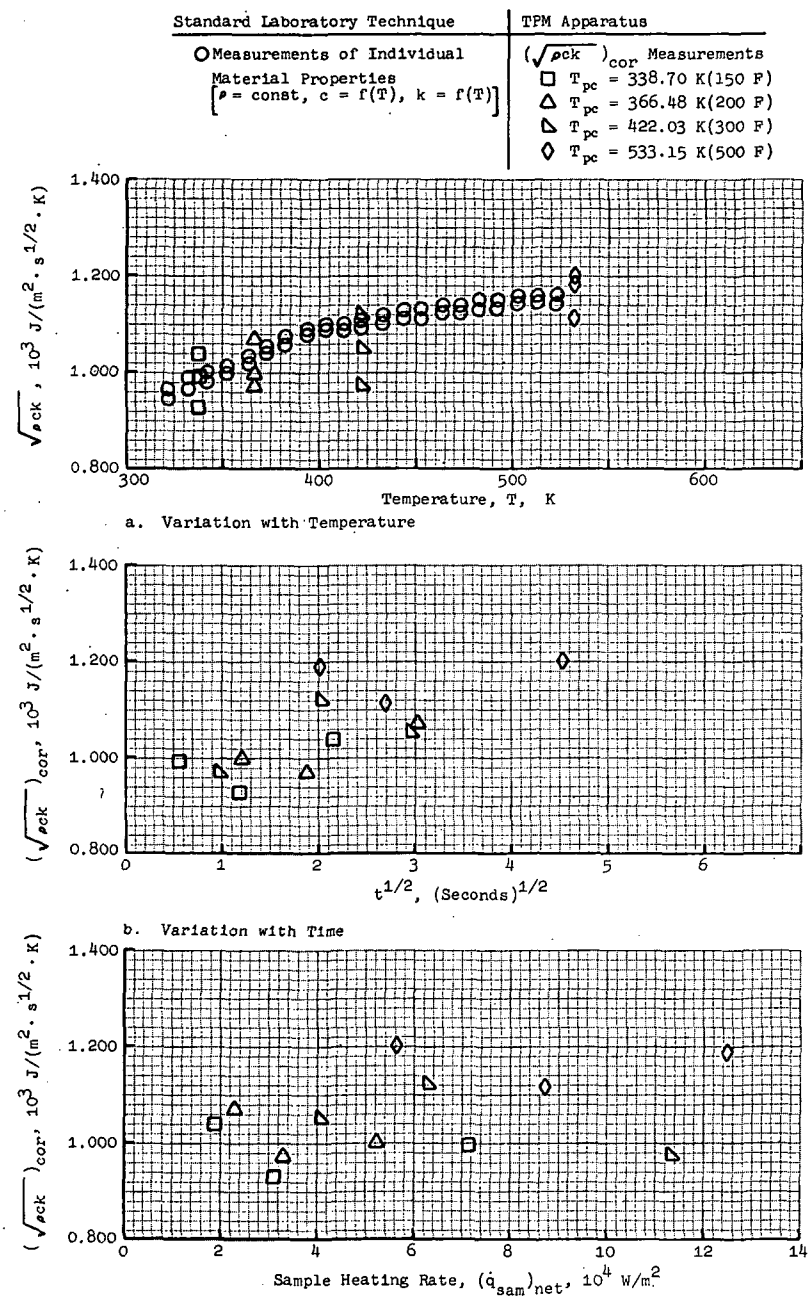

Figure 6-21 Comparison of TPM Apparatus $\sqrt{\rho ck}$ Measurements with Standard Laboratory Measurements

Section 7

EXTENDED CAPABILITY

7.1 CRYOGENIC COOLING

The following modifications to the TPM apparatus are required in order to perform testing with the samples at cryogenic temperatures:

- The base plate must be thermally isolated from the main assembly to reduce the temperature conditioning period and minimize thermal gradients over the test area; conditioning may be provided by circulation of gaseous N_2 through suitably insulated ducts located on the lower base plate surface, Figure 7-1(a).
- The existing shutters must be replaced, possibly by new shutters of sandwich construction that will insulate the sample front face from heat flux prior to shutter retraction, and thereby assist in efficient cooling, Figure 7-1(b).
- Condensation on the cooled surfaces must be eliminated, possibly by locating the test apparatus in an enclosure equipped with an adequate N_2 purge; a remote actuation device would be necessary in this case.

7.2 TESTING OF WIND TUNNEL MODELS

As described in Section 3, the thermophysical properties of samples can differ from those of concurrently cast wind tunnel models. Complete elimination of samples and determination of the thermophysical properties of the fabrication material on the model itself would be ideal. However, in order to accomplish this, the base plate must be modified. An insert arrangement such as shown in Figure 7-2 might be suitable. The insert shown in the figure contains two symmetrically positioned ports, located in zones of similar heating. The left portion of the insert is recessed to allow flat or nearly flat areas of the model to be placed reasonably close to the test plane. The model should be insulated to prevent heat conduction from the metal insert. A standard

calorimeter, as described in paragraph 5.3, would be positioned in the opposite port to measure the heating rate. Standard TPM apparatus test procedure and data reduction, as described in Section 8, may be used without modification.

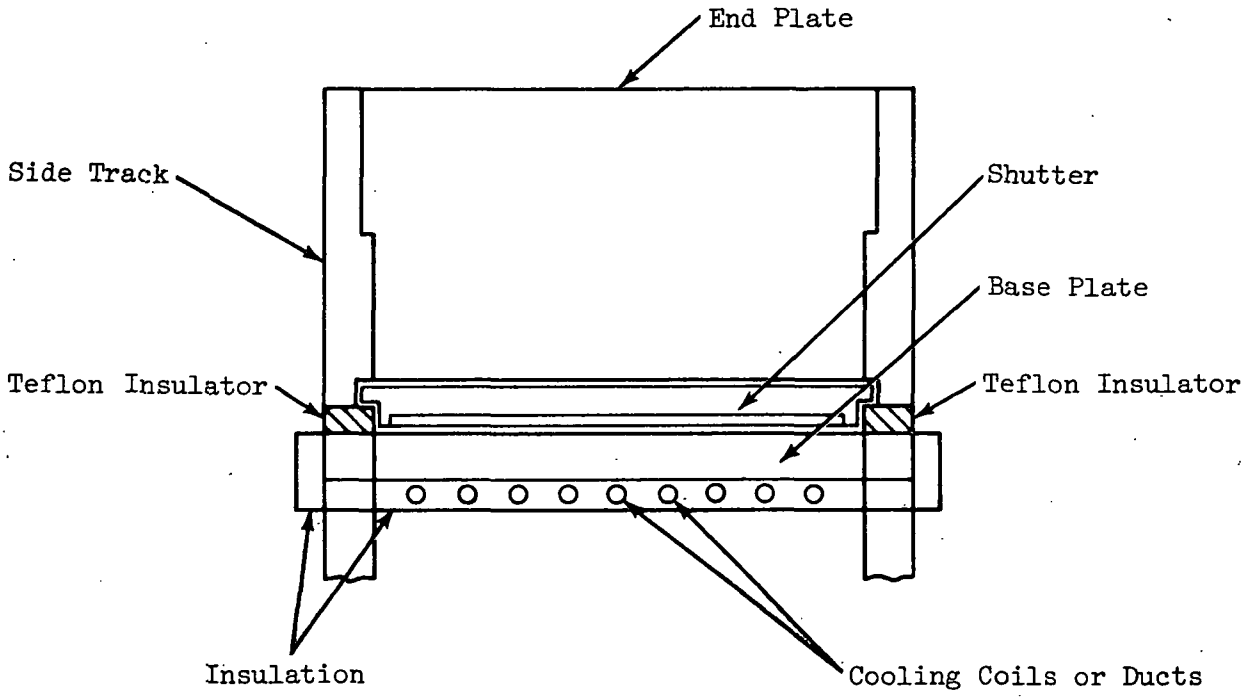

a. Apparatus Side View

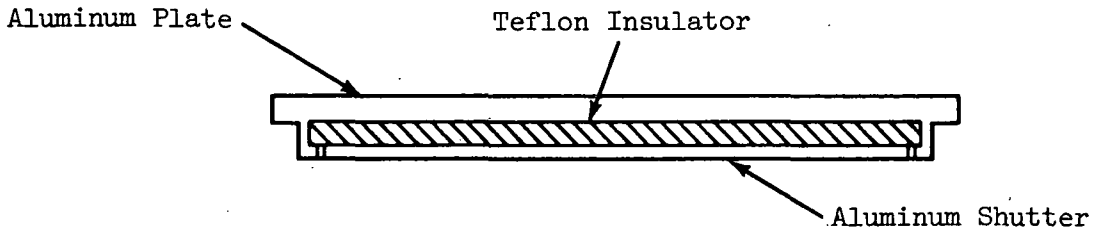

b. Shutter Assembly

Figure 7-1 Apparatus Modifications for Cryogenic Cooling

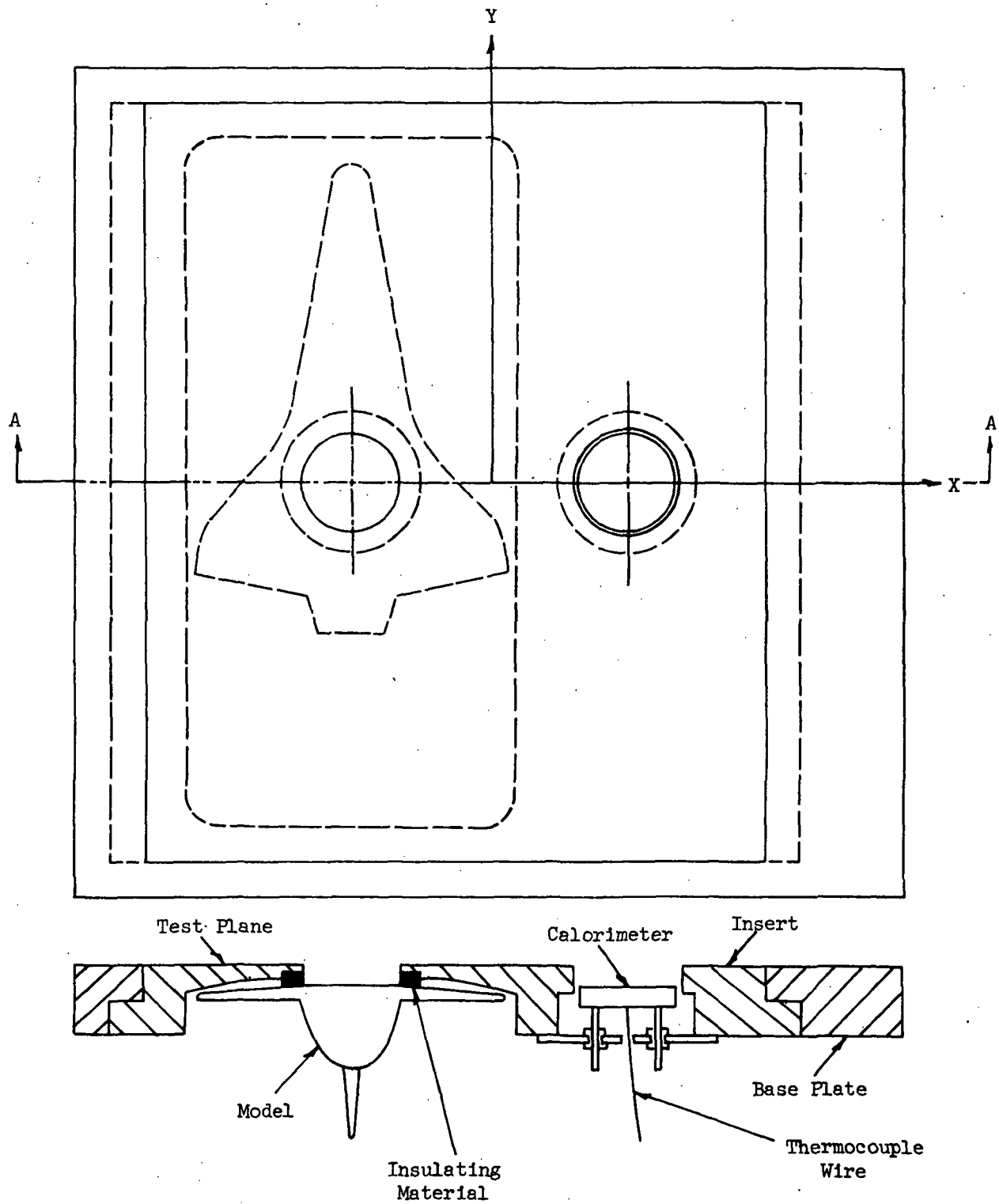

Figure 7-2 Wind Tunnel Model Installation

Section 8

OPERATING PROCEDURE

8.1 SPECIMEN PREPARATION/SELECTION OF TEST CONDITIONS

The following procedure is recommended for test specimen preparation:

1. Select a tempilaq phase-change coating for a specific melt temperature and mix in a household-type blender.

2. Thoroughly clean five test samples, 3.810 cm (1.5 in.) in diameter and 1.905 cm (0.75 in.) thick, with acetone.

3. From manufacturer specifications or existing properties data, estimate $\sqrt{\rho ck}$ in $J/(m^2 \cdot s^{\frac{1}{2}} \cdot K)$ for the test material, and determine the Figure 8-1 heating chart which most nearly corresponds to this estimated value of $\sqrt{\rho ck}$. For example, if the estimated value of $\sqrt{\rho ck}$ were 1.697×10^3 $J/(m^2 \cdot s^{\frac{1}{2}} \cdot K)$, Figure 8-1(e) would be selected. This chart gives the relationship between heating rate, phase-change temperature, and test time for one dimensional transient heating in a semi-infinite solid subjected to a step input of constant heating rate at the surface. Test conditions are obtained from this chart as follows:

   a. Calculate the temperature difference $(T_{pc} - T_i)$, where T_{pc} is the melt temperature of the selected phase-change coating and T_i is the initial sample temperature (assumed to be nominal room temperature, 294.26 K [70F].) If T_{pc} = 422.03 K (300 F),
   $T_{pc} - T_i = 422.03 - 294.26 = 127.77$ K

   b. Select a nominal test time, such as 9 seconds. (See Appendix D discussion of backface temperature response/minimum test time considerations.)

   c. Read the required heating rate of 6.246×10^4 W/m^2.

4. Determine the apparatus voltage setting, from Figure 6-19, based on the required heating rate; use the curve for tempilaq coated calorimeters. For example, a heating rate of 6.246×10^4 W/m^2 corresponds to a voltage setting of 105 V.

5. Select the calorimeter thickness which provides the better temperature response, using Figure 8-2 for thicknesses of 0.203 cm (0.08 in.) and 0.635 cm (0.25 in.). As an example, for the 6.246×10^4 W/m^2 required heating rate, enter the charts at $\dot{q} = 6.246 \times 10^4$ W/m^2 and proceed to t = 9 seconds. Note the following calorimeter temperature differences:

Calorimeter Thickness	$T_{cal} - T_i$
0.203 cm (0.08 in.)	76.38 K
0.635 cm (0.25 in.)	23.33 K

Select the calorimeter with the better temperature response: in this case, the one with the 0.203 cm (0.08 in.) thickness.

6. Check sample and calorimeter heat leakage errors for acceptability. Use Figures 5-2 and 5-4 to insure that these errors are not excessive.

7. Refer to Figure 8-3 to make sure that the selected test time is less than the maximum allowable test time for the chosen calorimeter. Figure 8-3 indicates that the maximum allowable test time for a 0.203 cm (0.08 in.) thick calorimeter, of the cited example, which absorbs 6.246×10^4 W/m^2, is 46 seconds: well above the selected 9 second test time. Note that maximum allowable test time is a limitation imposed by calorimeter h-film insulation; insulation service temperature is 699.81 K (800 F), and should not be exceeded.

8. Estimate the reflectance of the sample face. If sample reflectance is greater than 0.40, apply a 0.025 mm (0.001 in.) coating of high

emissivity black paint to all sample faces before applying the tempilaq. All calorimeters require such a coating; see paragraph 5.3.

9. Apply tempilaq to each of the five material samples and five calorimeters. Coating must be applied uniformly and in the same nominal thickness for all cases. Recommended nominal coating thicknesses are 0.127 mm (0.005 in.), 0.152 mm (0.006 in.), 0.177 mm (0.007 in.) or 0.203 mm (0.008 in.).

10. Allow tempilaq coatings to dry thoroughly before installing samples and calorimeters in the apparatus base plate.

8.2 TEST PROCEDURE

Figure 8-4 is a sequential series of photographs which illustrate the steps to be performed in the test procedure. The TPM apparatus, power source and temperature recording equipment are shown in Figure 8-4(a). This figure shows the shutter system in the initial, open position, with the radiant heater bank removed from its position above the test plane.

Figure 8-4(b) shows the test plane and specimen supports; these supports consist of ceramic stilts upon which the calorimeters and samples rest. The stilts protrude through rubber bushings anchored in a split panel arrangement which is suspended below the base plate, Figure 8-4(c). The two outer panels are free to move laterally, thereby providing sufficient space between panels.

The following procedural steps should be followed in the prescribed order:

1. Install the tempilaq coated calorimeters in the row of specimen mounting holes nearest the viewing port in the left end plate. Pass the thermocouple leads through the holes and then center the ceramic stilts in all ports by bringing the split panels together. Tighten the panel supports to prevent shifting.

2. Place the tempilaq coated samples in the row of specimen mounting holes nearest the camera port in the right end plate, Figure 8-4(d).

3. Align calorimeter and sample faces with the test plane by adjusting the height of the ceramic stilts. Each specimen must be carefully centered in order to maintain a circumferential gap between the specimen and base plate.

4. After test specimen installation, manually close the left shutter as shown in Figure 8-4(e and f). While holding the shutter closed, pivot the left handle to restrain the shutter linkage, Figure 8-4(g). Pivot the left safety latch, Figure 8-4(h), to lock the handle in place.

5. Repeat the procedure of step 4 with the right shutter: manually close the shutter, Figure 8-4(i and j), pivot the right handle to restrain the shutter linkage, Figure 8-4(k), and lock the right safety latch, Figure 8-4(l).

6. Rotate the interlock as shown in Figure 8-4 (m and r) to join both handle pieces; this primes the shutter release system for operation.

7. Install the radiant heater bank above the shielded test plane, and mount the motion picture camera so that it can view the test area through the right end plate port, Figure 8-4(o).

8. Connect all thermocouple leads to the temperature recording equipment.

9. Activate lamp cooling air to provide a 158.579×10^3 N/m^2 (23 psig) plenum gage pressure at port P (see Figure 5-1). This pressure corresponds to a flow rate of 0.877 m^3/min (31 ft^3/min).

10. Provide cooling water at 4.163×10^{-3} m^3/min (1.1 gal/min) to the lamps and shutters.

11. Allow calorimeter temperatures to stabilize under the influence of shutter cooling; the apparatus is now ready for testing.

12. While holding the handle in position, release both safety latches, Figure 8-4(p). Then bring the lamps to the desired intensity. When voltage is stabilized, activate the temperature recorder and motion picture camera.

13. Release the shutters by dropping the handle, Figure 8-4(q), and maintain power at a constant level for a predetermined test interval sufficiently long to allow the sample coatings to melt, Figure 8-4(r).

14. Terminate the run when the specified time has elapsed; turn off the temperature recorder and motion picture camera after the apparatus is turned off.

8.3 DATA REDUCTION

Data are reduced by the following equation:

$$\sqrt{\rho c k} = \frac{\dot{q}}{T_{pc} - T_i} \frac{2}{\sqrt{\pi}} \sqrt{t} \quad (J/[m^2 \cdot s^{\frac{1}{2}} \cdot K]) \qquad (8\text{-}1)$$

where T_{pc} = melt temperature of the tempilaq coating, K

T_i = initial sample temperature, K (assumed equal to the recorded initial calorimeter temperature)

t = elapsed time from initial shutter opening to sample coating phase change as determined from motion picture film, seconds.

The heating rate, $\dot{q}$, may be expressed as

$$\dot{q} = \frac{Mc}{A} \frac{dT}{dt} \quad (W/m^2) \qquad (8\text{-}2)$$

where M = calorimeter mass, kg

c = specific heat of copper = 401.932856 J/(kg·K)

A = calorimeter face area = 1.14009×10^{-3} m^2 for a 3.810 cm diameter

$\frac{dT}{dt}$ = slope of calorimeter temperature-time curve, K/s.

Equation 8-2 thus may be expressed

$$\dot{q} = \frac{M \times 401.932856}{1.14009 \times 10^{-3}} \frac{dT}{dt}$$

$$\dot{q} = M[35.25448 \times 10^{4}] \frac{dT}{dt} \quad (W/m^2) \qquad (8\text{-}3)$$

Mass measurements for the calorimeters supplied with the apparatus are given in Table 8-1.

Table 8-1. Calorimeter Mass Measurements

Thickness = 0.203 cm (0.08 in.)		Thickness = 0.635 cm (0.25 in.)	
Calorimeter	Mass, kg	Calorimeter	Mass, kg
1	0.01885	1	0.06440
2	0.01910	2	0.06445
5	0.02060	3	0.06430
8	0.01930	7	0.06425
9	0.02015	8	0.06435
10	0.01895	10	0.06440

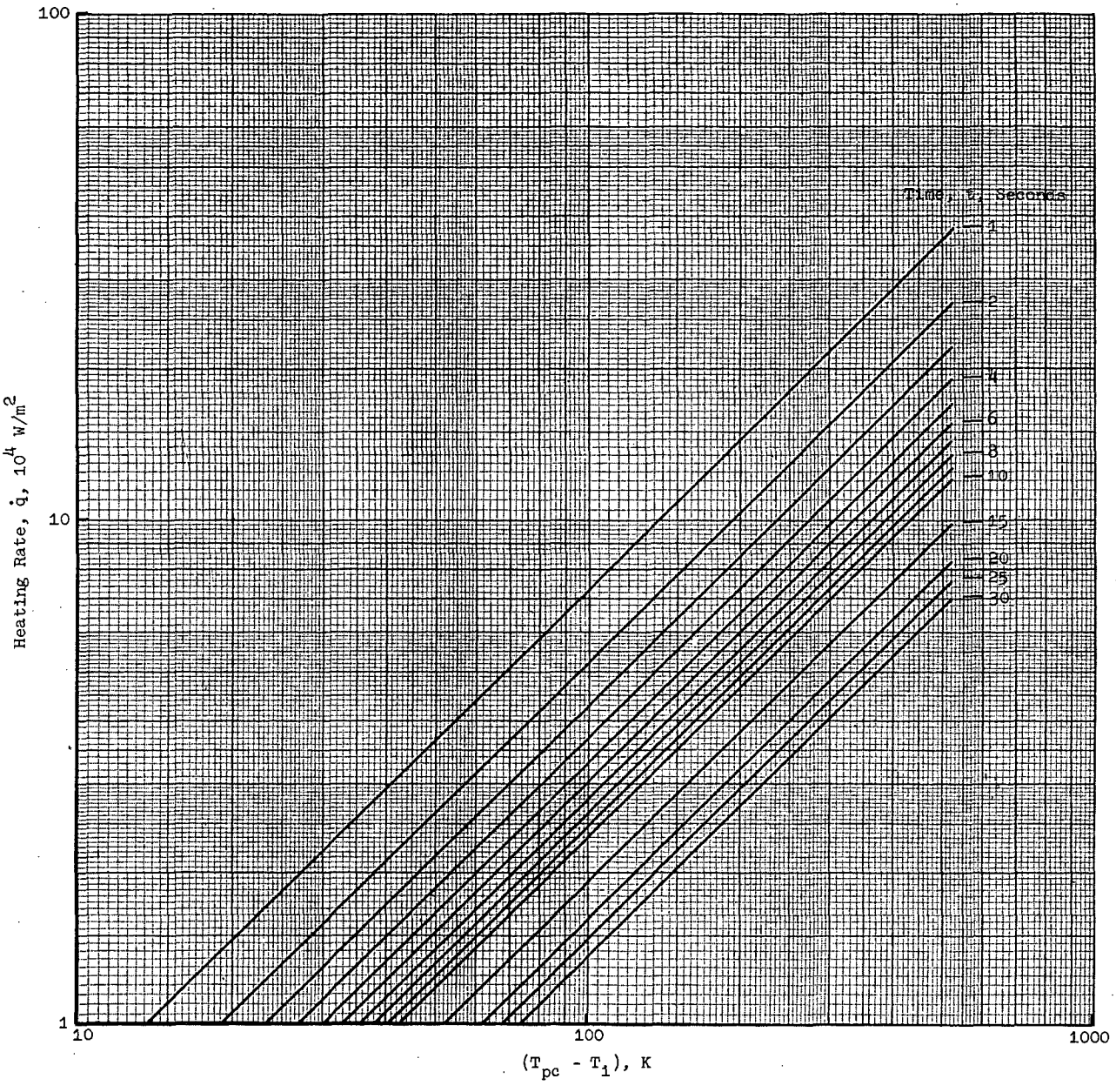

a. $\sqrt{\rho ck} = 0.817 \times 10^3$ J/(m$^2 \cdot$ s$^{1/2} \cdot$ K) [0.04 Btu/(ft$^2 \cdot$ s$^{1/2} \cdot$ F)]

Figure 8-1 One Dimensional Transient Heating in a Semi-Infinite Solid Subjected to a Step Input of Constant Heating Rate at the Surface $\left[\dot{q} = \sqrt{\rho ck}\,(\sqrt{\pi}/t/2)\,(T_{pc} - T_i)\right]$, Sheet 1 of 13

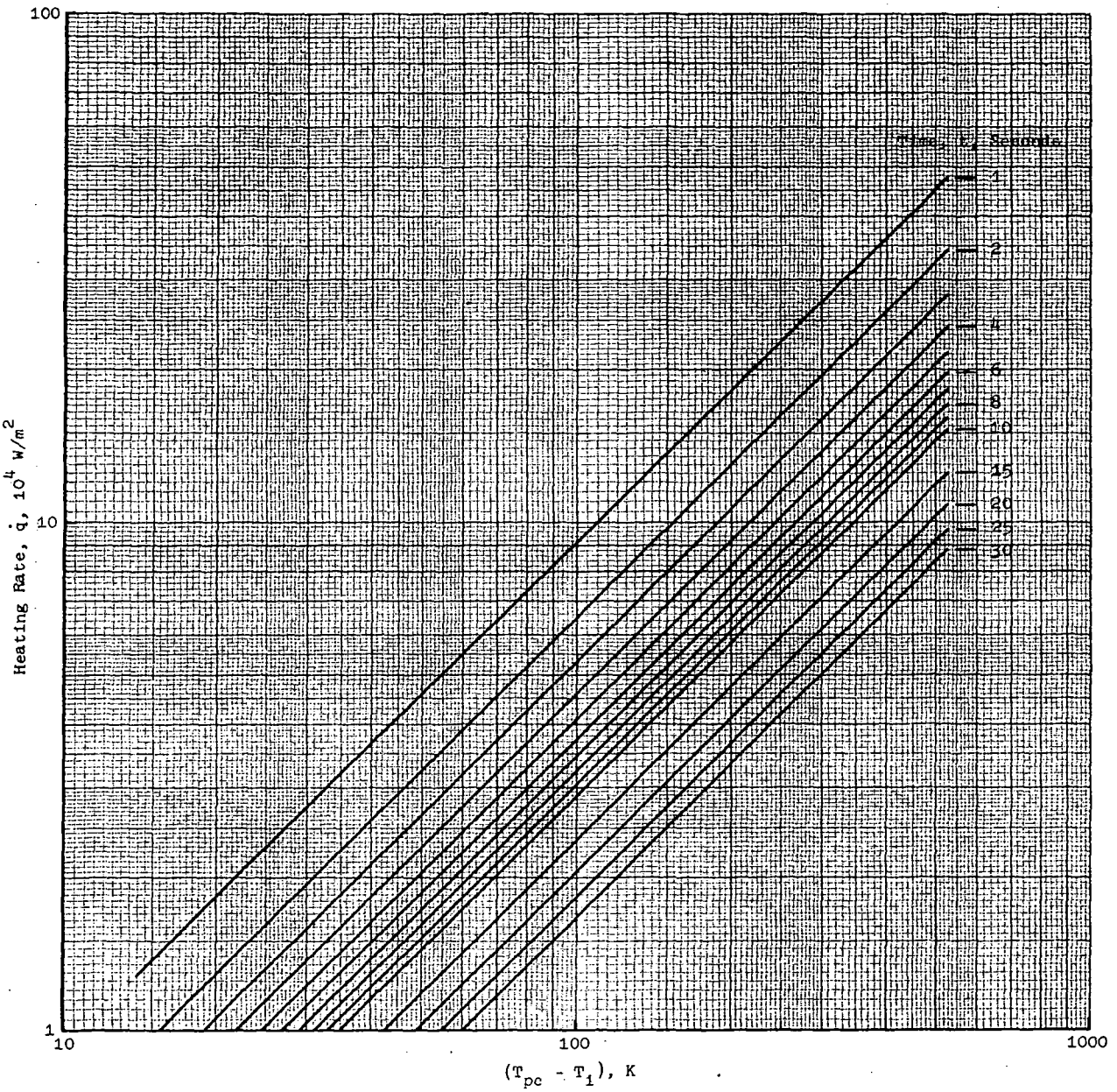

b. $\sqrt{\rho ck}$ = 1.022 x 10^3 J/($m^2 \cdot s^{1/2} \cdot K$) [0.05 Btu/($ft^2 \cdot s^{1/2} \cdot F$)]

Figure 8-1 One Dimensional Transient Heating in a Semi-Infinite Solid Subjected to a Step Input of Constant Heating Rate at the Surface $\left[\dot{q} = \sqrt{\rho ck}\ (\sqrt{\pi/t}/2)\ (T_{pc} - T_i)\right]$, Sheet 2 of 13

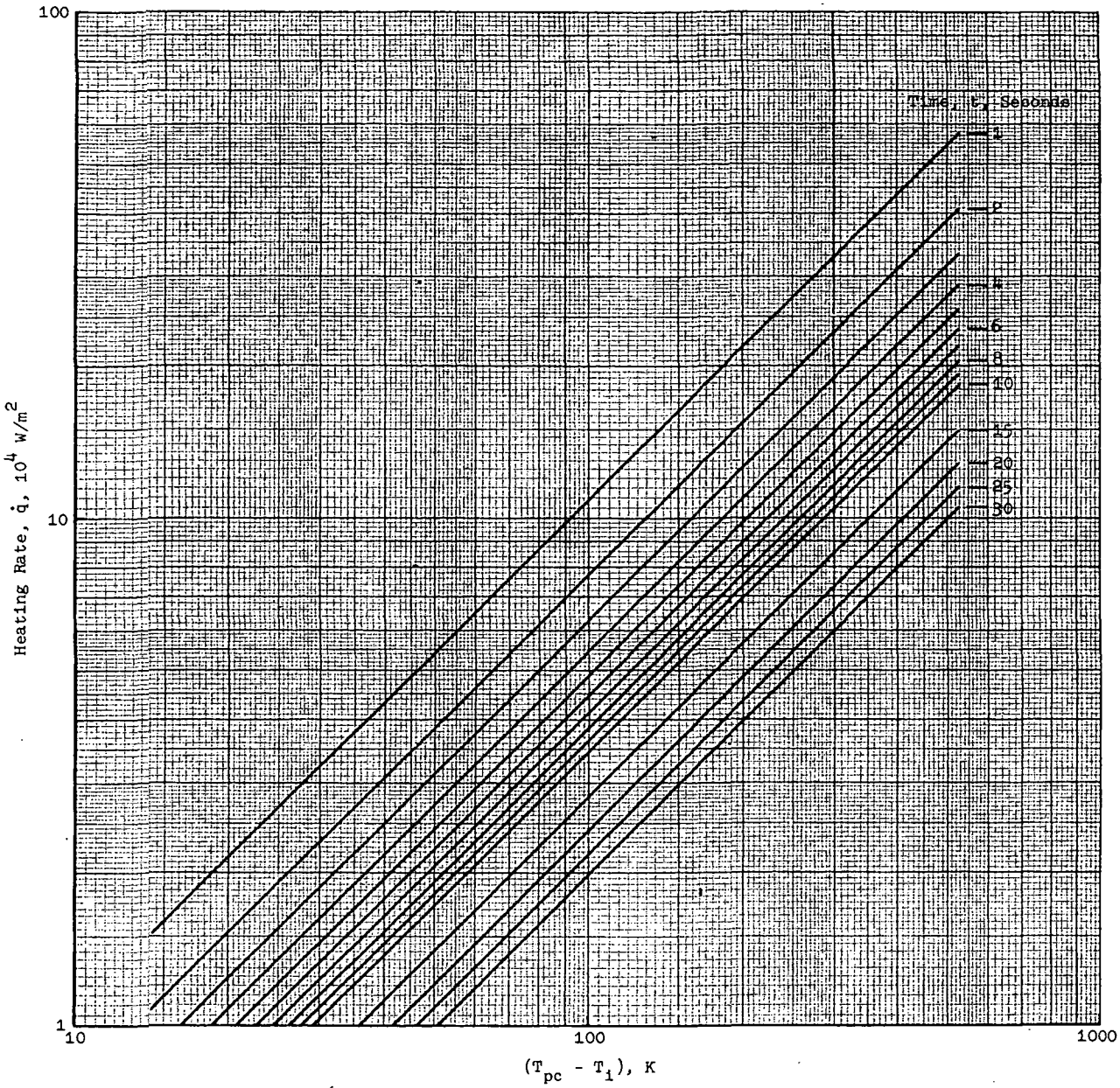

c. $\sqrt{\rho ck} = 1.226 \times 10^3$ J/(m^2. s$^{1/2}$.K) [0.06 Btu/(ft^2. s$^{1/2}$.F)]

Figure 8-1 One Dimensional Transient Heating in a Semi-Infinite Solid Subjected to a Step Input of Constant Heating Rate at the Surface $[\dot{q} = \sqrt{\rho ck}\ (\sqrt{\pi/t}/2)\ (T_{pc} - T_i)]$, Sheet 3 of 13

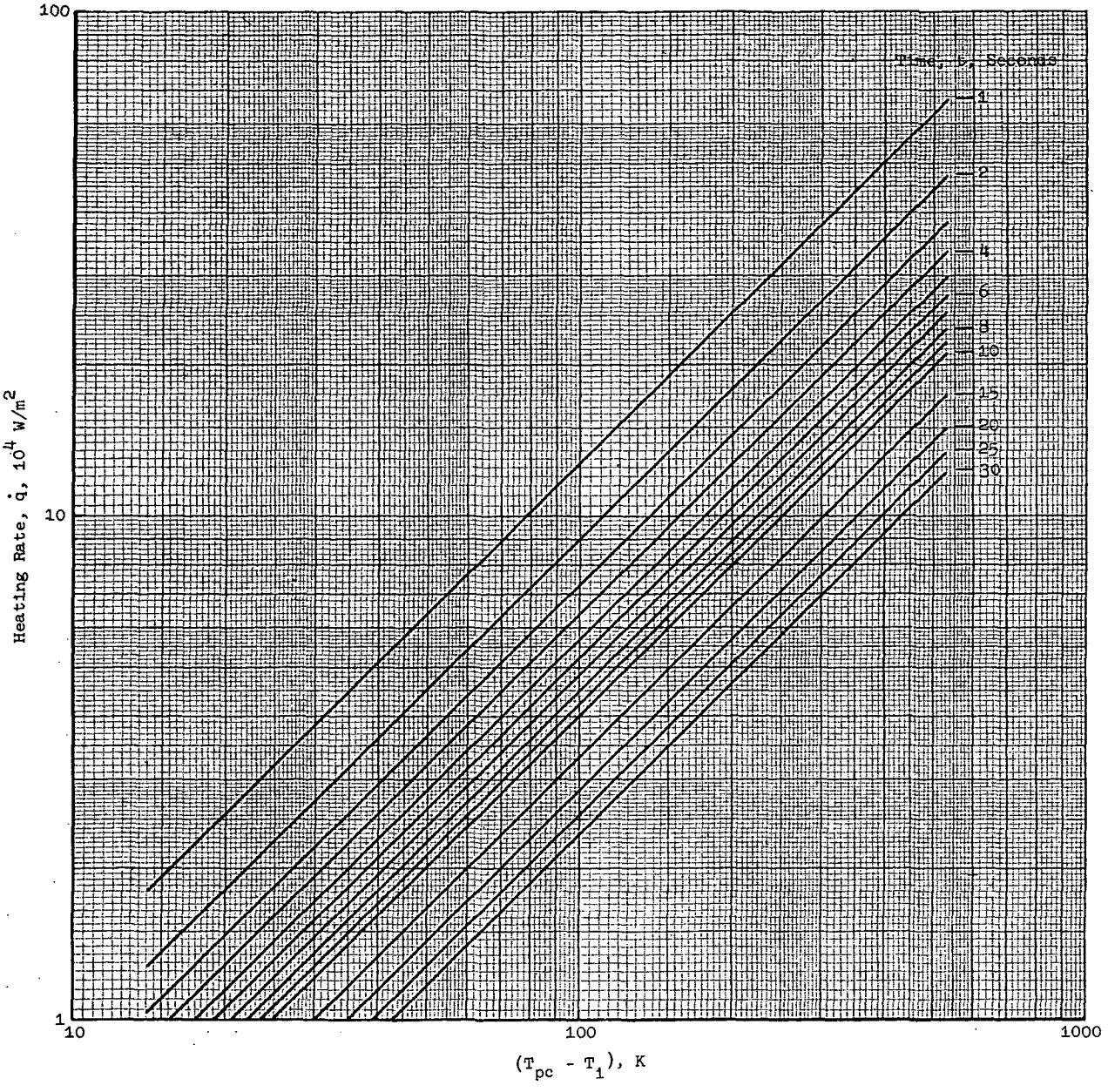

d. $\sqrt{\rho ck} = 1.430 \times 10^3$ J/(m^2.s$^{1/2}$.K) [0.07 Btu/(ft^2.s$^{1/2}$.F)]

Figure 8-1 One Dimensional Transient Heating in a Semi-Infinite Solid Subjected to a Step Input of Constant Heating Rate at the Surface $\left[\dot{q} = \sqrt{\rho ck}\ (\sqrt{\pi/t}/2)\ (T_{pc} - T_i)\right]$, Sheet 4 of 13

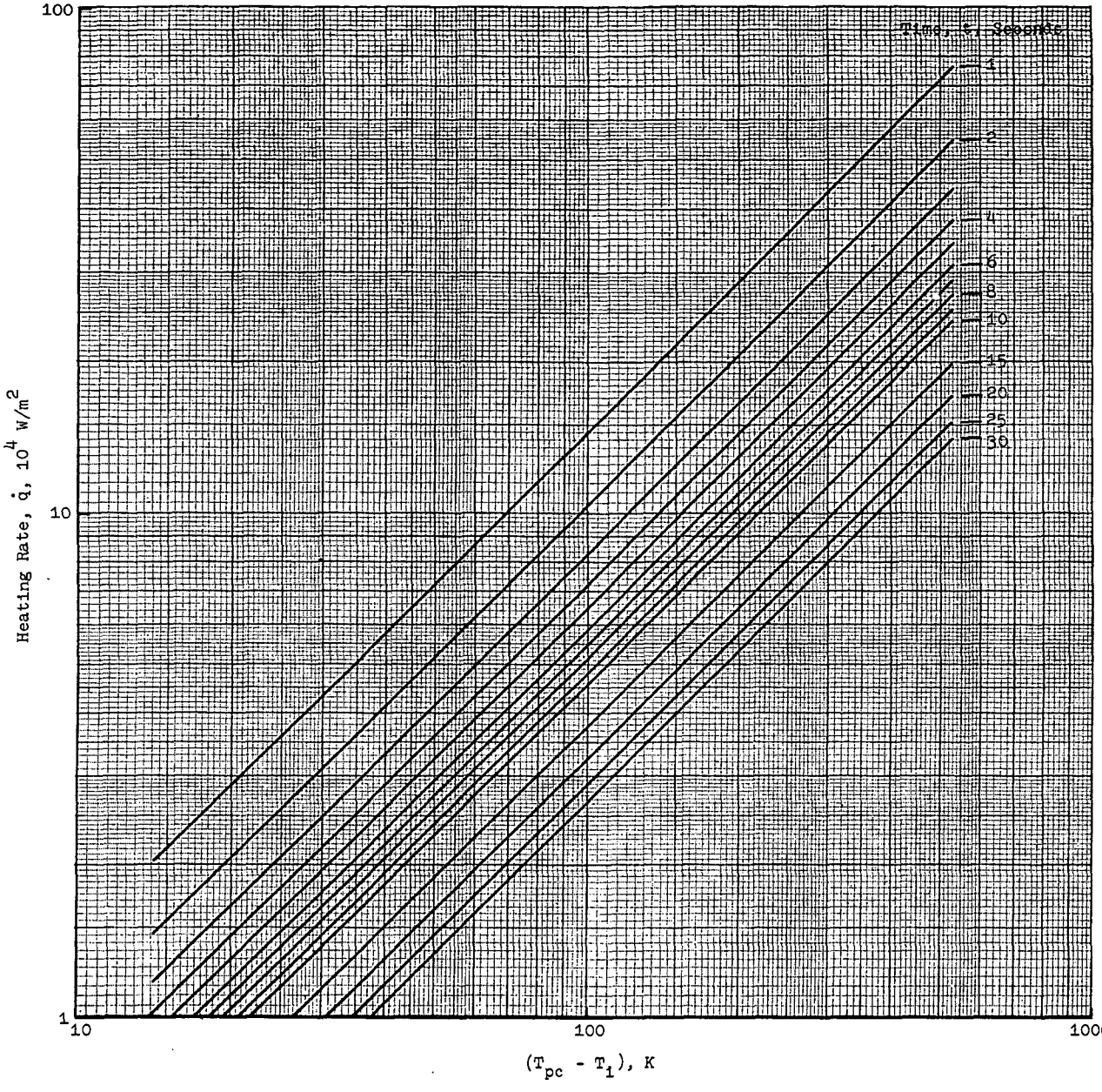

e. $\sqrt{\rho ck} = 1.635 \times 10^3$ J/(m^2.s$^{1/2}$.K) [0.08 Btu/(ft^2.s$^{1/2}$.F)]

Figure 8-1 One Dimensional Transient Heating in a Semi-Infinite Solid Subjected to a Step Input of Constant Heating Rate at the Surface $\left[\dot{q} = \sqrt{\rho ck}\ (\sqrt{\pi}/t/2)\ (T_{pc} - T_i)\right]$, Sheet 5 of 13

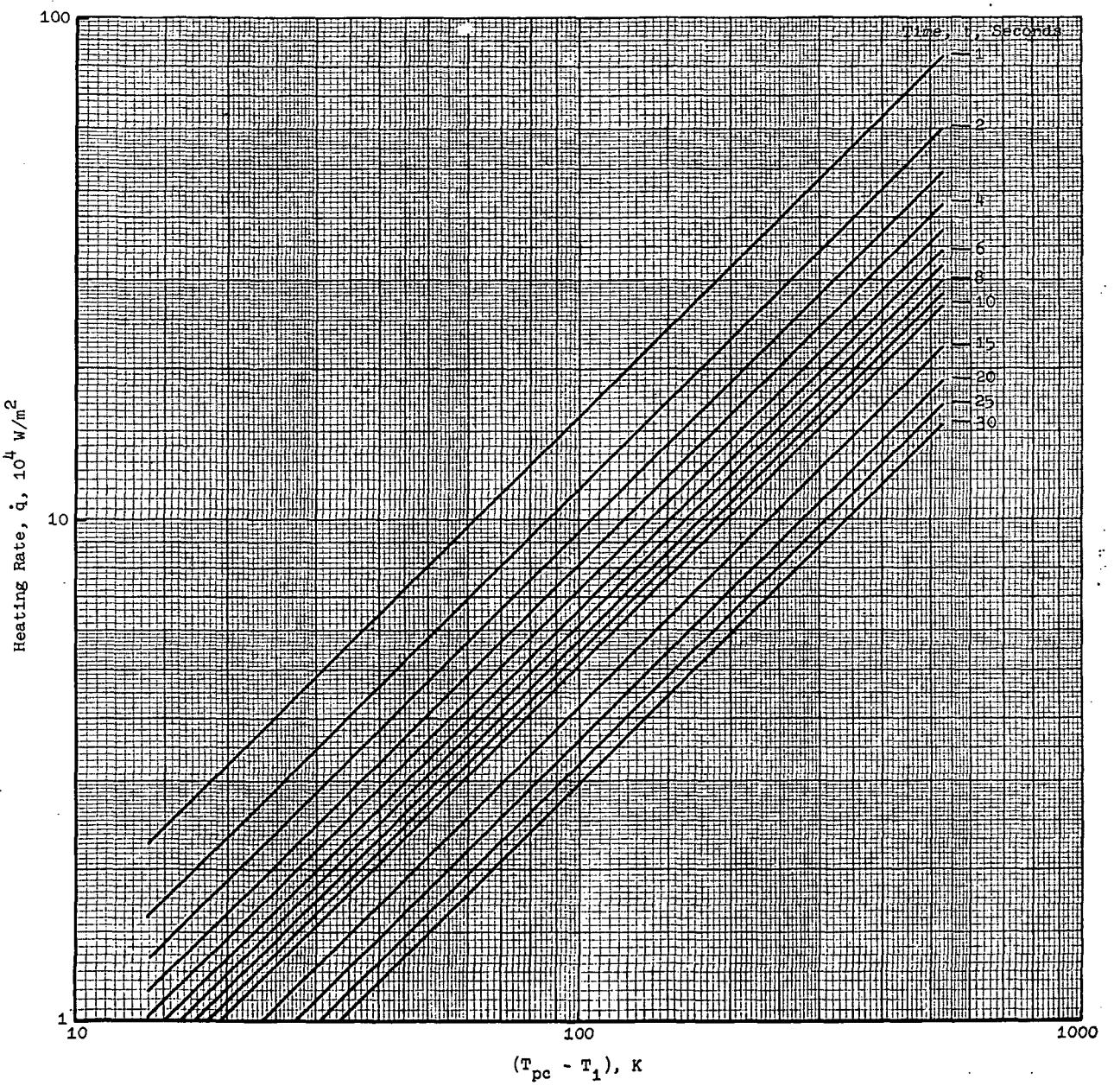

f. $\sqrt{\rho ck} = 1.839 \times 10^3$ J/(m^2.s$^{1/2}$.K) [0.09 Btu/(ft^2.s$^{1/2}$.F)]

Figure 8-1 One Dimensional Transient Heating in a Semi-Infinite Solid Subjected to a Step Input of Constant Heating Rate at the Surface $\left[\dot{q} = \sqrt{\rho ck}\,(\sqrt{\pi/t}/2)\,(T_{pc} - T_i)\right]$, Sheet 6 of 13

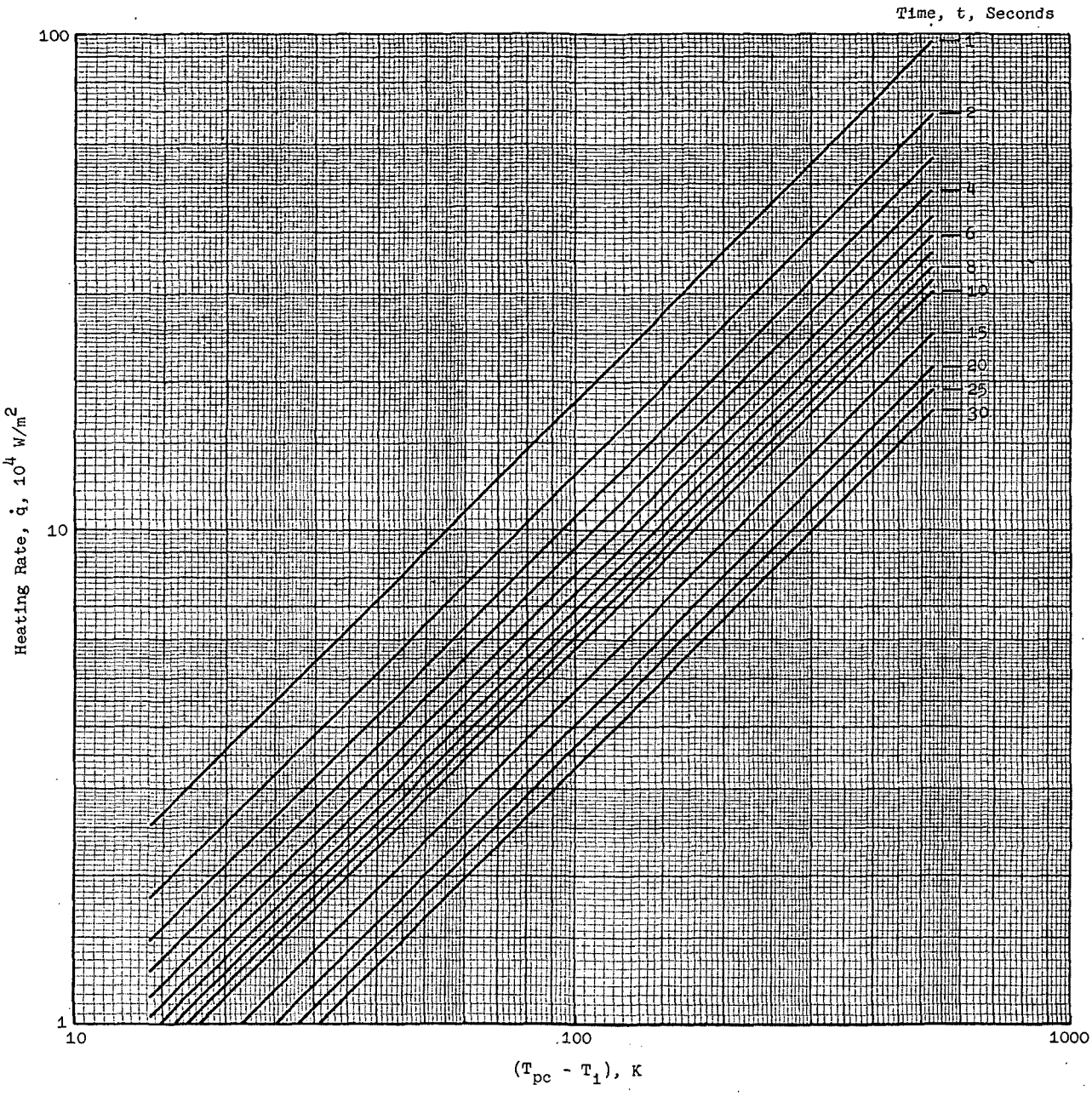

Figure 8-1 One Dimensional Transient Heating in a Semi-Infinite Solid Subjected to a Step Input of Constant Heating Rate at the Surface $[\dot{q} = \sqrt{\rho ck}\ (\sqrt{\pi/t}/2)\ (T_{pc} - T_i)$, Sheet 7 of 13

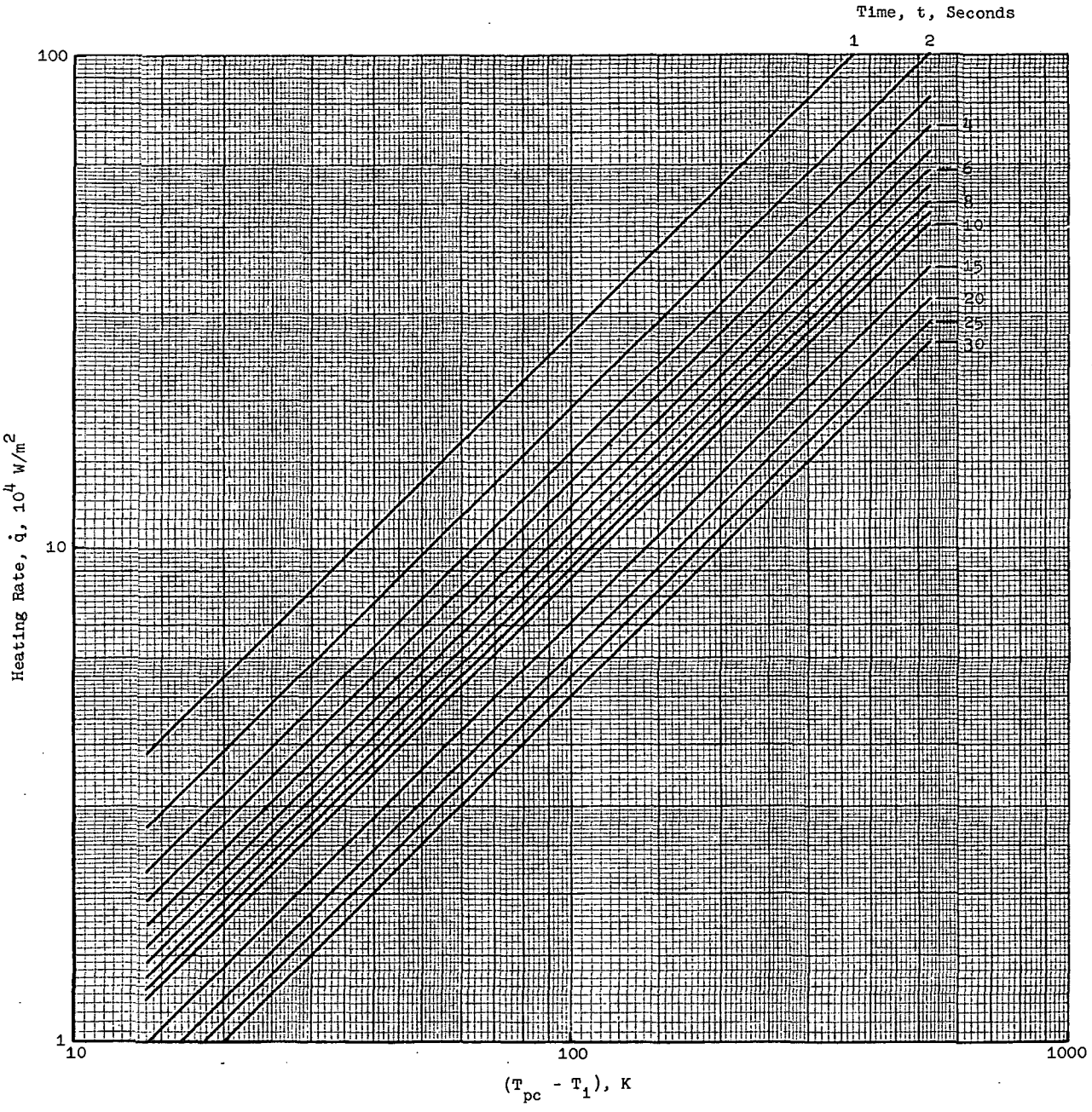

Figure 8-1 One Dimensional Transient Heating in a Semi-Infinite Solid Subjected to a Step Input of Constant Heating Rate at the Surface $[\dot{q} = \sqrt{\rho ck}\ (\sqrt{\pi/t}/2)\ (T_{pc} - T_i)\ ]$, Sheet 8 of 13

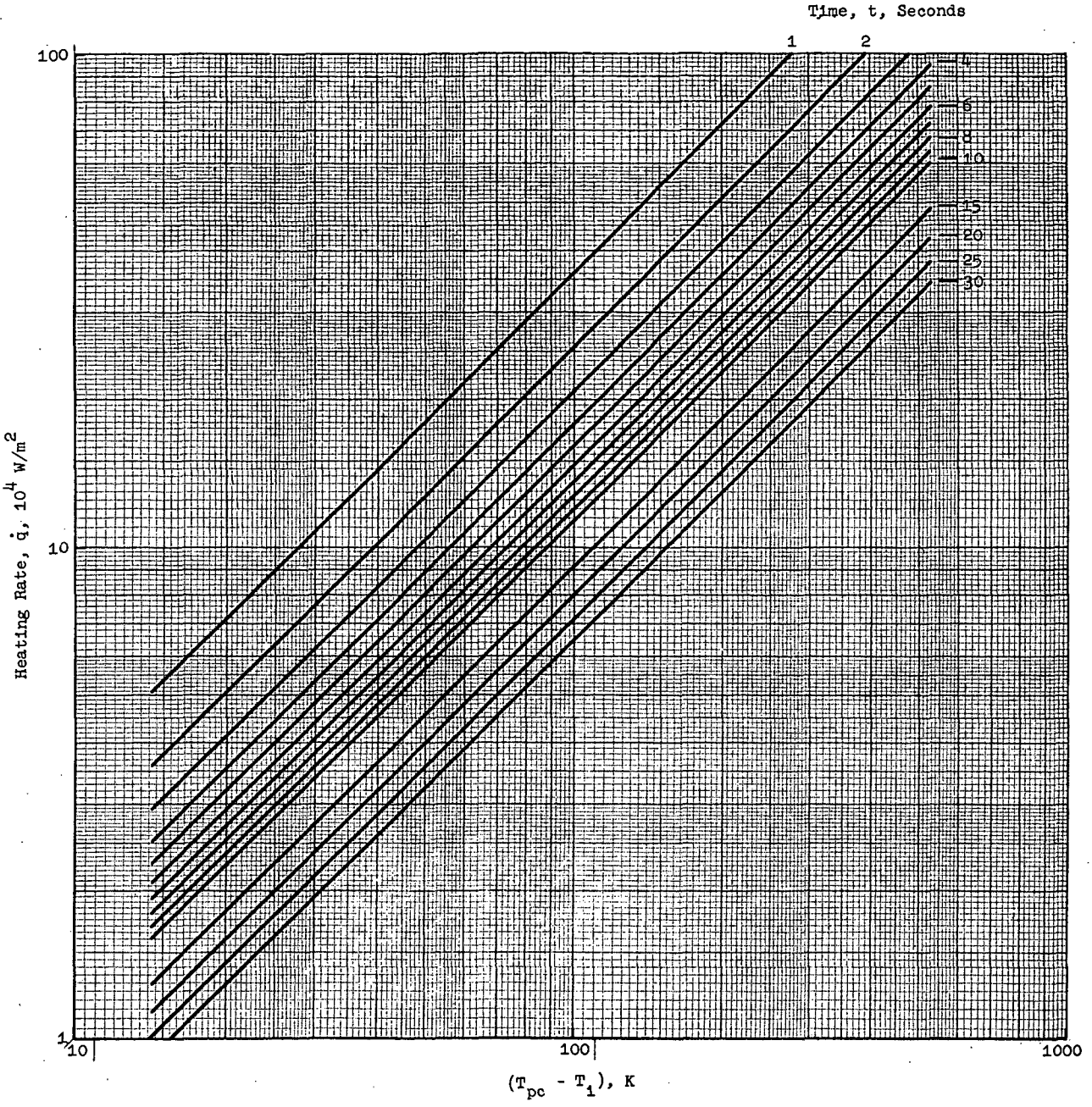

1. $\sqrt{\rho ck} = 4.088 \times 10^3$ J/(m^2.s$^{1/2}$.K) [0.20 Btu/(ft^2.s$^{1/2}$.F)]

Figure 8-1 One Dimensional Transient Heating in a Semi-Infinite Solid Subjected to a Step Input of Constant Heating Rate at the Surface $\left[\dot{q} = \sqrt{\rho ck}\,(\sqrt{\pi/t}\,/2)\,(T_{pc} - T_i)\right.$, Sheet 9 of 13

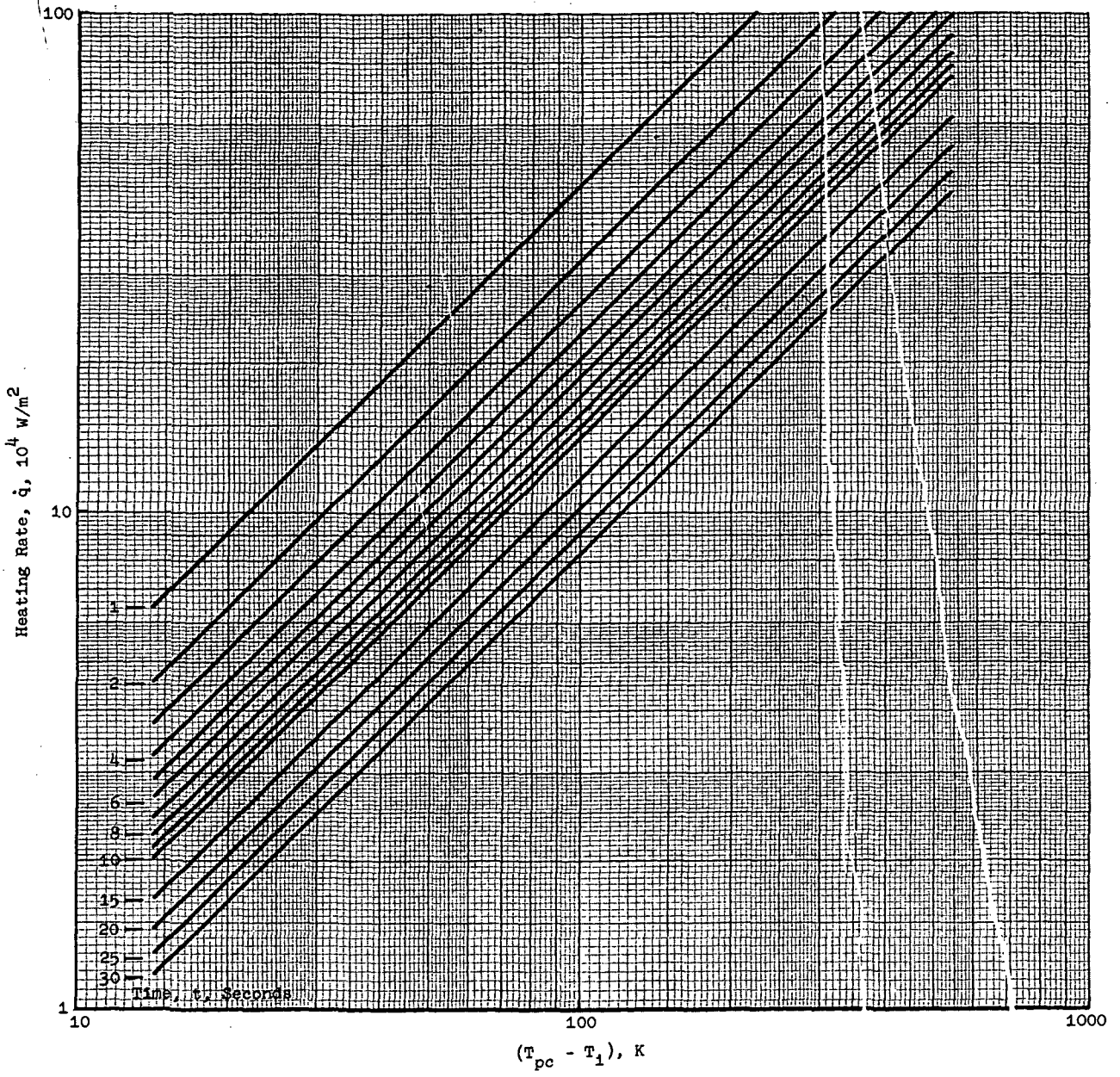

j. $\sqrt{\rho ck} = 5.110 \times 10^3$ J/(m^2·s$^{1/2}$·K) [0.25 Btu/(ft^2·s$^{1/2}$·F)]

Figure 8-1 One Dimensional Transient Heating in a Semi-Infinite Solid Subjected to a Step Input of Constant Heating Rate at the Surface $[\dot{q} = \sqrt{\rho ck}\ (\sqrt{\pi/t}/2)\ (T_{pc} - T_i)$, Sheet 10 of 13

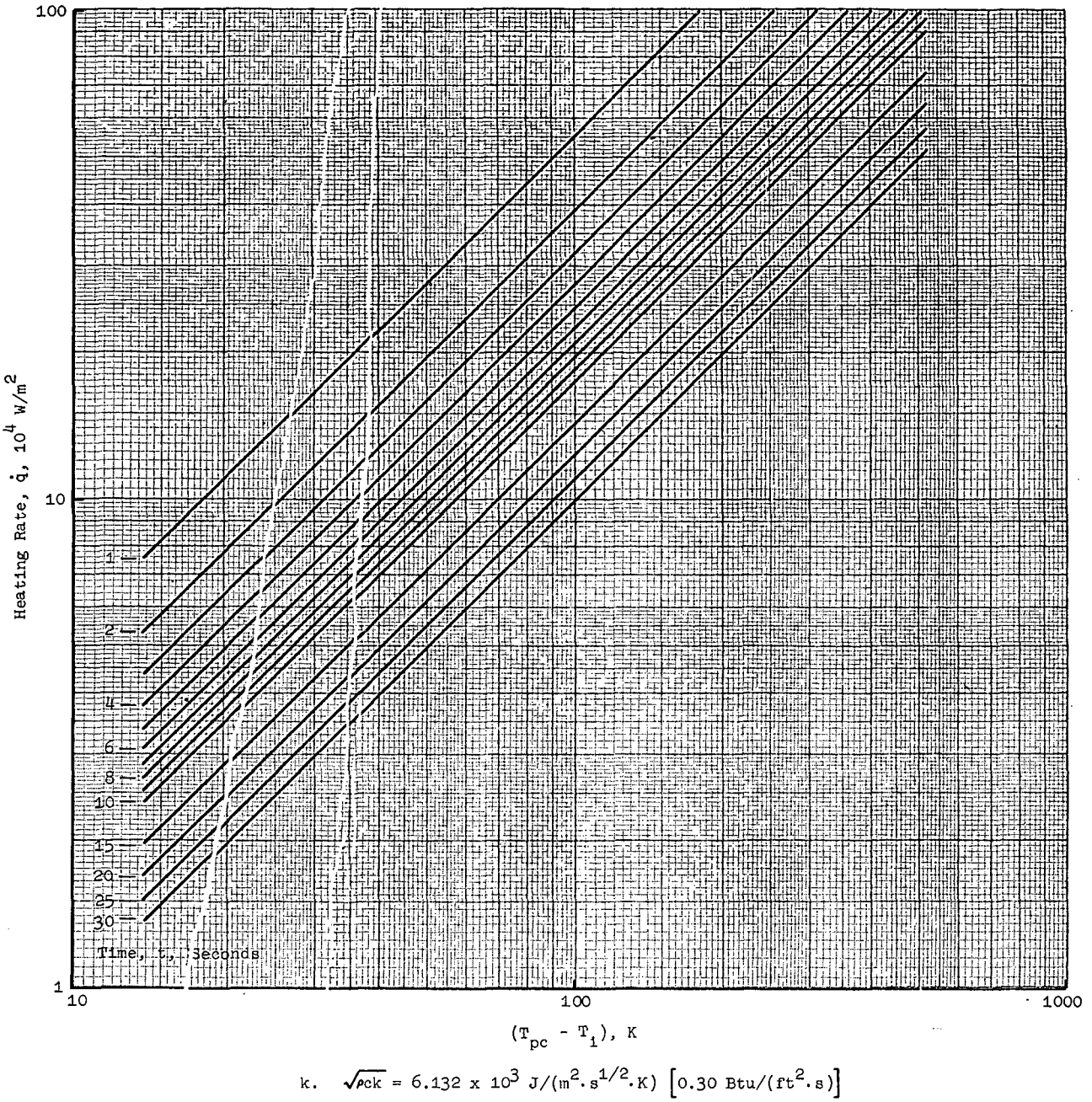

k. $\sqrt{\rho ck} = 6.132 \times 10^3$ J/(m^2.s$^{1/2}$.K) [0.30 Btu/(ft^2.s)]

Figure 8-1 One Dimensional Transient Heating in a Semi-Infinite Solid Subjected to a Step Input of Constant Heating Rate at the Surface, $\left[\dot{q} = \sqrt{\rho ck}\,(\sqrt{\pi/t}/2)\,(T_{pc} - T_i)\right]$, Sheet 11 of 13

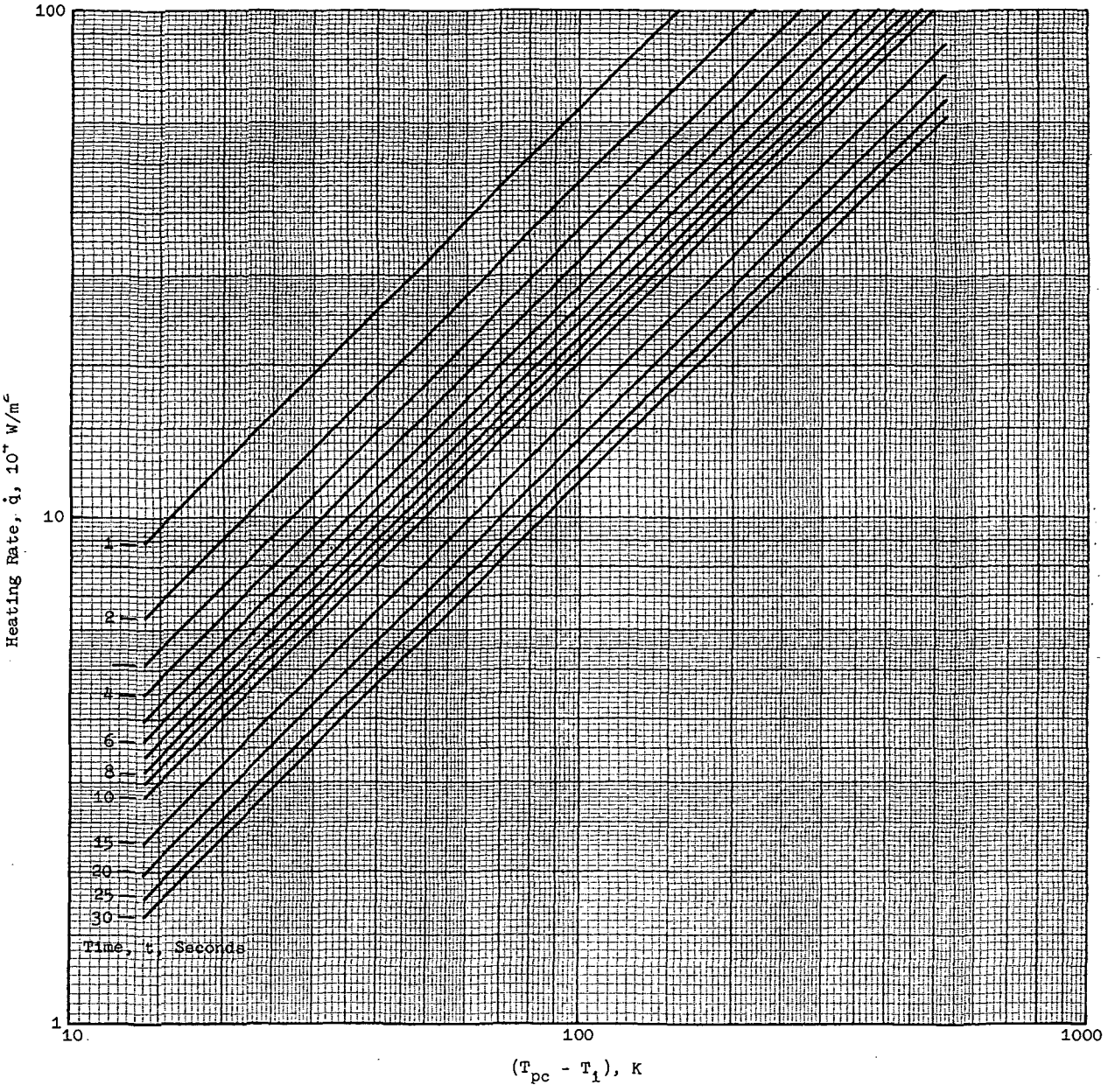

1. $\sqrt{\rho ck} = 7.154 \times 10^3$ J/(m^2.s$^{1/2}$.K) [0.35 Btu/(ft^2.s$^{1/2}$.F)]

Figure 8-1 One Dimensional Transient Heating in a Semi-Infinite Solid Subjected to a Step Input of Constant Heating Rate at the Surface $[\dot{q} = \sqrt{\rho ck}\,(\sqrt{\pi/t}/2)\,(T_{pc} - T_i)$, Sheet 12 of 13

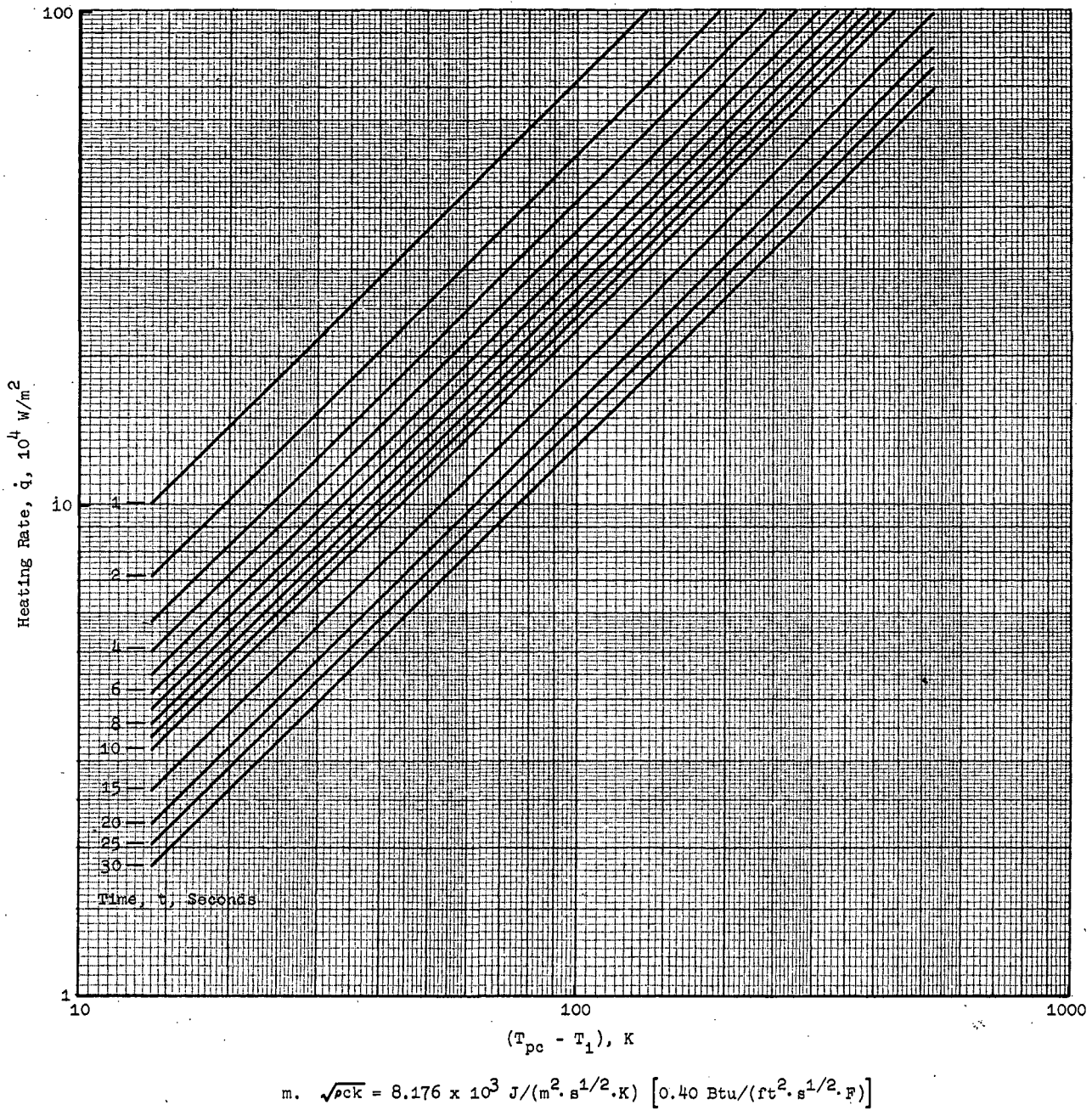

Figure 8-1 One Dimensional Transient Heating in a Semi-Infinite Solid Subjected to a Step Input of Constant Heating Rate at the Surface $\left[\dot{q} = \sqrt{\rho ck}\ (\sqrt{\pi t}/2)\ (T_{pc} - T_i)\right]$, Sheet 13 of 13

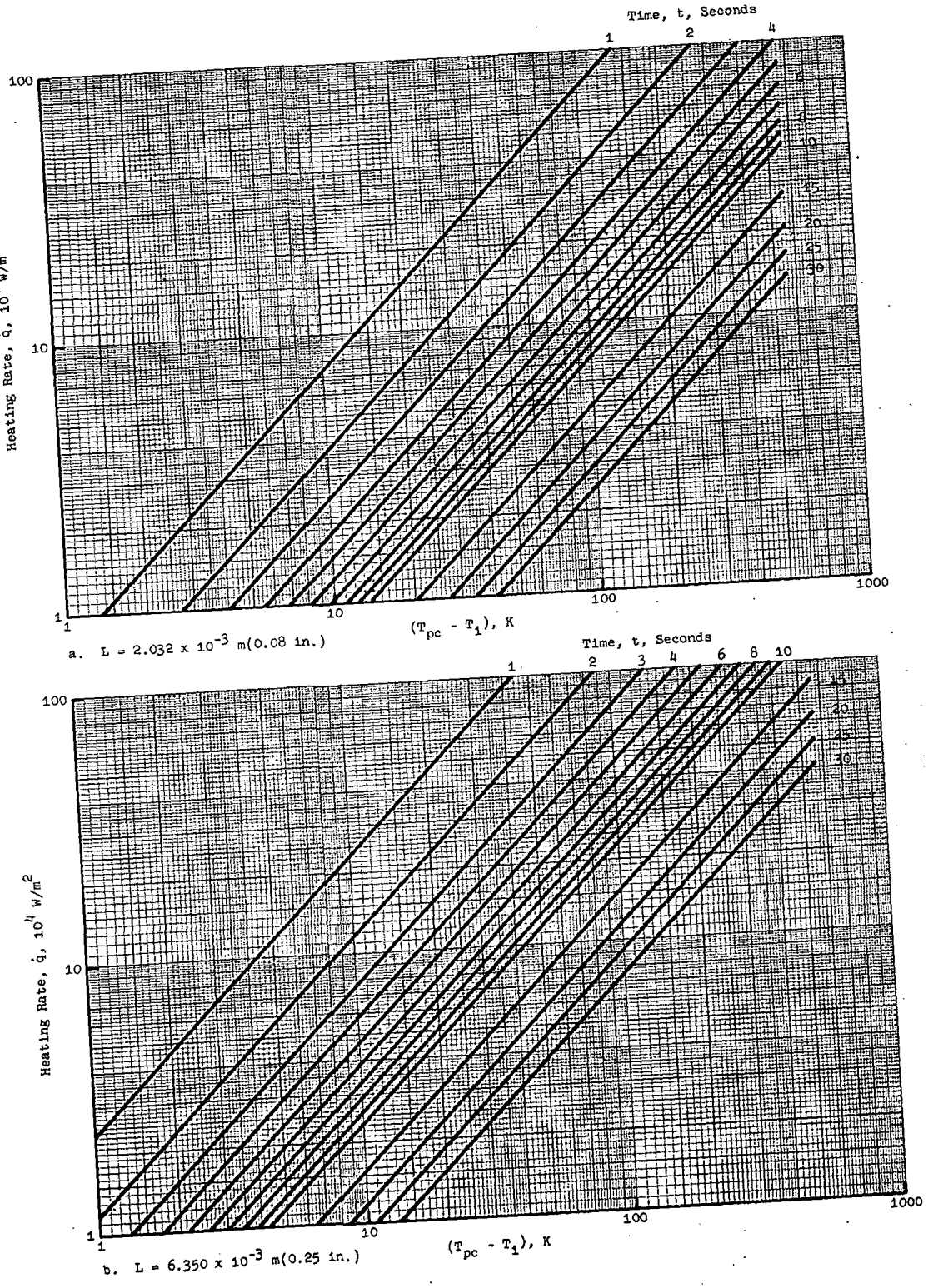

Figure 8-2 One Dimensional Transient Heating in a Copper Slug Calorimeter Subjected to a Step Input in Heating Rate at the Surface $[\dot{q} = (\rho c)_{cu} (L/t) (T_{pc} - T_i)]$, $(\rho c)_{cu} = 3.593 \times 10^6$ J/(m^3.K) [53.568 Btu/(ft^3.F)]

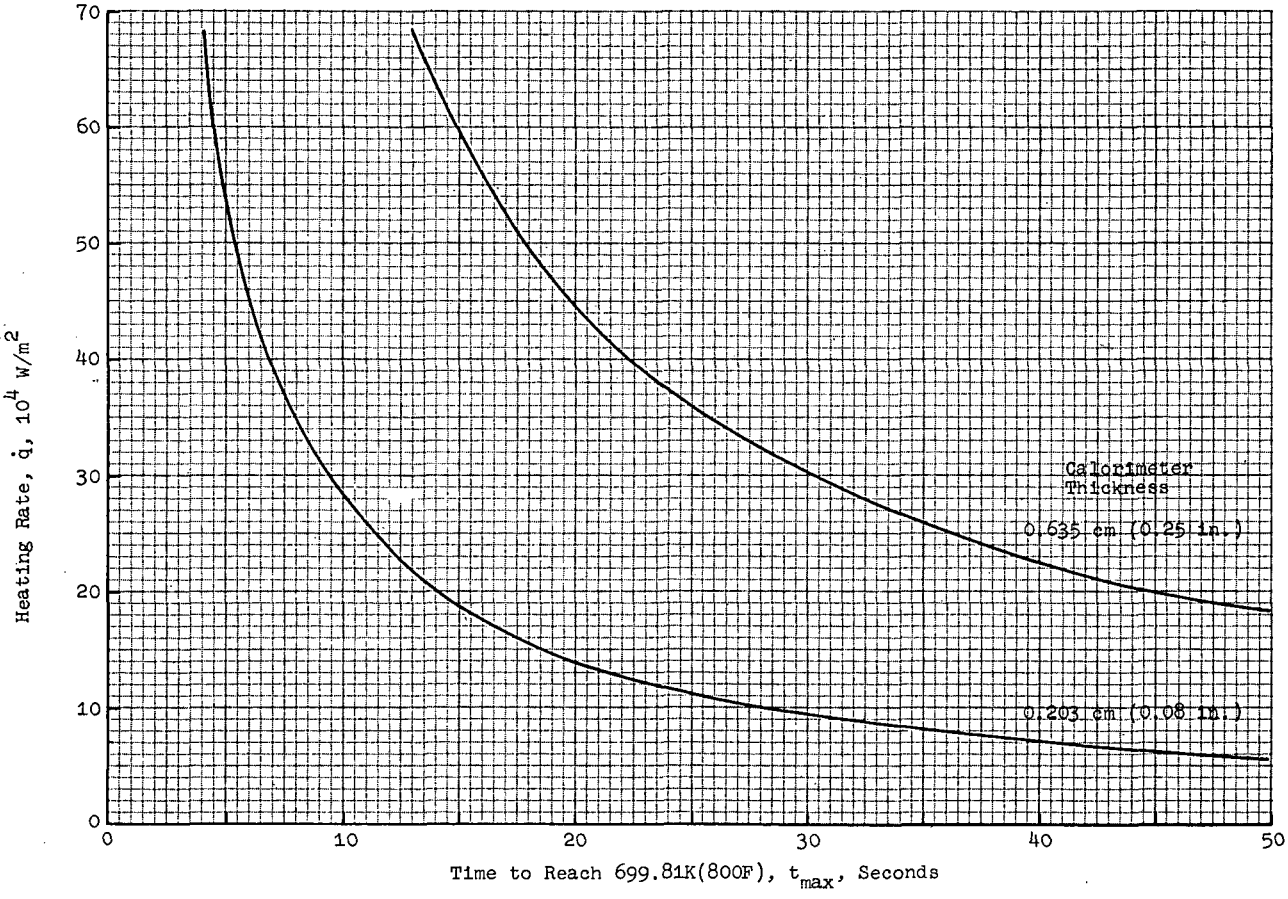

Figure 8-3 Maximum Allowable Calorimeter Test Time

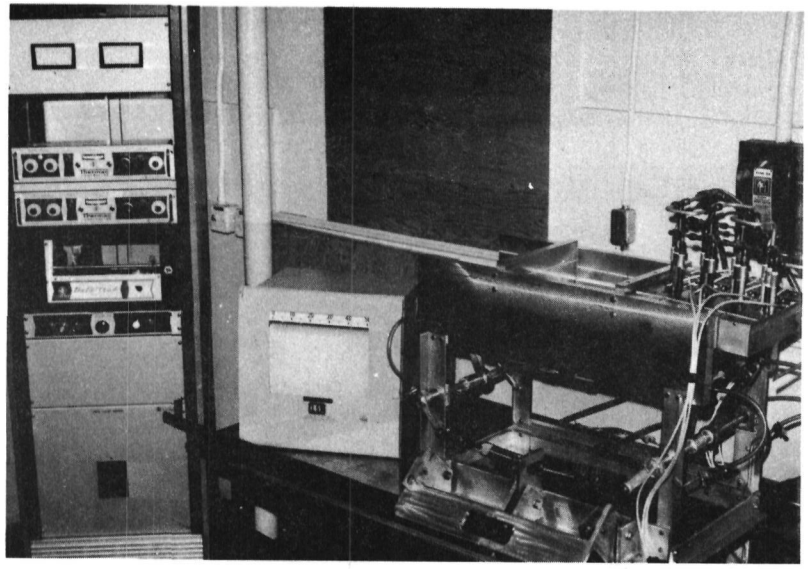

a. TPM Apparatus, Power Source and Temp Recorder

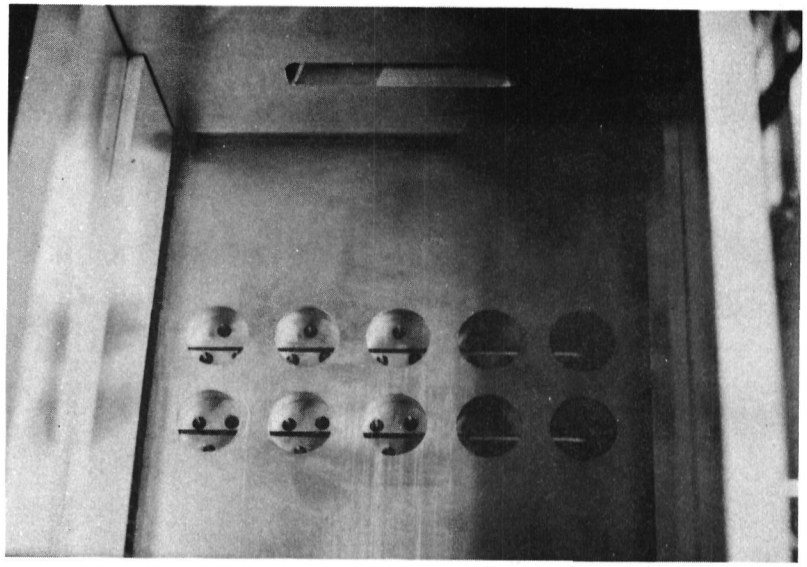

b. Test Plane and Specimen Support

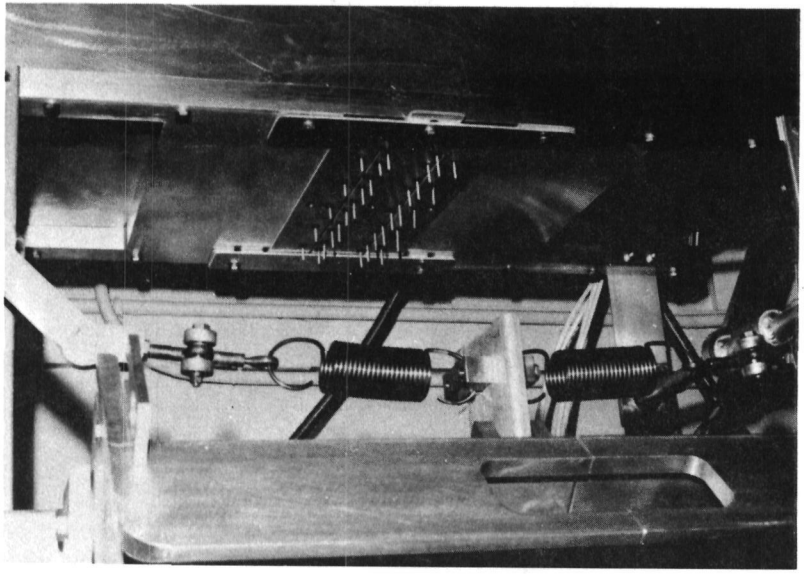

c. Stilts Protruding Through Rubber Bushing Anchored in Split Panel Arrangement Suspended Below Base Plate

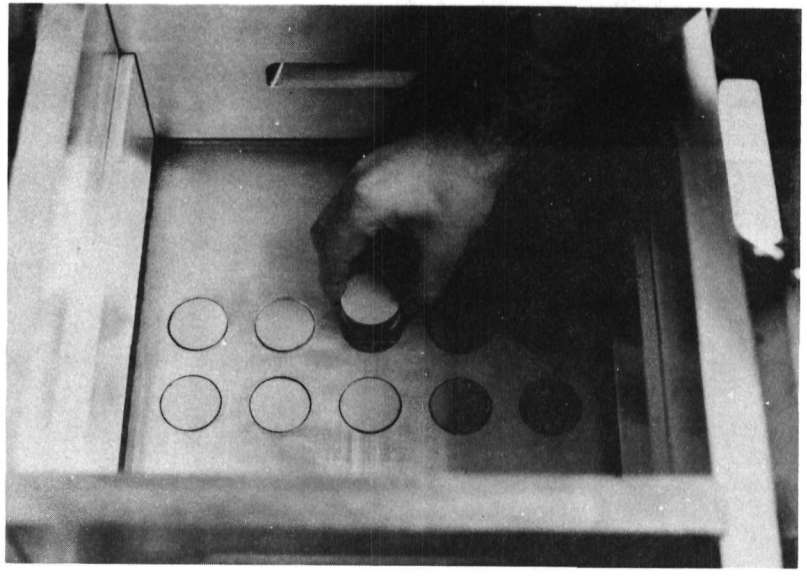

d. Tempilaq Coated Sample Placed in Mounting Hole

Figure 8-4 Test Procedure, Sheet 1 of 5

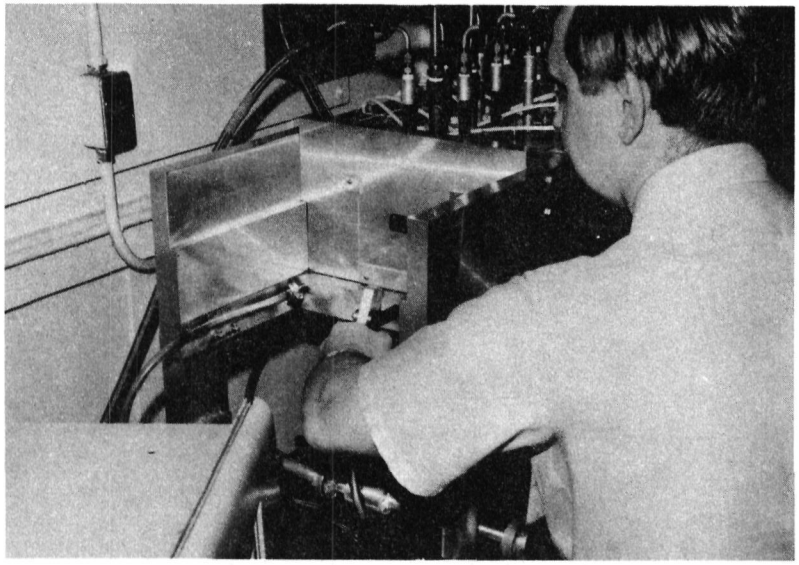

e. Manual Closing of Left Shutter

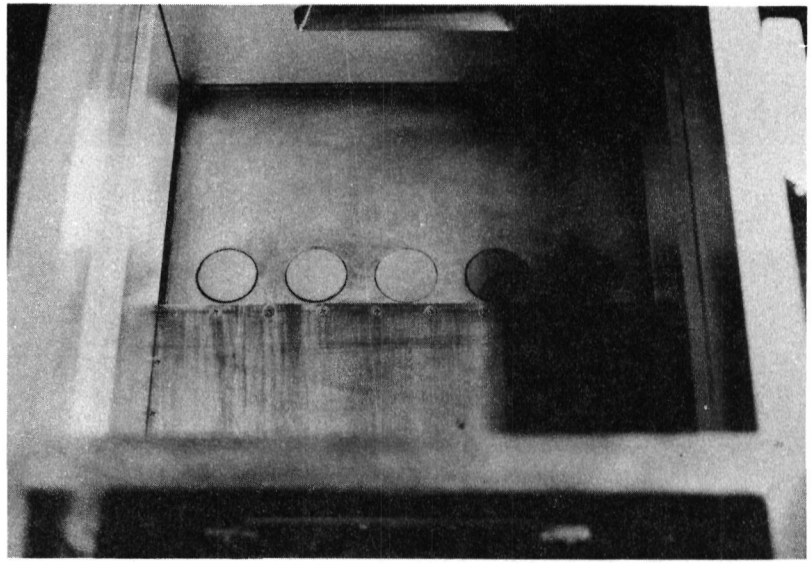

f. Left Shutter Closed

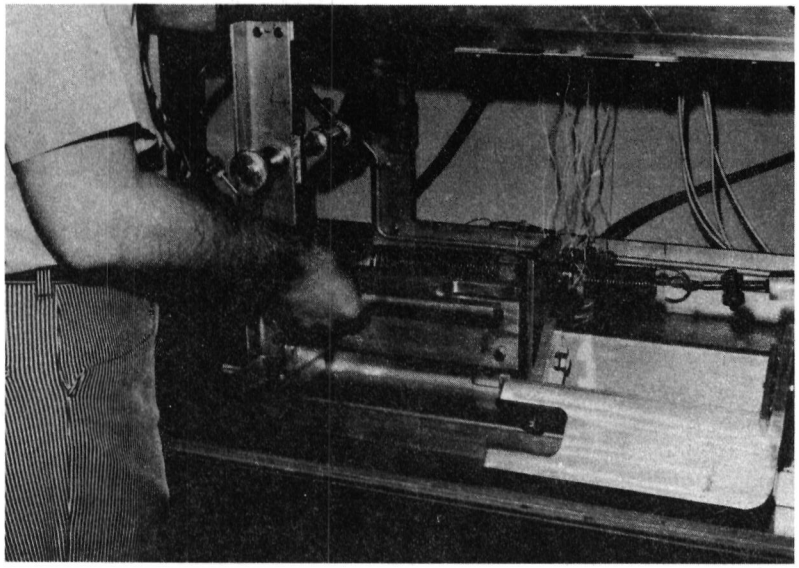

g. Left Handle Pivoted to Restrain Shutter Linkage

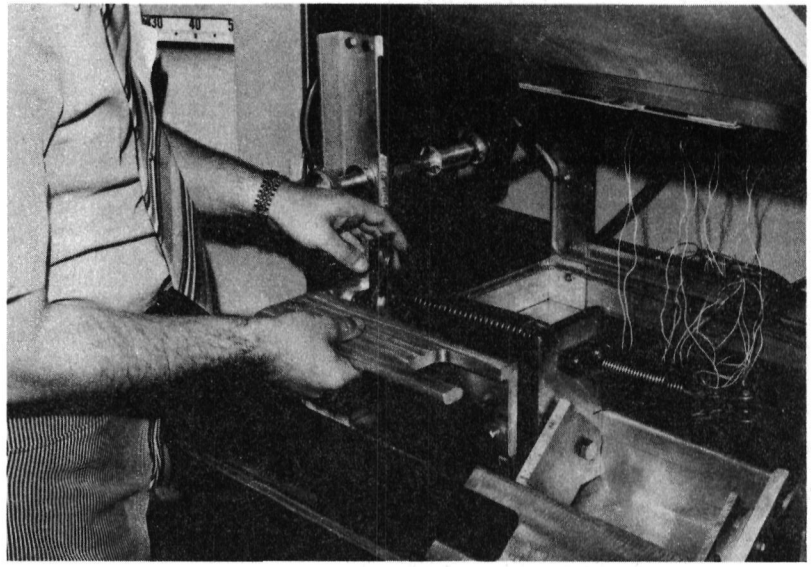

h. Left Safety Latch Pivoted to Lock Handle in Place

Figure 8-4 Test Procedure, Sheet 2 of 5

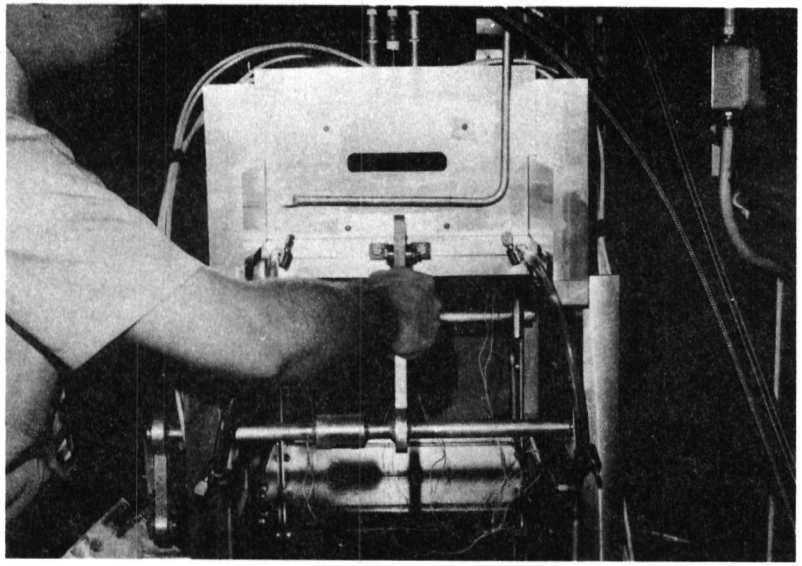

i. Manual Closing of Shutter

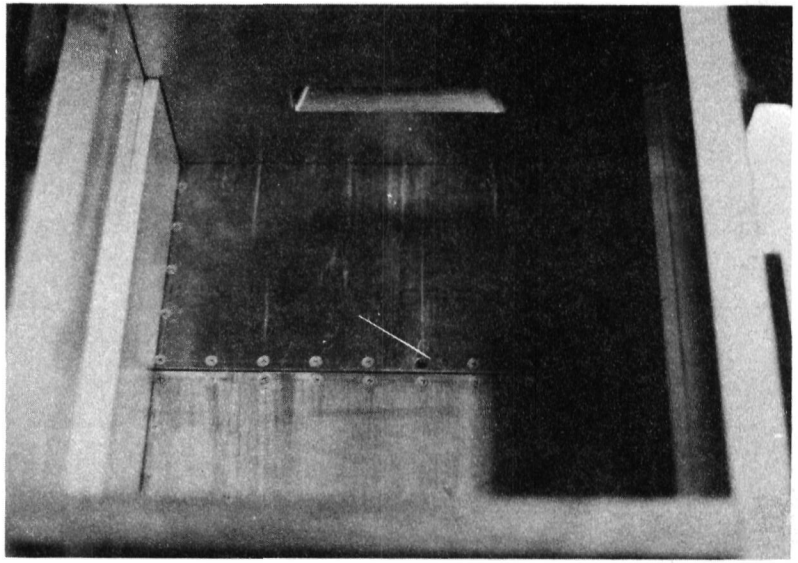

j. Shutter Closed

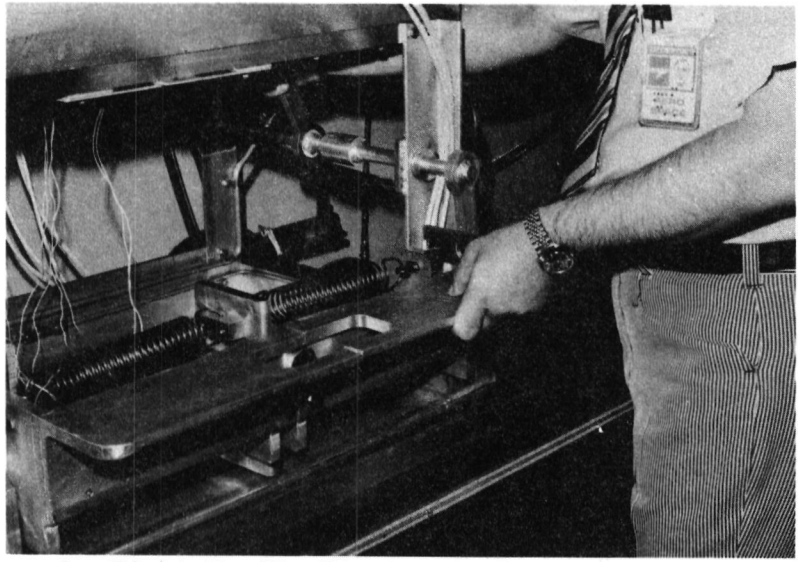

k. Right Handle Pivoted to Restrain Shutter Linkage

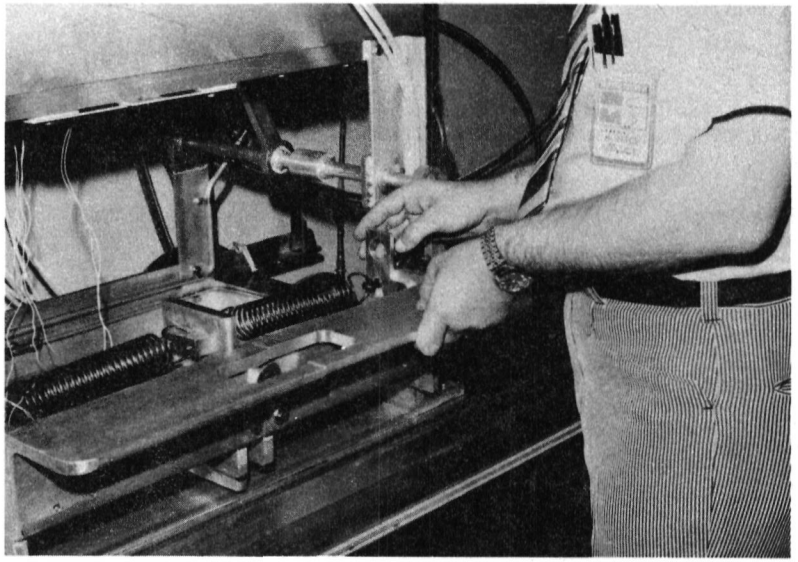

l. Right Safety Latch Locked

Figure 8-4 Test Procedure, Sheet 3 of 5

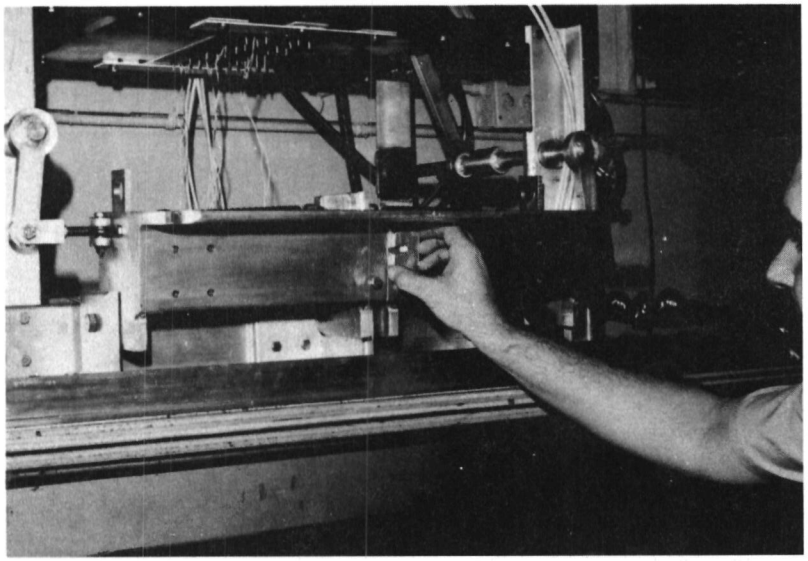

m. Rotating Interlock

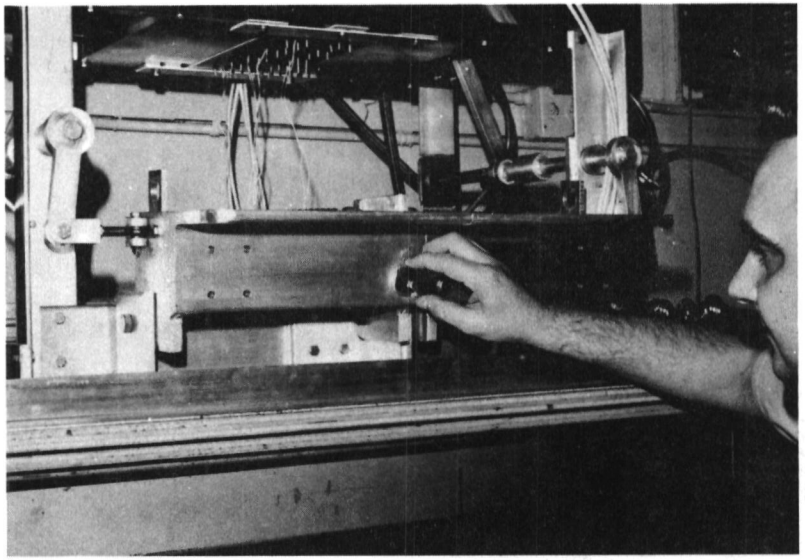

n. Interlock Rotated to Join Both Handle Pieces

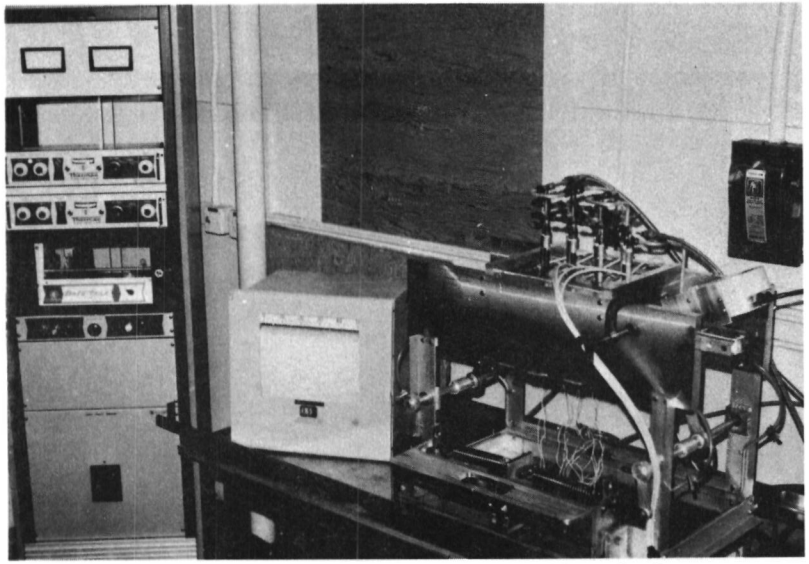

o. Motion Picture Camera Mounted to View Test Area

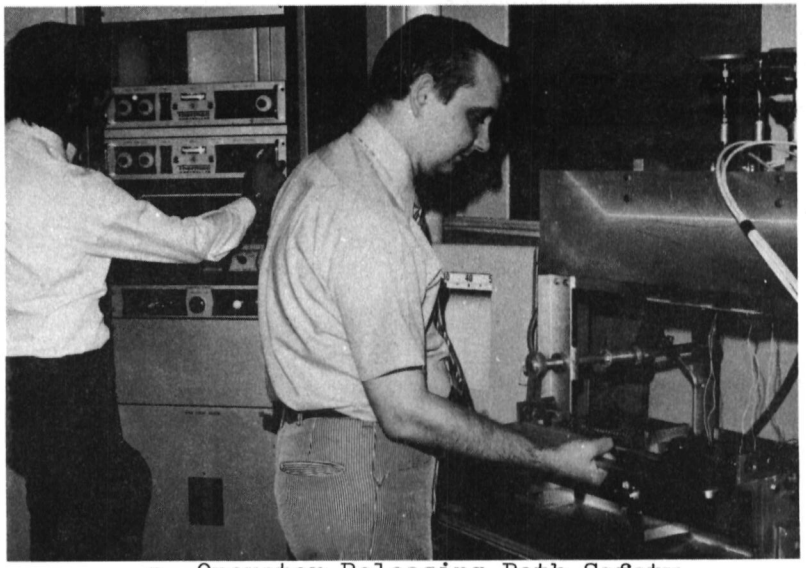

p. Operator Releasing Both Safety Latches

Figure 8-4 Test Procedure, Sheet 4 of 5

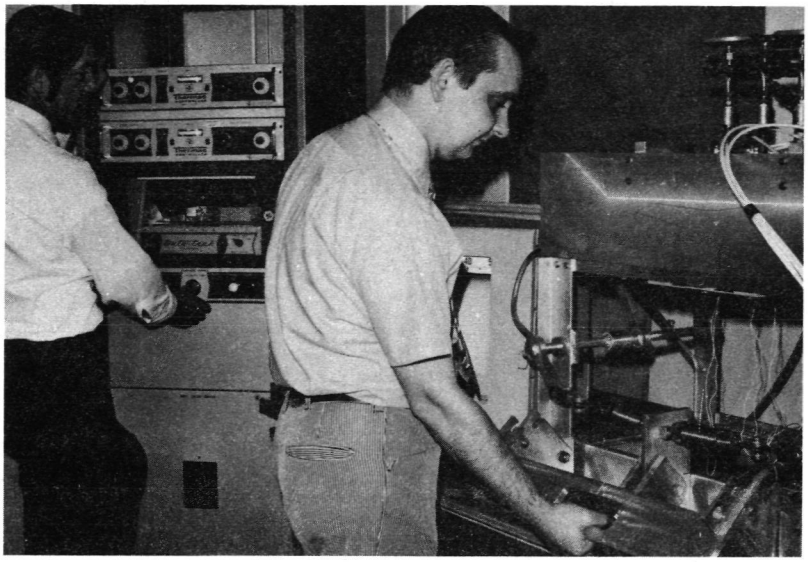

q. Releasing Shutters by Dropping Handle

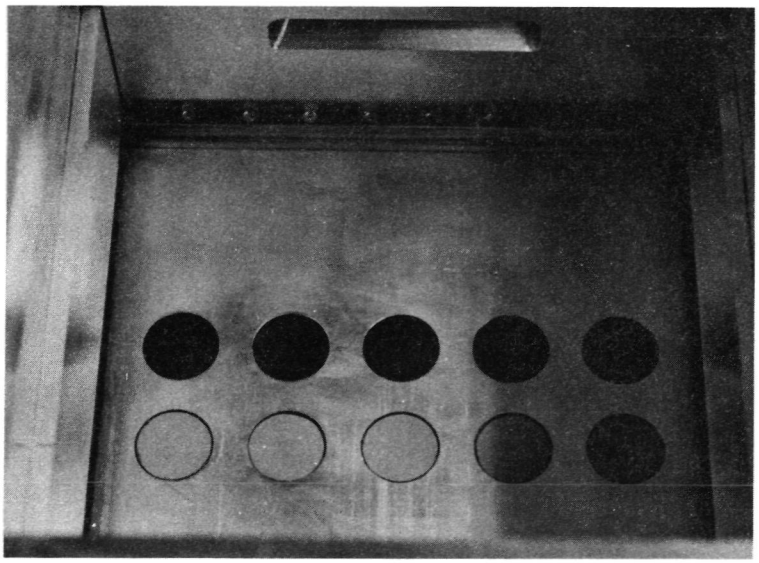

r. Power Maintained Until Sample Coatings Melt

Figure 8-4 Test Procedure, Sheet 5 of 5

Appendix A

TEST SAMPLE DESIGN AND INSTALLATION

A.1 SUMMARY

An analysis was performed to determine required design and installation characteristics of the test sample. These characteristics must enable the sample to be mounted in such a manner that no heat enters or leaves, other than through the face exposed to the lamps. The temperature response at that face thus could be calculated for a constant incident heating rate.

The initial design that was chosen was 2.382 cm (0.938 in.) in diameter and 1.905 cm (0.75 in.) thick; installation was on a three prong support, in a 2.54 cm (1.0 in.) diameter base plate hole, as shown in Figure A-1(a). The support is made from a very low conductivity material to prevent conduction losses, and provides a trapped air gap as additional insulation.

Results of the analysis showed that heat leaking into a stainless steel sample was less than 3 percent for test times up to 30 seconds (which is the maximum time before the semi-infinite slab assumption is violated). However, the effect is opposite for low conductivity plastics: heat leaking out of the sample exceeded 23 percent of the absorbed heat after 300 seconds. In order to reduce these errors, the sample diameter and gap between the sample and sample holder were increased, Figure A-1(b) shows the final sample design. This modification of the original design reduced leakage from the low conductivity plastic to 6 percent, over a 300 second test run.

A.2 DISCUSSION

The first design that was analyzed consisted of a 2.382 cm (0.938 in.) diameter, 1.905 cm (0.75 in.) thick sample mounted in a 2.54 cm (1.0 in.) thick aluminum slab on a three prong support made from a good insulating material. Two sample materials were analyzed for radiation and conduction heat loss through the sides. These sample materials, a low conductivity plastic and stainless

steel, cover a range of $\sqrt{\rho ck}$ from 0.408×10^3 to 8.176×10^3 J/($m^2 \cdot s^{\frac{1}{2}} \cdot K$) [0.02 to 0.40 Btu/($ft^2 \cdot s^{\frac{1}{2}} \cdot F$)]. The representative material properties used are listed in Table A-1.

The analysis was performed under the assumption that test time was limited to the maximum time before the semi-infinite slab assumption is violated. This time is 30 seconds for stainless steel and 300 seconds for the low conductivity plastic. The samples thus were assumed to behave as semi-infinite slabs, and to have their backfaces mounted above good insulators; since no temperature differences exist between the backfaces and the insulators, no heat transfer would exist at the backfaces. Leakage through the sides was assumed to be via radiation and conduction. Reference 3 shows that for enclosed annular air spaces, convection effects are negligible compared to conduction effects when the product of the Grashof and Prandtl numbers is less than 10^3. This criterion is applicable in this case for gaps between the sample and sample holder up to 1.524 cm (0.6 in.).

A.2.1 Radiation Leakage

The heating rate per unit area radiating from the inner to the outer cylinder of two concentric cylinders is expressed as:

$$\dot{q}_{rad} = \frac{0.477 \times 10^{-12} \, (T_i^4 - T_o^4)}{1/\varepsilon_i + (A_i/A_o)([1/\varepsilon_o] - 1)} \qquad (Btu/ft^2 \cdot s) \qquad (A-1)$$

where the subscripts i and o indicate inner and outer cylinder. Since the temperatures are not constant along the side of the sample or sample holder, the integrated value of the heating rate must be calculated:

$$\bar{\dot{q}}_{rad} = \frac{0.477 \times 10^{-12}}{1/\varepsilon_i + (A_i/A_o)([1/\varepsilon_o - 1])} \frac{1}{L} \int_0^L [T_i^4(x) - T_o^4(o)] \, dx \qquad (A-2)$$

where L is the sample thickness.

A.2.2 Conduction Leakage

The heating rate per unit area of heat conducted through the air gap, from the sample to the sample holder, is expressed as:

$$\dot{q}_{cond} = \frac{k\,(T_o - T_i)}{g} \qquad (Btu/ft^2 \cdot s) \qquad (A-3)$$

where g is the gap width and k is the thermal conductivity of air ($k = 4.36 \times 10^{-6}$ Btu/ft·s·F). As for the radiation calculation, the integrated value of the heating rate is used:

$$\bar{\dot{q}}_{cond} = \frac{k}{g}\frac{1}{L}\int_0^L [T_o(x) - T_i(x)]\,dx \qquad (A-4)$$

A.2.3 Total Heat Leakage

The total heat leakage, Q, in or out of the sample is calculated as a percentage of the absorbed heat entering through the top of the sample:

$$\frac{Q_{leak}}{Q_{abs}} = \frac{Q_{rad} + Q_{cond}}{Q_{abs}} \qquad (A-5)$$

where $Q_{rad} = \bar{\dot{q}}_{rad}\, A_i$

$Q_{cond} = \bar{\dot{q}}_{cond}\, A_i$

$Q_{abs} = \bar{\dot{q}}_{abs}\, (\pi/4)\, (D_i)^2$

Since A_i is the surface area of the side of the sample,

$$A_i = \pi D_i L$$

and Equation A-5 may be rewritten as

$$\frac{Q_{leak}}{Q_{abs}} = \frac{(\bar{\dot{q}}_{rad} + \bar{\dot{q}}_{cond})\, L}{0.25\, D_i\, \bar{\dot{q}}_{abs}} \qquad (A-6)$$

A.2.4 Temperature Distributions

The temperature distribution into the sample was calculated by approximating the solution for a constant heating rate into a semi-infinite slab. This

approximation was obtained by interpolation of a straight line on semi-log curve, Figure A-2, for the values $0 \leqq \alpha t/L^2 \leqq 0.25$. The equation of the approximate solution is:

$$T_i(x,t) = T(x,o) + \frac{1.13\ \dot{q}_{abs}\ \sqrt{\alpha t}}{k}\ e^{-2.41\ x/2\sqrt{\alpha t}}$$

Equation A-7 is suitable for closed form integration in Equations A-2 and A-4.

The temperature distribution in the aluminum sample holder was assumed uniform. Checking of the solution for a finite slab being heated at a constant heating rate showed that the ratios of the absolute temperatures on the front and back sides remained within 11 percent after 10 seconds. This narrow temperature range is due to the high conductivity of aluminum. The equation expressing the temperature is:

$$T(t) = T(o) + \frac{\dot{q}_{abs}\ \alpha t}{kL} \qquad \text{(A-8)}$$

A.3 RESULTS

The results of the analysis are presented in Table A-2. This table shows that the net heat leakage is into the stainless steel sample, and out of the low conductivity plastic sample. For both cases, the leakage increases with time as the wall temperature difference increases, but is relatively insensitive to the absorbed heating rate. Conduction effects are significantly greater than radiation effects in both cases.

For the initial design, heat leakage into the stainless steel sample was less than 2.8 percent. However, this value represents the heat leakage into the entire sample; the error at the center of the sample face is significantly less. Leakage out of the low conductivity plastic is significantly higher, reaching 23.3 percent after 300 seconds.

Two modifications were made to the sample design to reduce leakage. The between the sample and sample holder was increased from 0.078 cm (0.031 in.) .317 cm (0.125 in.) for all but a small, 0.160 cm (0.063 in.) length, re A-1(b), thereby reducing the conduction losses by a factor of four, ation A-3. A small flange was maintained at the top to keep incident heat of the space between the sample and sample holder. Increasing the sample diameter from 2.382 cm (0.938 in.) to 3.810 cm (1.5 in.) reduces the percentage of total heat leakage by a factor of 1.6. Improvements in the modified sample, Table A-2(b), are obvious.

Table A-1. Material Properties

Property	Material		
	Stainless Steel	Plastic	Aluminum
Diffusivity, α, m^2/s [ft^2/s]	3.772×10^{-6} [40.6×10^{-6}]	0.0353×10^{-6} [0.38×10^{-6}]	71.628×10^{-6} [771×10^{-6}]
Conductivity, k, W/(m·K) [Btu/(ft·s·F)]	16.013 [25.7×10^{-4}]	0.0754 [0.121×10^{-4}]	160.751 [258×10^{-4}]
Density, ρ, kg/m^3 [lb/ft^3]	8.265×10^3 [516]	2.130×10^3 [133]	2.627×10^3 [164]
Emissivity, ε	0.55	0.90	0.18

Table A-2. Sample Heat Leakage

Material	$\dot{q}_{abs}$, 10^4 W/m^2 (Btu/[ft^2·s])	Time, Seconds	$\bar{\dot{q}}_{rad}$, W/m^2(10^{-4} Btu/[ft^2·s])	$\bar{\dot{q}}_{cond}$, W/m^2 (10^{-4} Btu/[ft^2·s])	Q_{rad}/Q_{abs}, percent	Q_{cond}/Q_{abs}, percent	Q_{leak}/Q_{abs}, percent
Original Sample Design: 2.382 cm (0.938 in.) Diameter							
Stainless Steel	1.135 (1.0)	10	-0.363 (-0.32)	-24.757 (-21.8)	-0.01	-0.72	-0.73
		20	-1.249 (-1.1)	-53.375 (-47.0)	-0.03	-1.55	-1.58
		30	-2.044 (-1.8)	-85.855 (-75.6)	-0.06	-2.50	-2.56
	11.356 (10)	10	-5.451 (-4.8)	-244.164 (-215.0)	-0.02	-0.71	-0.73
		20	-15.104 (-13.3)	-530.348 (-467.0)	-0.04	-1.54	-1.58
		30	-28.618 (-25.2)	-856.280 (-754.0)	-0.08	-2.50	-2.58
	56.782 (50)	10	-27.369 (-24.1)	-1217.416(-1072.0)	-0.02	-0.71	-0.73
		20	-155.016 (-136.5)	-2654.014(-2337.0)	-0.09	-1.54	-1.63
		30	-459.256 (-404.4)	-4304.113(-3790.0)	-0.26	-2.50	-2.76
Low Conductivity Plastic	1.135 (1.0)	10	1.589 (1.4)	21.009 (18.5)	0.04	0.61	0.65
		100	42.586 (37.5)	213.502 (188.0)	1.20	6.20	7.40
		300	180.227 (158.7)	635.964 (560.0)	5.06	18.20	23.26
Modified Sample Design: 3.810 cm (1.5 in.) Diameter							
Stainless Steel	1.135 (1.0)	10	-0.363 (-0.32)	-6.189 (-5.45)	-0.01	-0.11	-0.12
		20	-1.249 (-1.1)	-13.343 (-11.75)	-0.02	-0.24	-0.26
		30	-2.044 (-1.8)	-21.463 (-18.90)	-0.04	-0.38	-0.42
	11.356 (10)	10	-5.451 (-4.8)	-61.041 (-53.75)	-0.01	-0.11	-0.12
		20	-15.104 (-13.3)	-132.587 (-116.75)	-0.03	-0.23	-0.26
		30	-28.618 (-25.2)	-214.070 (-188.50)	-0.05	-0.38	-0.43
	56.782 (50)	10	-27.369 (-24.1)	-304.354 (-268.00)	-0.05	-0.11	-0.16
		20	-155.016 (-136.5)	-663.503 (-584.25)	-0.27	-0.23	-0.50
		30	-459.256 (-404.4)	-1073.189 (-945.00)	-0.81	-0.38	-1.19
Low Conductivity Plastic	1.135 (1.0)	10	1.589 (1.4)	5.258 (4.63)	0.03	0.09	0.12
		100	42.586 (37.5)	53.375 (47.00)	0.75	0.94	1.69
		300	180.227 (158.7)	158.991 (140.00)	3.17	2.80	5.97

Dimensions in Centimeters

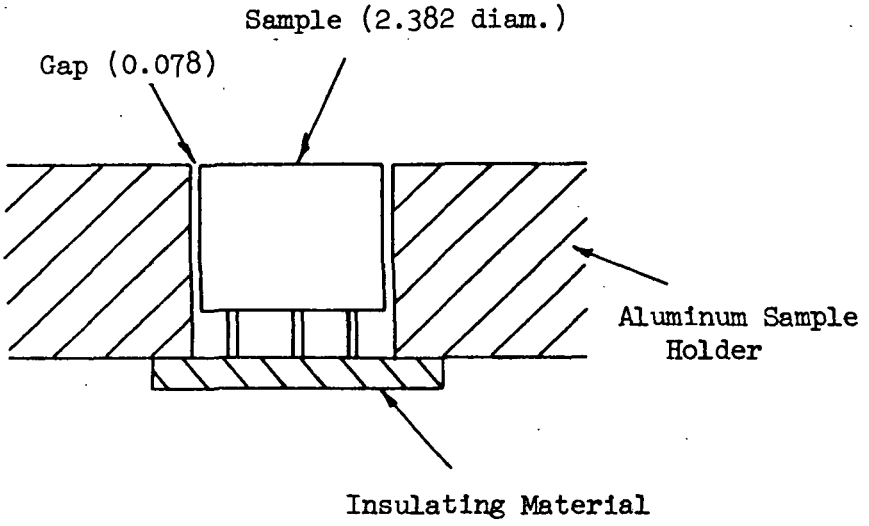

a. Original

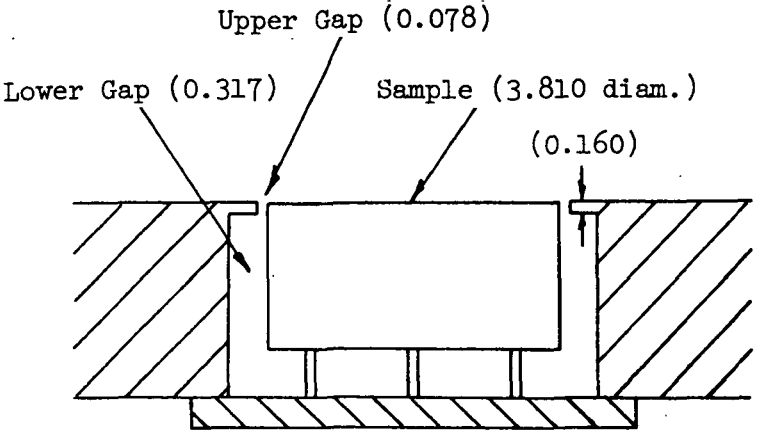

b. Final

Figure A-1 Sample Design and Installation

Note: Data Points Represent Exact Solution

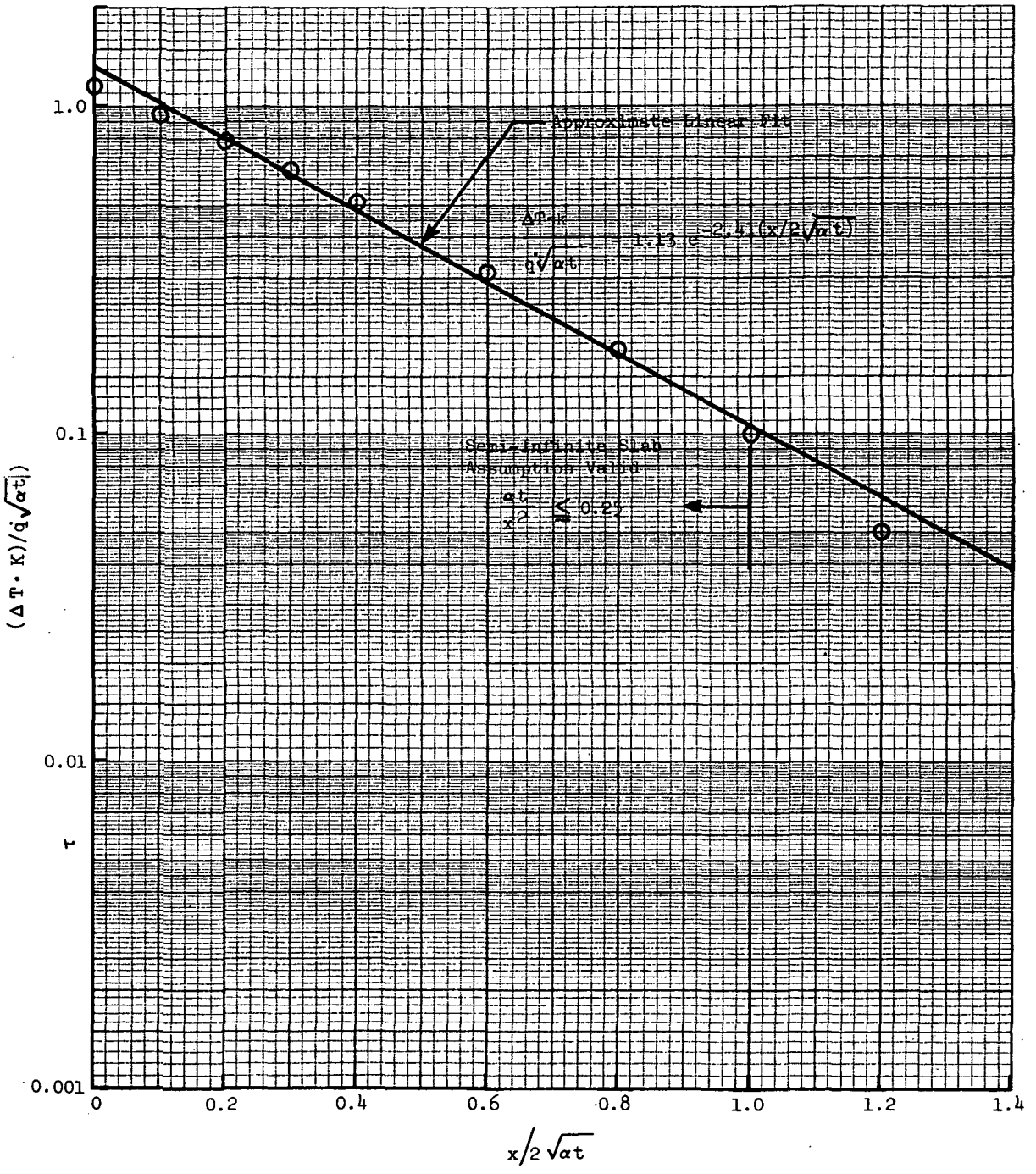

Figure A-2 Temperature Response of a Semi-Infinite Slab Heated by a Constant Heat Flux

Appendix B

CALORIMETER DESIGN

B.1 SUMMARY

An analysis performed to determine proper calorimeter design showed that at least three sizes are required. Thicknesses of 0.203 cm (0.08 in.), 0.635 cm (0.25 in.), and 1.270 cm (0.50 in.) are needed to cover the range of sample thermophysical properties: $0.408 \times 10^3 \leq \sqrt{\rho c k} \leq 8.176 \times 10^3$ J/($m^2 \cdot s^{\frac{1}{2}} \cdot K$) [$0.02 \leq \sqrt{\rho c k} \leq 0.40$ Btu/($ft^2 \cdot s^{\frac{1}{2}} \cdot F$)] and incident heating rates: $1.135 \times 10^4 \leq \dot{q}_i \leq 113.565 \times 10^4$ W/m^2 [$1 \leq \dot{q}_i \leq 100$ Btu/($ft^2 \cdot s$)]. Each calorimeter is 3.810 cm (1.5 in.) in diameter, and is mounted in the sample holder in the same manner as the samples. The calorimeters consist of pure copper slugs, insulated with a thin layer of h-film and instrumented with backface thermocouples.

B.2 DISCUSSION

Since the calorimeter is used to measure sample heating rate, it must be of high accuracy. The following five criteria were established to meet the accuracy requirements:

1. The calorimeter must be of the same diameter as the sample so that when each is located in zones of similar heating, the calorimeter measures the sample average heating rate.
2. Calorimeter temperature distribution should be as uniform as possible.
3. Heat leaking in or out of the sides of the calorimeter should be minimized.
4. The calorimeter surface temperature should always lag behind that of the sample so that the coating on the sample changes phase before the coating on the calorimeter.

5. Calorimeter temperature rise should be sufficiently large and fast for accurate heating rate readings to be made.

B.2.1 Material

Pure copper was chosen for calorimeter fabrication because of its high value of thermal conductivity, availability in a very pure form, and fully documented properties. The high value of conductivity helps to insure a uniform temperature distribution; the purity and full documented properties eliminate the need for calibration. The following property values are used in this analysis:

- Conductivity, k = 115.382 W/(m·K) [0.060 Btu/(ft·s·F)]
- Density, ρ, = 9595.059 kg/m^3 [559 lb/ft^3]
- Specific Heat, c, = 118.238 J/(kg·K) [0.0915 Btu/(lb·F)]
- Diffusivity, α, = 1.124 x 10^{-4} m^2/s [0.00121 ft^2/s]

B.2.2 Time to Reach Phase-Change Temperature

Based on criteria 4, the time required for the calorimeter surface to reach the phase-change temperature of a tempilaq coating must be greater than that for a similarly coated sample. Assuming that the sample heats up as a semi-infinite slab, and that the calorimeter heats up as a mass of uniform temperature, the time for each surface to reach the phase-change temperature can be expressed as

Sample:

$$t_{sam} = (T_{pc} - T_i)^2 \frac{\pi}{4} \frac{\rho c k}{\dot{q}^2} \qquad \text{(B-1)}$$

Calorimeter:

$$t_{cal} = (T_{pc} - T_i) \frac{\rho c L}{\dot{q}} \qquad \text{(B-2)}$$

Since $t_{cal} \geq t_{sam}$, the thickness of the calorimeter may be expressed

$$L \geq \frac{T_{pc} - T_i}{\dot{q}} \frac{\pi}{4} \frac{(\rho ck)_{sam}}{(\rho c)_{cal}} \qquad \text{(B-3)}$$

or

$$L \geq \frac{\sqrt{\pi}}{2} \frac{(\sqrt{\rho ck})_{sam} \sqrt{t_{sam}}}{(\rho c)_{cal}} \qquad \text{(B-4)}$$

Since the thickness is proportional to the square root of time, the minimum calorimeter thickness required is based on the maximum test time. Maximum test time is defined as the time at which the semi-infinite slab assumption is violated for the sample; this time is derived from the equation

$$\left[\frac{\alpha t}{L^2}\right]_{sam} \leq 0.30 \qquad \text{(B-5)}$$

By substituting Equation B-5 into Equation B-4, the required calorimeter thickness can be defined as a fraction of the sample thickness, L_{sam}:

$$\frac{L_{cal}}{L_{sam}} \geq 0.486 \frac{(\rho c)_{sam}}{(\rho c)_{cal}} \qquad \text{(B-6)}$$

The ρc product of most materials that will be tested varies from about 41.398×10^4 to 132.476×10^4 J/(m^3·K) [20 to 64 Btu/(ft^3·F)]. For the worst case, the required calorimeter thickness, L_{cal}, for a sample of 1.905 cm (0.75 in.) thickness must be greater than 1.168 cm (0.46 in.).

B.2.3 Backface Temperature Response

Though the calorimeter temperature distribution is assumed constant, a finite temperature difference does exist between the top, where it is heated,

and the backface, where the thermocouple is located. The error in assuming a uniform temperature distribution can be calculated by dividing the temperature rise at the backface by that of a body which behaves like a thin skin. Backface temperature response, Figure B-1, shows that the parameter $(T - T_i)k/\dot{q}\sqrt{\alpha t}$ is a function of $\sqrt{\alpha t/L^2}$. Thus,

$$T - T_i = \dot{q} \frac{\sqrt{\alpha t}}{k} \; f(\sqrt{\alpha t/L^2}) \tag{B-7}$$

Dividing Equation B-7 by Equation B-2, the error can be calculated as

$$\frac{(T - T_i)_{\text{backface}}}{(T - T_i)_{\text{thin skin}}} = \frac{f(\sqrt{\alpha t/L^2})}{\sqrt{\alpha t/L^2}} \tag{B-8}$$

Figure B-2 presents the error as a function of Fourier number, $\alpha t/L^2$, and also shows the relationship between heating time and error for copper calorimeters of 0.635 cm (0.25 in.) and 1.270 cm (0.50 in.) thicknesses. This figure shows that for a 1.270 cm (0.50 in.) thick calorimeter, the error is less than 5 percent only after four seconds of heating, the error may be reduced by decreasing calorimeter thickness.

B.2.4 Calorimeter Temperature Rise

The rate of calorimeter temperature rise and its final, overall temperature influences the accuracy of the heating rate measurement. Equation B-2 shows that the rate of temperature rise is directly proportional to the heating rate and inversely proportional to the calorimeter thickness. The increase in calorimeter temperature for the time it takes the sample surface to reach phase-change temperature can be calculated by combining Equations B-1 and B-2:

$$T - T_i = \frac{(T_{pc} - T_i)^2}{\dot{q}} \; \frac{\pi}{4} \; \frac{(\rho c k)_{\text{samp}}}{(\rho c L)_{\text{cal}}} \tag{B-9}$$

This equation shows that the samllest temperature rise occurs when samples with low values of ρck are tested using a low temperature phase-change coating and high heating rates. Reducing calorimeter thickness increases the temperature rise.

From Equation B-1, a sample for which $\sqrt{\rho ck} = 0.408 \times 10^3$ J/($m^2 \cdot s^{\frac{1}{2}} \cdot K$) [0.02 Btu/($ft^2 \cdot s^{\frac{1}{2}} \cdot F$)], coated with 533.15 K (500 F) phase-change coating, can be tested for 58 seconds with a heating rate of 1.135×10^4 W/m^2 (1.0 Btu/[$ft^2 \cdot s$]) or for 5 seconds with a heating rate of 3.861×10^4 W/m^2 (3.4 Btu/[$ft^2 \cdot s$]). The calorimeter temperature rise for these conditions, with L_{cal} = 1.168 cm (0.46 in.), are

Time, t (sec)	T_{pc}, K (F)	$T - T_i$, K (F)	dT/dt, K/s (F/s)
5	533.15 (500)	4.83 (8.7)	0.96 (1.74)
58	533.15 (500)	16.66 (30.0)	0.28 (0.51)

In both cases the overall temperature rise is low and should be increased by decreasing calorimeter thickness. Since the calorimeter size, L_{cal} = 1.168 cm (0.46 in.), was selected for a material with a very high value of ρck and tested for the maximum time (as defined in Equation B-5), more than one calorimeter would be required for materials with low values of ρck. However, the minimum calorimeter thickness can be reduced if the test time is reduced. Figure B-3 shows minimum calorimeter thickness as a function of test time, calculated as a percentage of the maximum test time for a given sample; maximum test time is defined by Equation B-5.

The calculations show that though a 1.168 cm (0.46 in.) thick calorimeter heated at 3.861×10^4 W/m^2 (3.4 Btu/[$ft^2 \cdot s$]) for 5 seconds has a 4.83 K (8.7 F) temperature rise, a 27.77 K (50 F) temperature rise is obtained under the same conditions with a 0.203 cm (0.203 cm (0.08 in.) thick calorimeter. This latter temperature rise is more desirable. As shown in Figure B-3, a 0.203 cm (0.08 in.) thick calorimeter (L_{cal}/L_{sam} = 0.107) would allow materials with ρc products up to 74.517×10^4 J/($m^3 \cdot K$) [36 Btu/($ft^3 \cdot F$)] to be tested for at least 10 percent of the maximum test time; for $74.517 \times 10^4 \leq \rho c \leq 132.476 \times 10^4$ J/($m^3 \cdot K$) [$36 \leq \rho c \leq 64$ Btu/($ft^3 \cdot F$)], a third calorimeter would be required for

medium to high heating rates, which produce overall temperature rises too large for the 0.203 cm (0.08 in.) thick calorimeter to measure. A 0.635 cm (0.25 in.) thickness (L_{cal}/L_{sam} = 0.333) is a logical choice since samples with ρc products up to 144.895 x 10^4 J/(m^3·K) [70 Btu/(ft^3·F)] could be tested for at least 25 percent of the maximum time.

B.2.5 Heat Leakage

Heat can leak in or out of the calorimeter through the side and bottom via radiation and conduction through the air gap (see Appendix A). Unlike the sample, where the backface never heats up, the temperature distribution in the calorimeter is uniform; the backface can heat up and radiate. This unfavorable condition for heat leakage requires that both the backface and sides be insulated. A suitable radiation barrier is aluminized h-film (emissivity = 0.05), which can be applied in 0.0127 mm (0.0005 in.) layers. This film is sufficiently thin that the thermal mass of the calorimeter is not affected. The one constraint that the h-film does impose, however, is that the maximum temperature of the calorimeter should not exceed 699.81 K (800 F). Maximum test time thus is limited by this constraint at each heating rate and calorimeter thickness, Figure B-4. An additional requirement is that the h-film be installed on the walls of the sample holder where the calorimeter is installed.

Estimates for the heat leakage are given in Table B-1. (These data are plotted in Figure 5-4.) These estimates were made based on the assumption that the calorimeter is mounted in the sample holder in the same manner as the sample. The 1.270 cm (0.50 in.) thick calorimeter shows very little error, but at low heating rates lengthy test times are needed to produce adequate temperature rises. Leakage rates for the 0.203 cm (0.08 in.) and 0.634 cm (0.25 in.) thick calorimeters are significantly higher due to the large conduction losses. These losses occur because the gap between the calorimeter and holder, which is 0.078 cm (0.031 in.) for the first 0.160 cm (0.063 in.) of thickness, widens to 0.317 cm (0.125 in.) for the remainder. Since 0.160 cm (0.063 in.) is a greater percentage of the overall thickness of the 0.203 cm (0.08 in.) and

0.635 cm (0.25 in.) calorimeters than of the 1.270 cm (0.50 in.) calorimeter, the percentage heat loss is greater. By limiting test time, calorimeter heat losses can be held within 2.1 percent.

Table B-1 Calorimeter Heat Leakage

$\dot{q}$, 10^4 W/m^2(Btu/[ft^2·s])	Time, s	$\left[\frac{Q_{rad}}{Q_{abs}}\right]$ side, percent	$\left[\frac{Q_{rad}}{Q_{abs}}\right]$ back-face, percent	$\left[\frac{Q_{cond}}{Q_{abs}}\right]$ side, percent	$\frac{Q_{leak}}{Q_{abs}}$, percent
Thickness = 1.270 cm (0.50 in.)					
102.208 (90)	10	0.01	0.01	0.09	0.11
	15	0.02	0.02	0.13	0.17
45.426 (40)	10	0.00	0.01	0.09	0.10
	20	0.02	0.02	0.17	0.21
	40	0.08	0.08	0.34	0.50
1.135 (1)	100	0.02	0.04	0.86	0.92
	200	0.05	0.09	1.71	1.84
	300	0.10	0.15	2.57	2.82
Thickness = 0.635 cm (0.25 in.)					
45.426 (40)	10	0.02	0.02	0.46	0.50
	20	0.07	0.08	0.92	1.07
22.713 (20)	10	0.01	0.01	0.46	0.48
	30	0.07	0.08	1.38	1.53
	50	0.26	0.28	2.30	2.84
1.135 (1)	40	0.02	0.03	4.60	4.65
	100	0.06	0.09	9.20	9.35
	200	0.18	0.23	18.40	18.81
Thickness = 0.203 cm (0.08 in.)					
22.713 (20)	5	0.01	0.02	0.44	0.47
	10	0.03	0.09	0.88	1.00
9.085 (8)	5	0.01	0.02	0.44	0.47
	10	0.01	0.04	0.88	0.93
	20	0.05	0.14	1.76	2.05
	30	0.11	0.35	2.63	3.09
1.135 (1)	20	0.02	0.05	1.76	1.83
	40	0.04	0.12	3.51	3.67
	60	0.07	0.21	5.27	5.55
	100	0.15	0.47	8.78	9.40

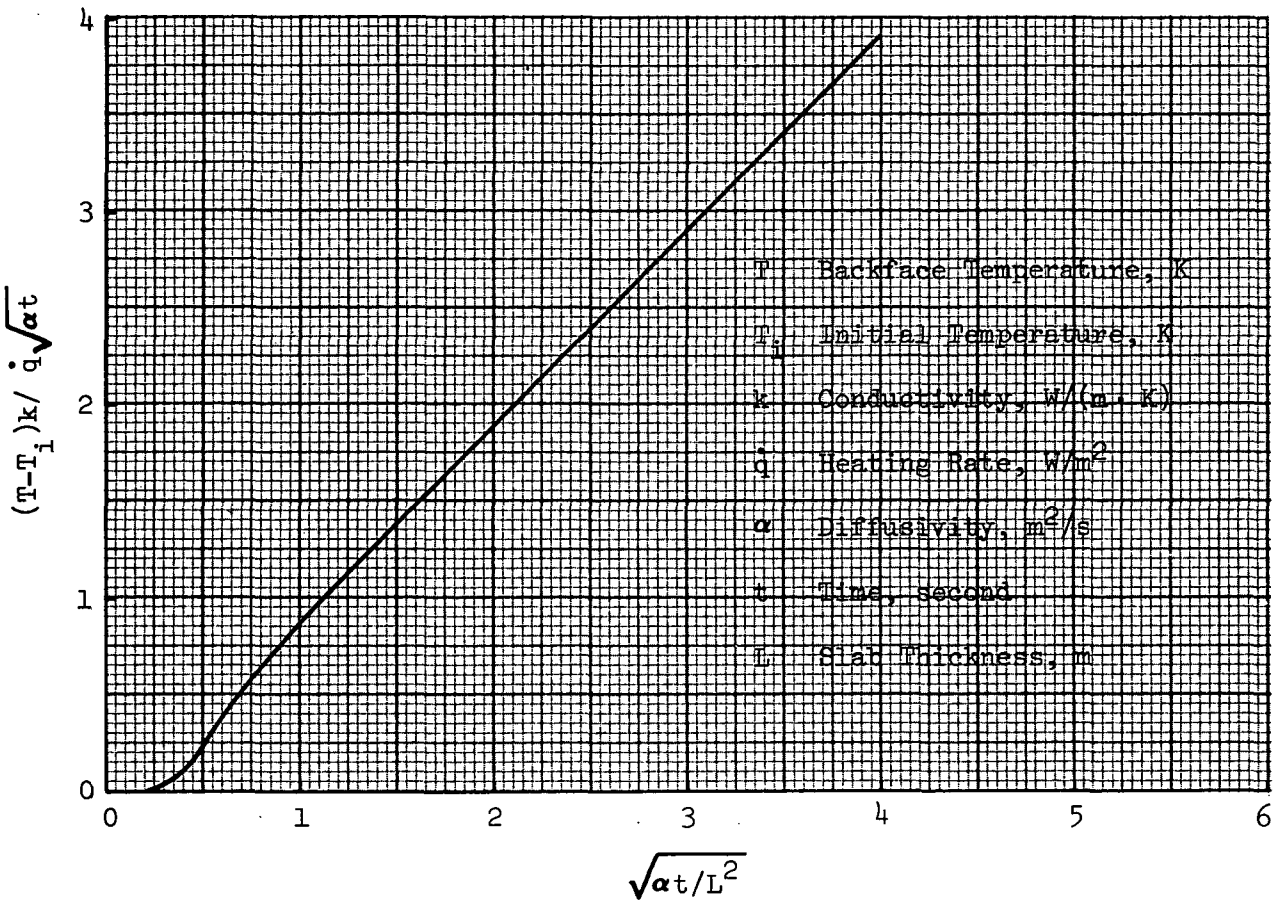

Figure B-1 Backface Response of a Slab of Finite Thickness Heated at a Constant Rate

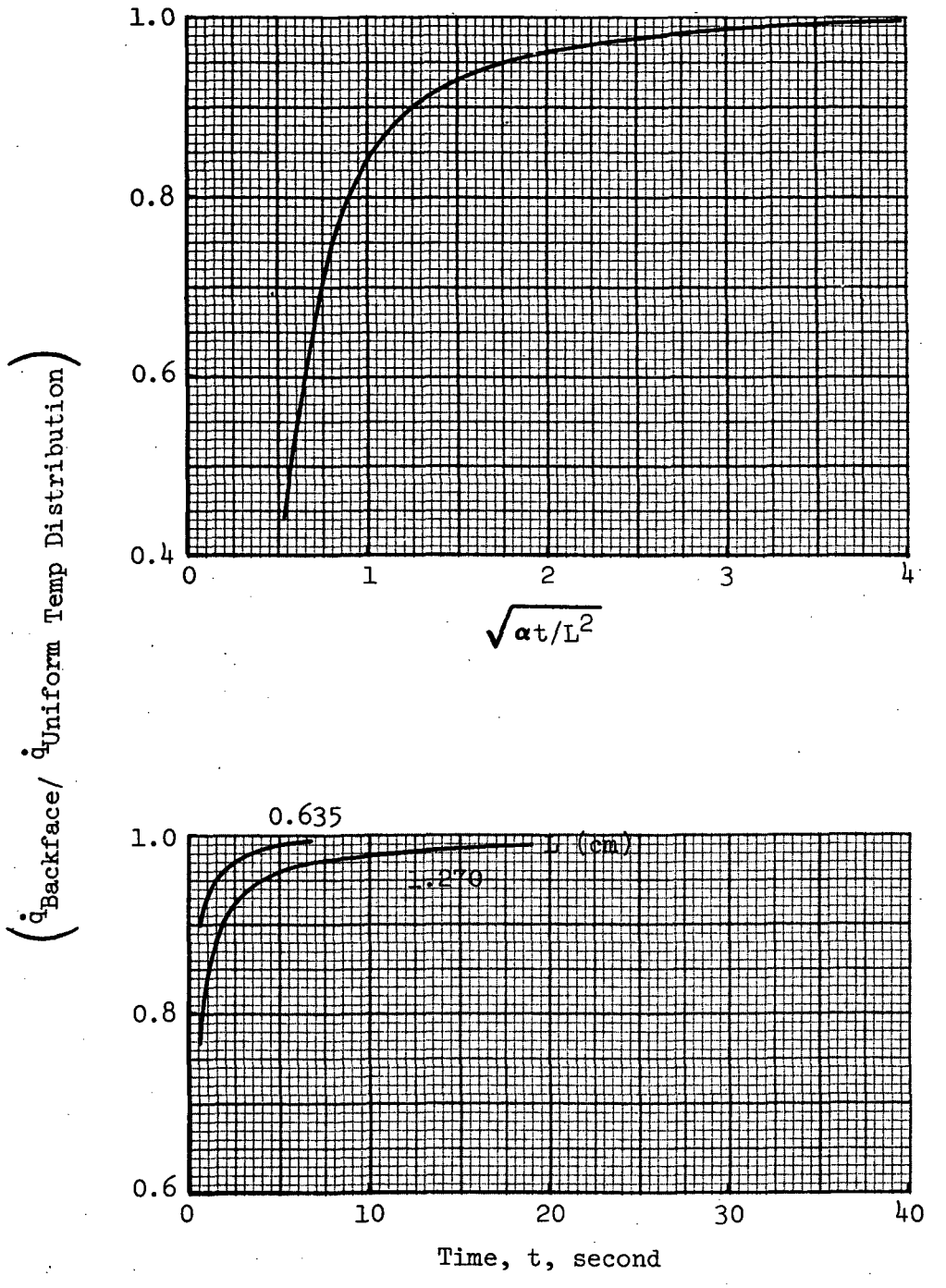

Figure B-2 Calorimeter Heating Rate Measurement Error as a Function of Fourier Number and Exposure Time

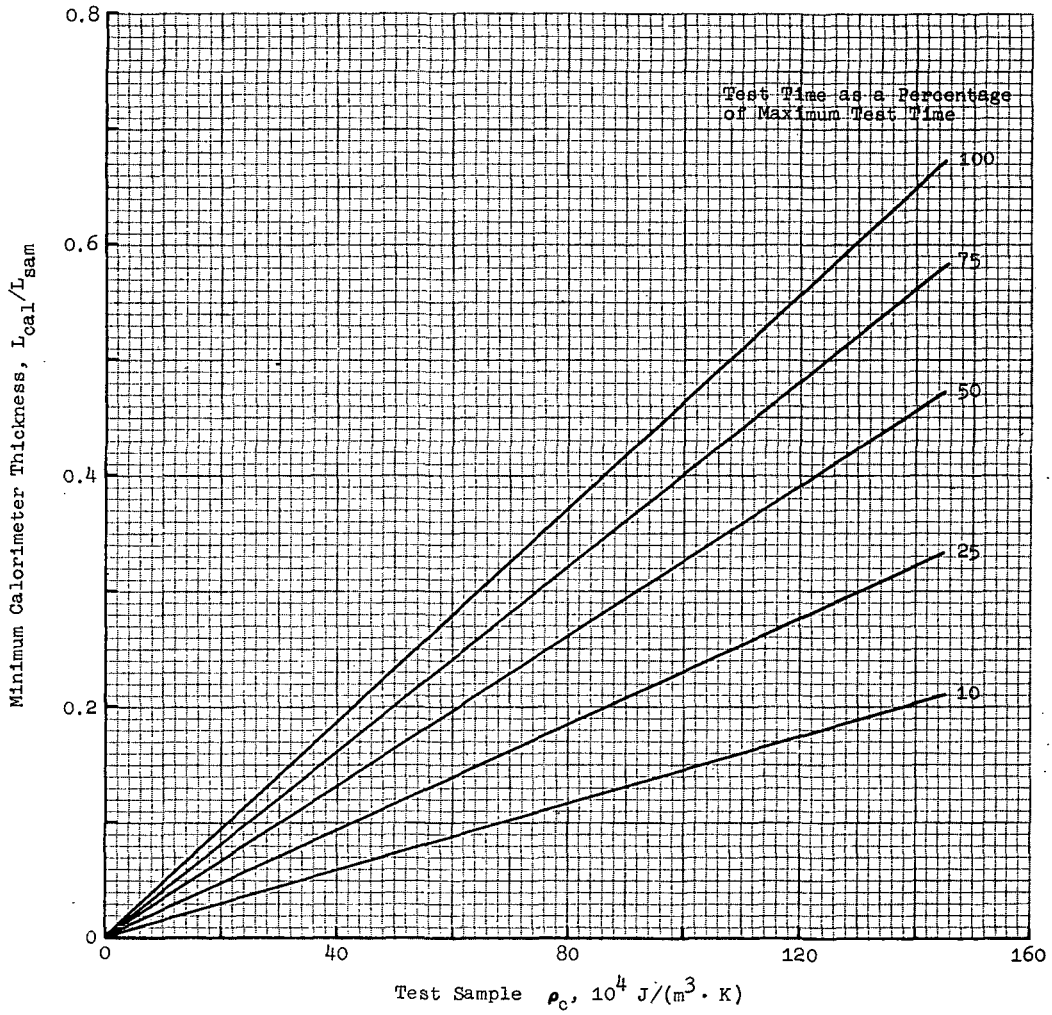

Figure B-3 Minimum Calorimeter Thickness for Calorimeter Surface Temperature to Lag behind that of the Sample [$t_{max} = (0.3\ L^2/\alpha)_{sam}$]

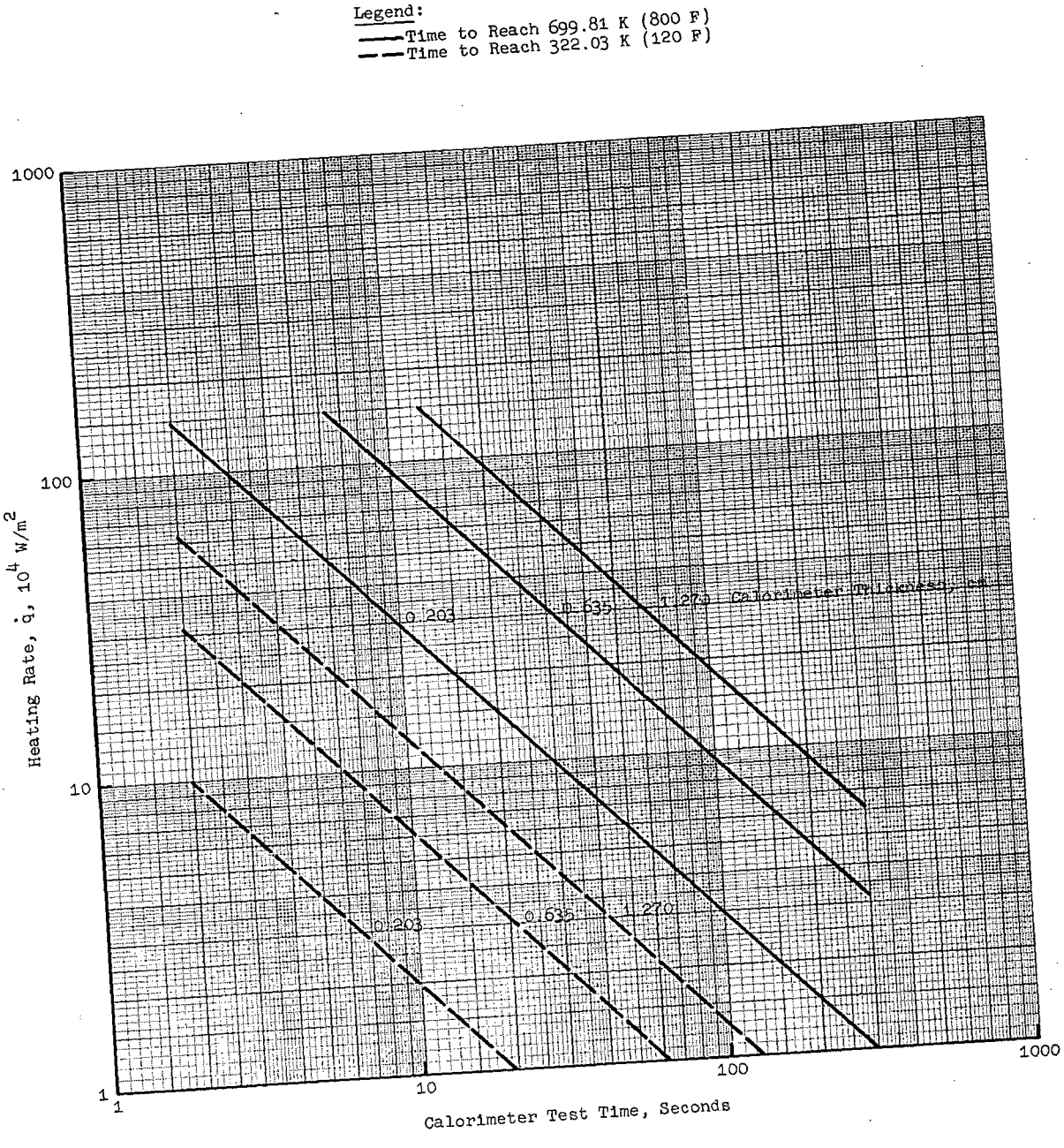

Figure B-4 Calorimeter Temperature Rise

LIST OF REFERENCES

1. Jones, R.A. and Hunt, J.L., "Use of Fusible Temperature Indicators for Obtaining Quantitive Aerodynamic Heat-Transfer Data," NASA TR R-230.

2. Traiger, H.L. and Wentworth, R.L., "Thermophysical Properties Measurements Performed for NASA," Dynatech Corporation, August 27, 1964.

3. Mc Adams, W.H., Heat Transmission, Mc Graw-Hill, 1954.

☆ U.S. GOVERNMENT PRINTING OFFICE: 1974—635-044/30

NATIONAL AERONAUTICS AND SPACE ADMINISTRATION
WASHINGTON, D.C. 20546

OFFICIAL BUSINESS
PENALTY FOR PRIVATE USE $300

SPECIAL FOURTH-CLASS RATE
BOOK

POSTAGE AND FEES PAID
NATIONAL AERONAUTICS AND
SPACE ADMINISTRATION
451

U.S.MAIL

POSTMASTER: If Undeliverable (Section 158 Postal Manual) Do Not Return

"The aeronautical and space activities of the United States shall be conducted so as to contribute . . . to the expansion of human knowledge of phenomena in the atmosphere and space. The Administration shall provide for the widest practicable and appropriate dissemination of information concerning its activities and the results thereof."

—NATIONAL AERONAUTICS AND SPACE ACT OF 1958

NASA SCIENTIFIC AND TECHNICAL PUBLICATIONS

TECHNICAL REPORTS: Scientific and technical information considered important, complete, and a lasting contribution to existing knowledge.

TECHNICAL NOTES: Information less broad in scope but nevertheless of importance as a contribution to existing knowledge.

TECHNICAL MEMORANDUMS: Information receiving limited distribution because of preliminary data, security classification, or other reasons. Also includes conference proceedings with either limited or unlimited distribution.

CONTRACTOR REPORTS: Scientific and technical information generated under a NASA contract or grant and considered an important contribution to existing knowledge.

TECHNICAL TRANSLATIONS: Information published in a foreign language considered to merit NASA distribution in English.

SPECIAL PUBLICATIONS: Information derived from or of value to NASA activities. Publications include final reports of major projects, monographs, data compilations, handbooks, sourcebooks, and special bibliographies.

TECHNOLOGY UTILIZATION PUBLICATIONS: Information on technology used by NASA that may be of particular interest in commercial and other non-aerospace applications. Publications include Tech Briefs, Technology Utilization Reports and Technology Surveys.

Details on the availability of these publications may be obtained from:

SCIENTIFIC AND TECHNICAL INFORMATION OFFICE

NATIONAL AERONAUTICS AND SPACE ADMINISTRATION

Washington, D.C. 20546